To the Graduate Council:

I am submitting herewith a thesis written by Rajen M. Patel entitled "Rheological Properties of Low Molecular Weight Polypropylenes". I have examined the final copy of this thesis for form and content and recommend that it be accepted in partial fulfillment of the requirements for the degree of Master of Science, with a major in Polymer Engineering.

Donald C. Bogue, Major Professor

We have read this thesis
and recommend its acceptance:

Accepted for the Council:

Vice Provost
and Dean of The Graduate School

STATEMENT OF PERMISSION TO USE

In presenting this thesis in partial fulfillment of the requirements for a Master's degree at The University of Tennessee, Knoxville, I agree that the Library shall make it available to borrowers under rules of the Library. Brief quotations from this thesis are allowable without special permission, provided that accurate acknowledgement of the source is made.

Permission for extensive quotation from or reproduction of this thesis may be granted by my major professor, or in his absence, by the Head of Interlibrary Services when, in the opinion of either, the proposed use of the material is for scholarly purpose. Any copying or use of the material in this thesis for financial gain shall not be allowed without my written permission.

Signature Rajen Patel

Date 29th Jan. 1998

RHEOLOGICAL PROPERTIES OF LOW MOLECULAR WEIGHT POLYPROPYLENES

A Thesis

Presented for the

Master of Science

Degree

The University of Tennessee, Knoxville

Rajen M. Patel

March 1988

This Thesis is Dedicated To my Parents

Manubhai and Ramaben Patel

ACKNOWLEDGEMENTS

First, the author wishes to express his profound appreciation to his research advisor, Professor Donald C. Bogue for the opportunity to work with him in this project and for his encouragement when it was needed the most, guidance and invaluable advice throughout his master's program.

Second, the author expresses his appreciation to Professor Larry C. Wadsworth for providing supplementary support for this research and for providing the necessary polymer samples.

Third, the author wishes to thank the Polymer Consortium for a research assistantship and the department of Materials Science and Engineering for a teaching assistantship.

Fourth, the author would like to extend his many thanks to all his many associates and faculty advisor in the Polymer Engineering program, particularly David Lewis, Russell Wong and Young D. Lee, for their advice, constructive conversations, and input during his master's program.

Fifth, the author wishes to thank the members of the mechanical shop and electronics shop for their help throughout the process of this work.

Finally, the author expresses his appreciation to the members of his master's committee, Professors, Donald C. Bogue, Joseph E. Spruiell and Larry C. Wadsworth.

ABSTRACT

Rheological properties of a series of low molecular weight polypropylenes (being used in the manufacture of melt blown fabrics and also in the melt spinning studies) were studied with particular emphasis on elongational properties. Shear viscosities and normal stresses in the low shear rate region were measured using a cone-and-plate rheometer and shear viscosities in the high shear rate region were measured using a capillary rheometer. One of the samples studied was remelted web of fabrics prepared from PP-300 MFR at 500 ^{o}F. Comparison of shear viscosity data of PP-300 MFR with the remelted web sample obtained from it suggest that significant thermal degradation occurred in the screw extruder of the melt blown unit. Because of the very thin nature of the materials studied, it is difficult to measure small stretching forces; therefore, isothermal spinning under the force of gravity (gravity spinning) was carried out.

The shear viscosity and the normal stress data were correlated by analytical expressions provided by the convected Maxwell model, with deformation rate dependent relaxation times as proposed by Bogue and White. The zero shear viscosity data were used for theoretical predictions for gravity spinning assuming Newtonian behavior. Such predictions depicted many features of gravity spinning and provided the base case for later comparison.

For the deformation rates observed in the gravity spinning experiments, the apparent elongational viscosities for PP-700 MFR and

PP-1400 MFR in the upper part of the spinline were close to three times the zero-shear viscosities, in agreement with Trouton's viscosity result for Newtonian fluids. But the corresponding results for PP-300 MFR were lower than three times the zero-shear viscosity. However, to understand the dynamics of the entire spinline, viscoelastic modelling is necessary. The convected Maxwell model provides a convenient framework for analyzing viscoelastic fluids. But the use of a deformation rate dependent relaxation times (as used in the Bogue-White model and the Phan-Thien and Tanner model) is necessary to account for the shear thinning behavior and for quantitative predictions of the gravity spinning data. The viscoelastic modelling shows that the time constants obtained from fitting the shear data cannot be used to predict the gravity spinning data quantitatively. A higher value of the average relaxation time is therefore necessary. These higher values of the average relaxation times give quantitative fits of the elongational flow data.

Under certain conditions (those giving higher elongation rates than observed for stable spinning), draw resonance, a kind of spinline instability, was observed in all the materials studied. Draw resonance data were correlated semi-quantitatively.

TABLE OF CONTENTS

CHAPTER		PAGE
1	INTRODUCTION	1
2	BACKGROUND	3
	2.1 Formulation of Constitutive Equations	3
	2.2 Behavior of Viscoelastic Fluids in Shear and Elongational Flows	9
	2.3 Rheological Properties of Polypropylenes and Molecular Weight Effects	18
3	MATERIALS AND EXPERIMENTAL PROCEDURES	21
	3.1 Materials	21
	3.2 Experimental procedures	21
4	PRESENTATION OF SHEAR FLOW DATA	31
5	PRESENTATION OF ELONGATIONAL FLOW DATA	48
	5.1 Theoretical Analysis of Newtonian Gravity Spinning	48
	5.2 Experimental Results	53
6	MODELLING OF SHEAR FLOW AND ELONGATIONAL FLOW DATA	80
	6.1 Modelling of Shear Flow Data	80
	6.2 Theoretical Simulation of Gravity Spinning Experiments	87
7	CONCLUSIONS	128
LIST OF REFERENCES		131

CHAPTER PAGE

APPENDICES 136

A 137

B 142

C 156

VITA 159

LIST OF TABLES

TABLES	PAGE
III.I. Polypropylenes used in the experiments	22
IV.I. The zero-shear viscosities and the shift factors at different temperatures for the materials studied	42
V.I. Conditions under which draw resonance was observed	76
VI.I. Tabulation of important parameters	127
A-1. Shear flow data of PP-35 MFR	137
A-2. Shear flow data of PP-300 MFR	138
A-3. Shear flow data of PP-WEB	139
A-4. Shear flow data of PP-700 MFR	140
A-5. Shear flow data of PP-1400 MFR	141

LIST OF FIGURES

FIGURE		PAGE
3.1.	Schematic diagram of equipment	26
3.2.	Experimental set-up	27
3.3.	A typical slide of a part of the spinline	29
4.1.	Shear viscosity as a function of shear rate for various polypropylene melts at 180 °C	32
4.2.	Shear viscosity as a function of shear rate for various polypropylene melts at 190 °C	33
4.3.	Shear viscosity as a function of shear rate for various polypropylene melts at 200 °C	34
4.4.	First normal stress difference as a function of shear rate for various polypropylene melts at 180 °C	35
4.5.	First normal stress difference as a function of shear rate for various polypropylene melts at 200 °C	36
4.6.	First normal stress difference as a function of shear rate for PP-300 MFR at three temperatures	38
4.7.	First normal stress difference as a function of shear stress for PP-300 MFR for data at three temperatures ...	39
4.8.	First normal stress difference coefficient as a function of shear rate at 180 °C	40
4.9.	Effective relaxation times in shear at 180 °C	43
4.10.	Master curves obtained from the data of Figures 4.1, 4.2 and 4.3. Reference Temperature = 180 °C	44
4.11.	Shift factors (a_T) as a function of reciprocal of absolute temperature	45
4.12.	Zero-shear viscosities at 180 °C as a function of weight average molecular weight	46
5.1.	Theoretical prediction of the velocity profiles along the spinline for gravity spinning of Newtonian fluids	50

5.2. Theoretical prediction of the elongation rate profiles along the spinline for Newtonian gravity spinning 51

5.3. Theoretical prediction of the stress profiles along the spinline for Newtonian gravity spinning 52

5.4. Profiles of the thread diameter for various polypropylene melts studied at 180 °C. 54

5.5. Profiles of thread diameter for PP-300 MFR at 180 °C and 200 °C 55

5.6. Polynomial curve fittings of diameter versus distance data 58

5.7. Elongation rates along the spinline, computed using polynomial curve fitting of diameter versus distance data of Figure 5.6 59

5.8. The polynomial curve fitting of (1/D) versus distance data for various polypropylene melts at 180 °C 60

5.9. Elongation rate profiles along the spinline for various polypropylene melts. Solid lines are the data at 180 °C and the dashed line is data for PP-300 MFR at 200 °C ... 64

5.10. Stress profiles along the spinline for various polypropylene melts 65

5.11. The apparent elongational viscosities as a function of the elongation rates for various polypropylene melts. The arrow shows the direction along the spinline 66

5.12. The curve fitted profiles of thread diameter for PP-300 MFR at 180 °C at two different take-up velocities 69

5.13. The apparent elongational viscosity as a function of elongation rate for PP-300 MFR at 180 °C for the runs shown in Figure 5.12 (without taking into account a small applied take-up force) 70

5.14. Profiles of thread diameter for PP-300 MFR at 180 °C for two different spinline length 72

5.15. The apparent elongational viscosities as a function of elongation rates for PP-300 MFR at 180 °C for two different spinline length 73

5.16. Plot of $D_R^{1/2}$ as a function of Re/Fr for Re=Re/We=0. The solid line is calculations of Denn et al. and the dashed line is the calculations of Shah and Pearson, as reproduced in Denn et al. (62) 78

6.1. Fitting of shear viscosity data for PP-300 MFR using the Bogue-White model 83

6.2. Fitting of shear viscosity data for PP-700 MFR and PP-1400 MFR at 180 °C using the Bogue-White model 84

6.3. Fitting of the first normal stress difference coefficient data using the Bogue-White model (using the same model parameters as used for fitting the shear viscosity data) 85

6.4. Predictions of the apparent elongational viscosities as a function of the elongational rates using the BW model using the model parameters obtained from the shear data 92

6.5. Comparison of the experimental data for PP-700 MFR at 180 °C with predictions of the BW model using three different values of average relaxation times and a=0.57 95

6.6. Comparison of the experimental data for PP-700 MFR at 180 °C with predictions of the BW model using three different values of average relaxation times and a=0.57 96

6.7. Comparison of the experimental data for PP-700 MFR at 180 °C with predictions of the BW model using three different values of average relaxation times and a=0.57 97

6.8. Comparison of the experimental data for PP-700 MFR at 180 °C with the predictions of various models using τ=0.18 sec. Model prediction for the Maxwell model with τ=0.09 sec. is also shown as solid line 99

6.9. Comparison of the experimental data for PP-700 MFR at 180 °C with the predictions of various models using τ=0.18 sec. and with the prediction assuming Newtonian behavior 100

6.10. Comparison of the experimental data for PP-700 MFR at 180 °C with the predictions of various models using τ=0.18 sec. and with the prediction assuming Newtonian behavior 101

6.11. Comparison of the experimental data for PP-700 MFR at 180 °C with the predictions of various models using τ=0.18 sec. and with the prediction assuming Newtonian behavior 102

6.12. Comparison of the experimental data for PP-700 MFR at 180 °C with the predictions of various models using τ=0.18 sec. 103

6.13. Comparison of the experimental data for PP-700 MFR at 180 °C with the BW model predictions using two different boundary conditions 107

6.14. Comparison of the experimental data for PP-700 MFR at 180 °C with the BW model predictions using two different boundary conditions 108

6.15. Comparison of the experimental data for PP-1400 MFR at 180 °C with the predictions of the BW model using τ=0.08 sec. and a=0.55 110

6.16. Comparison of the experimental data for PP-1400 MFR at 180 °C with the predictions of the BW model using τ=0.08 sec. and a=0.55 and the predictions assuming Newtonian behavior 111

6.17. Comparison of the experimental data for PP-1400 MFR at 180 °C with the predictions of the BW model using τ=0.08 sec. and a=0.55 and the predictions assuming Newtonian behavior 112

6.18. Comparison of the experimental data (solid line) for PP-300 MFr at 180 °C at the take-up velocity of 12.5 cm/sec with the predictions of the BW model (dashed line) using τ=0.45 sec. and a=1.1 and subtracting an estimated take-up force of 4.0 dyne from the model predictions .. 114

6.19. Comparison of the experimental data (solid line) for PP-300 MFr at 180 °C at the take-up velocity of 12.5 cm/sec with the predictions of the BW model (dashed line) using τ=0.45 sec. and a=1.1 and subtracting an estimated take-up force of 4.0 dyne from the model predictions .. 115

6.20. Comparison of the experimental data for PP-300 MFR at 180 °C at the take-up velocity of 10.3 cm./sec with the predictions of BW model using τ=0.45 sec. and a=1.1 ... 117

6.21. Comparison of the experimental data for PP-300 MFR at 180 °C at the take-up velocity of 10.3 cm./sec with the predictions of BW model using τ=0.45 sec. and a=1.1 ... 118

6.22. Comparison of the experimental data for PP-300 MFR at 180 °C at the take-up velocity of 10.3 cm./sec with taking into account small estimated take-up forces with the BW model predictions using extreme values of (T_{11}/T_{22}) ratio (τ=0.45 sec. and a=1.1) 120

6.23. Comparison of the experimental data for PP-1400 MFR at 180 °C with the predictions of the BW model using extreme values of (T_{11}/T_{22}) ratio (τ=0.08 sec. and a=0.55) 121

6.24. Comparison of the experimental data for PP-300 MFR at 200 °C with the predictions of the BW model using τ=0.22 sec. and a=1.1 122

6.25. Comparison of the experimental data for PP-300 MFR at 200 °C with the predictions of the BW model using τ=0.22 sec. and a=1.1 and the predictions assuming Newtonian behavior 123

6.26. Plot of the average relaxation times versus the zero-shear viscosities 125

6.27. Plot of the average relaxation times versus the Z-average molecular weights 126

CHAPTER 1

INTRODUCTION

Traditionally, polypropylene has been the dominant resin for making melt blown fabrics. During the past few years there has been a trend toward high melt flow rate (MFR) resins which have lower molecular weights and narrower molecular weight distributions than conventional polypropylenes (1). They can be melt blown at higher throughputs and much lower temperatures, depending on the processing conditions. The melt spinning of these low molecular weight resins is also of current interest (2). In a typical melt blown process, polymer is extruded through a slit die containing a horizontal row of small orifices. The fibers are rapidly attenuated by convergent streams of hot air exiting from both sides of the die tip. The ultrafine fibers are blown onto a collector screen forming a white, opaque web (3). If processes of this complexity are to be modelled, it will be necessary to have an independent rheological characterization of the materials. It is the purpose of the present work to provide that characterization.

There are two fundamental rheological properties that are of primary concern in polymer processing: viscous and elastic properties. These rheological properties in turn depend, among many other things, on the molecular structure, the molecular weight

distribution, and on processing conditions such as melt temperature, pressure, and flow rate (4). Therefore a better understanding of the interrelationships of these variables is essential for evaluating the processability of polymeric materials. The rheological behavior of polymer melts must be considered in terms of deformation under shear and, in view of the processes being considered, under elongation as well. Both kinds of deformation play an important role in the melt blown fabrics process and the melt spinning process.

It is the purpose of this research to study the rheological properties of these low molecular weight polypropylenes, with particular emphasis on elongational viscosity.

CHAPTER 2

BACKGROUND

Polymer rheology combines two quite different approaches: a phenomenological approach (continuum mechanics) which aims to find relations between stress and strain history in a general way; and a molecular approach which looks for understanding in terms of molecular structure (5,6).

One of the fundamental problems of rheology is to establish the relationship between stress and deformation rate. Polymeric melts are like viscous liquids, in that they flow, but they also show elastic or memory effects, in that the present stress state depends on the previous history of deformation. They are thus viscoelastic fluids. Viscoelasticity theory, which originated in one dimensional mechanical models for small strains, has been generalized to three dimensional, large deformation theories, the so-called constitutive equations.

2.1 Formulation of Constitutive Equations

Constitutive equations are formulated in two different ways: a differential type formulation and an integral type formulation.

Integral formulations : Viscoelastic theory can be organized around the idea of an integral constitutive equation of the form (7,8)

$$\sigma_{ij} = -P\delta_{ij} + \int_{-\infty}^{t} m_1(t-t')\, C_{ij}^{-1}\, dt' \qquad [2.1.1]$$

where $m_1(t-t')$ is the so-called "memory function", C_{ij}^{-1} is the Finger strain tensor, t is the present time and t' is some arbitrary past time.

The simplest memory function is of the form

$$m_1(t-t') = G/\tau \; e^{-(t-t')/\tau} \qquad \text{(one element memory)} \qquad [2.1.2]$$

where G and τ are an elastic modulus and a relaxation time, respectively.

Unfortunately, however, practical polymeric materials do not show just one relaxation time and one must use a relaxation spectrum $H(\tau)$ defined by the equation

$$m_1(t-t') = \int_{-\infty}^{\infty} H(\tau)/\tau \exp(-(t-t')/\tau)\, d\ln\tau \qquad \text{(continuous spectrum memory)} \qquad [2.1.3a]$$

or

$$m_1(t-t') = \Sigma\, G_n/\tau_n \; e^{-(t-t')/\tau_n} \qquad \text{(discrete multi-element memory)} \qquad [2.1.3b]$$

In practice, as many as eight discrete memory elements have been used to represent whole relaxation spectrum. The integral models of the

form of eq. [2.1.1] with one element memory or spectrum memory predicts constant viscosity in shear flow. A variety of forms of the memory functions have been suggested to account for the shear thinning behavior and non-linear behavior under elongation (8-15). Many of the integral formulations of constitutive equation can be cast in differential form. Two constitutive equations in particular, the Bogue-White model (based on continuum mechanics) and the Phan-Thien-Tanner Model (based on polymer network theories) in their differential formulations, will be discussed in the subsequent section. They will be used subsequently to analyze shear flow and elongational flow data.

Differential formulations : The historical development of the differential type constitutive equation is based on the classical "Maxwell model", which consists of a viscous element (dashpot) and an elastic element (elastic spring) in series. The simplest derivative-type model is any of several variations of the so-called convected Maxwell equation :

$$T_{ij} + \tau(\delta T_{ij}/\delta t) = G\tau d_{ij} \qquad [2.1.4]$$

where d_{ij} is a deformation rate tensor ($d_{ij} = dv_i/dx_j + dv_j/dx_i$), $(\delta T_{ij}/\delta t)$ denotes any suitable derivative which moves and deforms or rotates with a fluid element. Three convected derivatives which satisfy the principle of material objectivity are the contravariant and covariant formulations of the Oldroyd derivative (16), and the

Jaumann derivative discussed by Oldroyd (17) and Prager (18). Of the three convected time derivatives, the contravariant formulation possesses the correct characteristics of predicting high stress levels in elongational flows and a finite first normal stress differences and zero second normal stress difference in shear flow. Experimental data show a second normal stress difference which is about -0.2 to -0.3 times the first normal stress difference (31,32), but the approximation of a zero second normal stress difference is still often used. A zero second normal stress difference is also predicted by a number of molecular theories. Thus, if eq. [2.1.3] is to be used, the choice of the contravariant time derivative appears to be the most realistic one.

Convected Maxwell model with the Oldroyd contravariant derivative gives following predictions in simple shear :

$$T_{12} = 2G\tau\dot{\gamma}$$

$$N_1 = \sigma_{11} - \sigma_{22} = 2G\tau^2\dot{\gamma}^2 \qquad [2.1.5]$$

$$N_2 = \sigma_{22} - \sigma_{33} = 0$$

Note that the model predicts constant viscosity and zero second normal stress difference in shear and the first normal stress difference is predicted to be proportional to the square of the relaxation time and the shear rate.

Bogue-White model : The convected Maxwell model with a contravariant time derivative predicts a constant viscosity, independent of shear rate, while it is known experimentally that both the viscosity and the relaxation time are decreasing functions of shear rate. This dependence has generally been introduced by making these parameters functions of the second invariant of the deformation rate tensor, as in the Bogue-White model (7,8). The Bogue-White model in differential form is the same as convected Maxwell model with a contravariant time derivative with τ_n replaced by τ_{neff} where, τ_{neff} is an effective (deformation rate dependent) relaxation time given by

$$\tau_{neff} = \frac{\tau_n}{1+(a\tau_n\langle\pi_d{}^{1/2}\rangle)^b} \qquad [2.1.6]$$

where "b" is an adjustable (empirical) factor to obtain correct asymptotic slop of viscosity-shear rate curve at large shear rates. The Bogue-White model, when originally proposed, assumed the value of this adjustable factor "b" to be unity, which did not have the correct asymptotic slope of viscosity-shear rate curve at large shear rates (8). For this modified Bogue-White model, the value of "b" usually lies between 0.75-0.8. $\langle\pi_d\rangle$ is the second invariant of the deformation rate tensor. In simple shear, $\langle\pi_d{}^{1/2}\rangle$ is just the shear rate $\dot{\gamma}$, while in uniaxial elongation it is $\sqrt{3}$ E. The Bogue-White model with b=1, both in differential and integral form

has been found to successfully correlate data on bulk polymers (19-24).

Phan-Thien Tanner model : Several constitutive equations derived from a network picture of polymer solutions and melts have been proposed. A nonlinear constitutive equation for polymer melts and concentrated solutions is that due to Phan-Thien and Tanner (25,26,27), derived from a Lodge-Yamamoto type of network theory. The constitutive equation proposed by them (the PTT model) can be described by the following set of equations.

$$T = \Sigma\, T^{(i)}$$

$$\tau_i \frac{DT^{(i)}}{Dt} + K(\mathrm{tr}\, T^{(i)})T^{(i)} = G_i \tau_i D \qquad [2.1.7]$$

Equation [2.1.7] represents a spectral decomposition of the stress tensor. τ_i and G_i are the relaxation times and moduli, respectively, which can be measured from the equilibrium relaxation spectrum of the fluid. D/Dt is the convected derivative defined by

$$\frac{DT}{Dt} = \frac{dT}{dt} - \Gamma T - T\Gamma^T \qquad [2.1.8]$$

where $\Gamma = L - \xi D$ is the effective gradient, L and D are the velocity gradient and the symmetric part of the velocity gradient tensor

respectively. ξ is an adjustable parameter found from the ratio of the second to the first normal stress difference, as given by

$$N_2 = -\xi/2\ N_1 \qquad [2.1.9]$$

$K(\text{tr } T^{(i)})$ is closely related to the rate of destruction of junctions and takes the approximate form

$$K(\text{tr } T^{(i)}) = \exp(\varepsilon/G_i\ \text{tr } T^{(i)}) \qquad [2.1.10]$$

where,

$$\text{tr } T^{(i)} = T_{11} + T_{22} + T_{33}$$

The value of ε is found by fitting elongational viscosity data to the model prediction. Thus, the PTT model contains two adjustable parameters: one is found from the ratio of the second to the first normal stress differences and the other from elongational viscosity data. The PTT model can also be regarded as a convected Maxwell model with stress dependent relaxation times (28).

Both models, the Bogue-White model and the PTT model, can also be represented in an integral formulation.

2.2 Behavior of Viscoelastic Fluids in Shear and Elongational Flows :

The two most important basic flows are shear flow and elongational flow. Some of the important characteristics of these flows will now be discussed.

For many years most rheological studies have centered on long duration simple shear flow measurements as a means to study polymer melt behavior and to help develop viscoelastic theories.

The imposed kinematics can be written as

$$v = (v_1(X_2),\ 0\ ,\ 0) \qquad [2.2.1]$$

where "1" denotes the flow direction, "2" the normal direction, and "3" the neutral direction. The simple shear flow of polymer melts gives rise not only to shear stresses but also to two unequal normal stress differences which arise in the direction and perpendicular to the direction of flow. The character of the shear viscosity is well-known to be a decreasing function of shear rate for polymer solutions and melts, as reviewed by several authors (4,8,29,30). Less rheological data is available for the first and the second normal stress difference, especially the second normal stress difference. It is known that the first normal stress difference coefficient is positive and a stronger decreasing function of shear rate than the shear viscosity and second normal stress difference is negative and its magnitude is about 20-30 percent of the first normal stress difference (31,32). One can define the first normal stress difference coefficient as

$$\Psi_1 = (T_{11} - T_{22})/\dot{\gamma}^2 \qquad [2.2.2]$$

and similarly, the second normal stress difference coefficient. This particular definition of a normal stress difference coefficient is taken because polymeric liquids exhibit a quadratic dependence of normal stresses on shear rate in the limit of low shear rate. For such liquids Ψ_1 would approach a constant value $\Psi_{1(0)}$ characteristic of the liquid. This parallels the observation that many non-newtonian fluids exhibit a linear dependence of T_{12} on $\dot{\gamma}$ in the limit of small $\dot{\gamma}$, and so η approaches a constant value η_0 (the "zero-shear" viscosity) characteristic of the fluid. Oda, White and Clark (33) found from their correlation of the first normal stress difference against shear stress in polystyrene melts that the first normal stress difference is a unique function of shear stress and molecular weight distribution, independent of temperature.

One may define an effective relaxation time in shear using eq. [2.1.5] as follows :

$$\tau = \frac{\sigma_{11} - \sigma_{22}}{2\tau_{12}\dot{\gamma}} \qquad [2.2.3]$$

where the values of $(\sigma_{11} - \sigma_{22})$ and τ_{12} are to used at the same shear rate. One can then obtain relative relaxation time data as a function of shear rate, which can then be extrapolated to obtain an average value of a zero shear relaxation time.

Because of the great sensitivity of polymer viscosity to both temperature and shear rate, a large amount of data is required to characterize the flow behaviour of a particular polymer. Thus, there

is a strong need to predict the viscosity function from a small amount of experimental data. There also is the need to be able to compare the behavior of one polymer to another. Several schemes have been developed for doing this by superposition rules in which one curve is shifted relative to another curve to obtain a master curve (34). One of the proposed methods for the prediction of flow behavior at various temperatures is by using the time-temperature superposition method. In the case of shear rate as the variable, curves of shear stress T are plotted as a function of shear rate $\dot{\gamma}$, with temperature as the parameter. A curve at one convenient temperature can be chosen as the reference curve. The other curves can then be superimposed onto the reference curve by shifting them horizontally along the shear rate axis by means of a shift factor a_T. Mathematically,

$$a_T = \frac{\dot{\gamma}\,(\text{reference})}{\dot{\gamma}\,(T)} \qquad [2.2.4]$$

where $\dot{\gamma}$(reference) is the shear rate for a constant value of shear stress at a reference temperature curve, and $\dot{\gamma}(T)$ is the shear rate at temperature T for the same value of shear stress. Usually the shift factors are correlated in terms of the Williams-Landel-Ferry (WLF) equation (35). An alternate simpler way to correlate a_T, giving almost the same result when used over a limited range of temperature, is given by the following equation.

$$a_T = \frac{\eta(T)}{\eta(\text{reference})} = K_1 e^{E/RT} \qquad [2.2.5]$$

where K_1 is a constant, and E is the energy of activation for flow evaluated. The procedure can be reversed by using the master curve to calculate the flow behavior at any arbitrary temperature or to estimate the behavior of a polymer of different molecular weight but a similar structure with a minimum of information.

Although simple shear flow has been most widely studied, the occurrence of elongational flow in polymer processing operations such as melt spinning, film drawing and the melt blown fabric process makes it an important area of study (36,37,38). The stress accompanying the extension of the material is of particular importance in defining operating conditions for such processes. For this reason one defines an uniaxial elongational viscosity η_e (sometimes called a tensile viscosity) as

$$\eta_e = \sigma_{11}/E \qquad [2.2.6]$$

where E is the elongation rate. Note that η_e is defined in terms of the total stress σ_{11} and not in terms of the deviatoric stress T_{11}.

Qualitatively, the shear flow of all polymer melts shows similar behavior, whereas the elongational flow can show significant differences from one polymer to another. An important point is that it is not, in general, possible to predict behavior in elongation

from behavior in shear (11). Furthermore, for polymeric liquids there is evidence that in flows involving both shear and elongation, the elongation will have a dominant influence, e.g. in sharply converging or diverging flows.

As early as 1906, Trouton (39) showed that the uniaxial elongational viscosity (hereafter to be referred to as simply elongational viscosity) of a Newtonian fluid is three times the shear viscosity. This result is related mathematically to the fact that the Young's modulus for an incompressible isotropic Hookean solid is three times the shear modulus. Polymer melts are, however, both viscous and elastic in nature and thus one must use viscoelastic theory. Differential or integral equivalent of the convected Maxwell model, with constant G and τ (one element models) (refer Eqs. [2.1.1], [2.1.2] and [2.1.4]), gives the following steady state prediction (40):

$$\eta_E = \sigma_{11}/E = \frac{3G_o\tau_o}{(1-2E\tau_o)\ (1+E\tau_o)} \qquad [2.2.7]$$

where E is the elongation rate. From the above equation it is apparent that the elongational viscosity approaches the Trouton viscosity (note $\eta_o=G_o\tau_o$) at low E and becomes unbounded at $E=1/(2\tau_o)$. There are a large number of more complicated (non-linear) models (40).

From the mid 1960's there were several investigators who measured the elongational viscosity of polymer melts with different

experimental methods. There were often difficulties in measuring the elongational viscosity under controlled kinematics. Methods of measuring elongational viscosity have been reviewed by several authors (41,42,43,44). Many of these methods were developed for highly viscous melts which involve elongation with constant elongation rates, constant stress, etc. Elongation experiments should be carried out at constant elongational rate or stress, if they are to specify true material properties. For polymers of lower viscosity (lower molecular weights), isothermal melt spinning under the influence of gravity only (called "gravity spinning") or isothermal melt spinning with external take-up force are suitable methods for measuring apparent elongational viscosity. Isothermal melt spinning enables one to separate the effects of elongation rate on the elongational viscosity from those of temperature. Here the elongation rate varies along the spinline. The flow is not spatially homogeneous, but is steady in the Eulerian sense by which one means that at any point in space the velocity of the fluid is constant. One notes that a particle of fluid will experience a changing velocity and velocity gradient as it moves along the spinline; in other words that the flow is unsteady in the Lagrangean sense. Hence one obtains only an apparent elongational viscosity. Hence, the resulting elongational deformation in isothermal melt spinning is history dependent and so data reduction must be made in terms of a constitutive equation.

Isothermal melt spinning with take-up : In such an experiment, one must measure the axial profile of fiber diameter and thread tension at the take-up device, and ensure that the molten fiber travels through a heated chamber maintained at the same temperature as the melt. The fiber velocity U(x) is calculated from the continuity equation,

$$U(x) = 4W/\rho\pi d(x)^2 \qquad [2.2.8]$$

where ρ is the density of a melt, W is the mass flow rate through the die and d(x) is the fiber diameter at the position x.

Once the fiber diameter, fiber velocity and the fiber tension are measured, the apparent elongational viscosity η_{eapp} can be calculated (4),

$$\eta_{eapp} = \frac{F_R/A(x)}{dU/dx|_x} \qquad [2.2.9]$$

In an isothermal melt spinning experiment, F_R may be calculated from the overall force balance equation,

$$F_R = F_L + F_G - F_D - F_I \qquad [2.2.10]$$

In which F_L is the actually measured tension at x=L, F_G is the gravitational force, F_I is the inertial force and F_D is the drag force.

Viscous jets under gravity : For very low viscosity polymer melts, the take-up force that can be applied is very small and difficult to measure accurately. Isothermal melt spinning under the influence of gravity is one possible method for measuring the apparent elongational viscosity of these low viscosity melts. In case of gravity spinning, all the forces except gravity can be neglected and hence $F_R = F_G$ in eq. [2.2.10].

Let us consider an axisymmetric jet of a Newtonian fluid under isothermal conditions. In the case where viscosity and gravity are the dominant effects, the governing differential equation is (11)

$$U''(x) - U'(x)^2/U(x) = - \rho g/(3\eta) \qquad [2.2.11]$$

where ρ is the density and η is the shear viscosity. Eq. [2.2.11] has the solutions (11),

$$U(x) = (\rho g/6\eta A^2)\sinh^2(A(x+B)) \qquad [2.2.12a]$$

$$U(x) = (\rho g/6\eta)(x+B)^2 \qquad [2.2.12b]$$

and $$U(x) = (\rho g/6\eta A^2)\sin^2(A(x+B)) \qquad [2.2.12c]$$

where A and B are arbitrary constants to be determined by the boundary conditions. For gravity spinning, where molten fiber elongates under its own weight and enters a bath of the same or higher density as that of the fiber such that the gravity effect is offset by buoyancy, one obtains

$$F_L=0, \text{ at } x=L \quad (\equiv du/dx=0 \text{ for Newtonian fluids})$$

$$\text{and} \quad U=U_0, \text{ at } x=0 \qquad [2.2.13]$$

The constants in the above equation cannot be determined explicitly. Hence, the above second order differential equation would have to be solved numerically to obtain the velocity profile along the spinline. The theoretical predictions for Newtonian gravity spinning obtained from the numerical solution of the above second order differential equation would be presented in chapter V.

In an actual experiment, the diameter profile of the spinline is measured under isothermal conditions. The fiber velocity U(x) is calculated from the continuity equation [2.2.8]. The stress can be calculated from the weight of spinline fiber below a point x, from which the apparent elongational viscosity can be obtained by using the equation,

$$\eta_{eapp} = \frac{F/A(x)}{dU/dx\big|_x} \qquad [2.2.14]$$

where F is the force due to the weight of threadline below a point x and dU/dx is the elongation rate at that point.

2.3 Rheological Properties of Polypropylenes and Molecular Weight Effects :

Polypropylene melts, like many other polymeric materials, deviate considerably from ideal Newtonian behaviour in simple shear.

The apparent shear viscosity of most polymer melts decreases rapidly with increasing shear rate. The zero-shear melt viscosity (η_o) is an important material property. As is well-known from many studies with bulk polymers, the dependence of the zero-shear viscosity on the molecular weight varies from a linear one at low molecular weights to a dependence on approximately the 3.5 power at high molecular weights (45). The transition point between these two regions is referred to as the critical molecular weight, M_c, and also marks the begining of significant non-Newtonian effects at high shear rates. The deviation of polymer melt from Newtonian behavior is strongly dependent on its molecular weight and molecular weight distribution. In particular, melts of higher molecular weight deviate from Newtonian behavior at lower shear (or elongational) rates.

Several investigators have studied the shear and elongational rheology of conventional polypropylenes. Polypropylene shows mosts of the kinds of behavior described above. Minoshima, White and Spruiell (46,47) have reported measurements of steady shear and elongational flow properties, extrudate swell and apparent isothermal spinline elongational viscosities for a series of conventional polypropylenes. Han and Lamonte (48) and Nokubo, Koyama and Ishizuka (49) have also measured apparent elongational viscosities from isothermal melt spinning experiments. Han and Kim (50) have investigated the effects of deformation history on elongational viscosity, spinnability, and thread instability of polypropylene melt by carrying out isothermal melt spinning experiments. Trzebiatowski and Wilski (51) have measured the steady state elongational

viscosities of a series of polypropylenes using the Rheometrics Extensional Rheometer RER 9000.

There is some work reported in the literature on molecular weight distribution effects in shear and elongational rheology : Onogi and coworkers (52,53), Graessley and Segal (54), Graessley (55), Prest, Porter, and O'Reilly (56,57,58). A general theoretical observation is that the mixing of molecular weight fractions must be done by a quadratic (or even higher) mixing law, rather than by a linear one, if the molecular weights are above the entanglement molecular weight (53,59).

CHAPTER 3

MATERIALS AND EXPERIMENTAL PROCEDURES

3.1 Materials

The materials used in this study were polypropylenes, with varying molecular weight and narrow molecular weight distribution, prepared by Exxon Chemical Company, which are used in the manufacture of melt blown fabrics. They are listed in the order of increasing Melt Flow Rate (MFR) in Table III-I. All of the samples but one were in the form of pellets as received from Exxon Chemical Company. One of the samples was the remelted webs of fabric obtained after melt blowing operation; prepared from 300 MFR polypropylenes at 500 ^{o}F.

3.2 Experimental Procedures

Shear flow measurements : A cone-and-plate apparatus (Rheometrics Mechanical Spectrometer) was used to measure the shear stresses and first normal stress differences at different temperatures in the low shear rate region. The cone has a 25 mm diameter with 0.1 radian cone angle.

The shear stress and the first normal stress difference are determined by measuring the torque (τ) and the thrust (F). To obtain

Table III.I :- Polypropylenes used in the experiments*.

SAMPLE/MFR	M_w X 10^{-5}		M_w/M_n		M_z/M_w	
	GPC #1	GPC #2	GPC #1	GPC #2	GPC #1	GPC #2
PP-35 MFR	1.78	1.51	2.53	2.61	1.86	1.91
PP-300 MFR	1.24	1.03	2.87	2.74	2.05	2.04
PP-WEB**	-	0.81	-	2.40	-	1.82
PP-700 MFR	-	0.88	-	3.67	-	2.27
PP-1400 MFR	-	0.83	-	3.01	-	1.94

* GPC data provided by Exxon Chemical Company.

** Subsequently remelted to measure rheological properties.

the shear stress and the first normal stress difference the following equations were used.

$$\dot{\gamma} = \Omega/\alpha$$

$$\eta = \sigma_{12}/\dot{\gamma} = 3\tau/(\dot{\gamma}2\pi R^3) \qquad [3.1]$$

$$N_1 = \sigma_{11} - \sigma_{22} = 2F/\pi R^2$$

where Ω is the angular velocity of the cone; α is the cone angle; τ is the torque; F is the thrust; and R is the radius of the cone. Sheet samples to place in the gap were made on a hot press at 180 ^{o}C.

In the high shear rate region an Instron Capillary Rheometer was used to measure the shear viscosity at different temperatures. A close-fitting plunger was driven through the barrel at constant speed, extruding the melt through a capillary die fixed to the bottom of the barrel. By recording the plunger force from a load cell and knowing the plunger speed, a total pressure drop and volumetric flow rate are obtained. The sensitivity of load cell limits lowest achievable shear rate. The web sample was excluded from the Instron measurements as uniform pallets could not be obtained from it.

The appropriate equations for computing viscous properties of fluids in a capillary rheometer are

$$\Delta P_{total} = \Delta P_{ends} + 4\tau_w L/D$$

$$\dot{\gamma}_w = 32Q/\pi D^3 \left((3n'+1)/4n'\right) \qquad [3.2]$$

where $$n' = \frac{d\ln\tau_w}{d\ln(32Q/\pi D^3)}$$

where Q = flow rate, L = length of capillary, and D = diameter of capillary.

Capillaries of diameter 0.040 in. were used to measure the total pressure drop. The L/D ratios were 11.3,22.3,36.8.

Elongational flow measurements : The measurement of elongational viscosity is among the most difficult challenges in rheometry and this is particularly true for low-viscosity polymer melts and solutions (60). Because of the very thin nature of the materials (PP 300-1400 MFR) to be investigated, it is impossible to carry out elongational measurements in instruments such as the Meissner device (61), in which the elongation rate (E) is kept constant. Similarly, isothermal melt spinning experiments with external take-up force would be very difficult to carry out as the applied take-up force would be too small to measure accurately. Rather, isothermal melt spinning experiments without external take-up force ("gravity spinning") were carried out using the Instron Capillary Rheometer in order to measure the apparent elongational viscosity. PP-35 MFR was excluded from the elongation measurements as its change in diameter would not be large enough to measure the elongation rates accurately. The web sample was also excluded from the elongational measurements as uniform pallets could not be obtained from it.

The polymer melt was extruded at different temperatures using Instron Capillary Rheometer through a capillary die (diameter = 0.058" with die aspect ratio = 30) into an isothermal chamber (about 8.9 cm. and 15.6 cm. long) maintained at the same temperature as the melt; the chamber was equipped with a wide glass window. The plunger speed was set at 0.5 in./min for all runs. Temperature was controlled by thermocouples and controller feed back systems operating on sets of cartridge heaters. For gravity spinning, where the molten fiber extends under its own weight, the fiber was quenched in a water bath and was taken up very slowly on a take-up roll to prevent piling up of polymer so as to avoid applying any external take-up force. A variable speed (B and B motor, 86 r.p.m. max.) motor with a cylindrical take-up roll constituted the take-up device. The schematic diagram of the isothermal melt spinning apparatus is shown in Figure 3.1 and the experimental set up in Figure 3.2.

Photographs of the spinline were taken to measure the diameter profile of the spinline. For the photographs, a 35 mm Nikon SLR type camera was used with a 135 mm lens mounted on a bellows for maximum enlargement. Depth of field is very narrow for this macro-photographic technique. Kodak Ektachrome (ASA 100) color slide film was used. Shutter speeds of 1/60 sec. to 1/120 sec. were used with f-stops ranging from 5.6 to 8.3. The spinline was photographed in 4 to 6 parts to achieve maximum magnification. A fluorescent light source was kept on the other side of the camera just behind the window glass to illuminate it. Color slides contained a dark edged fiber in a bright background with a good contrast to mark off the

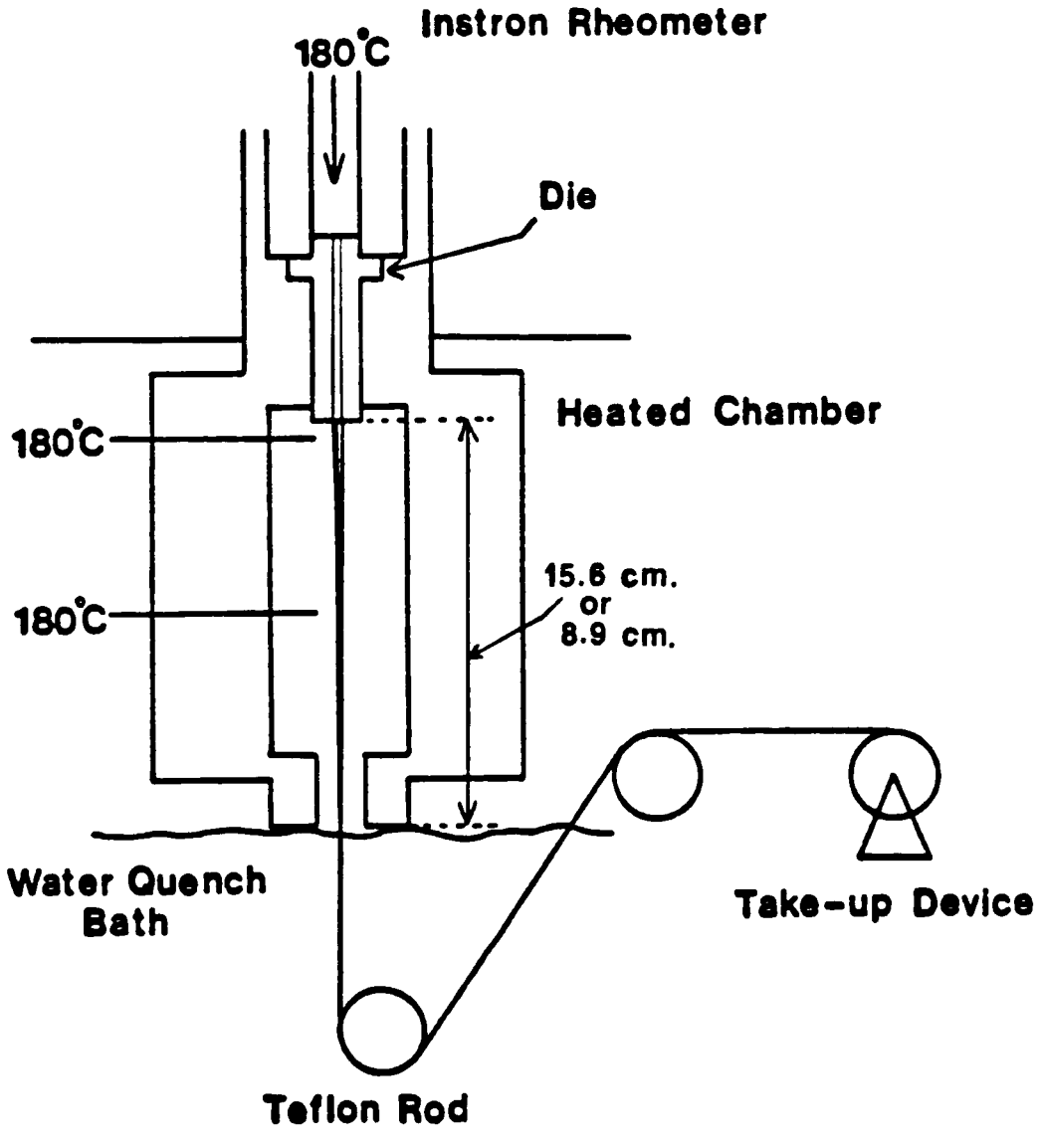
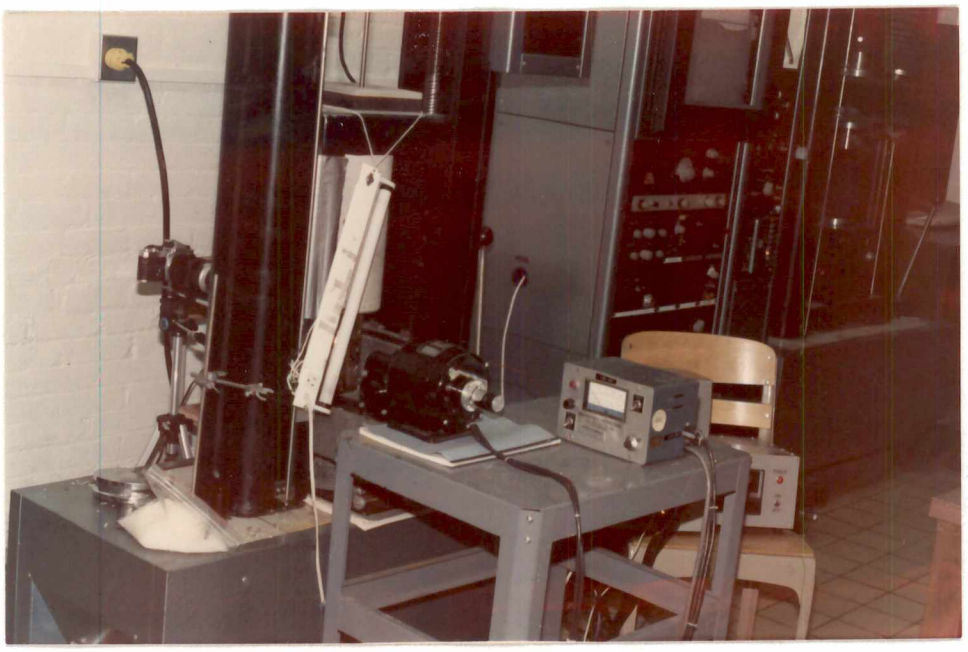
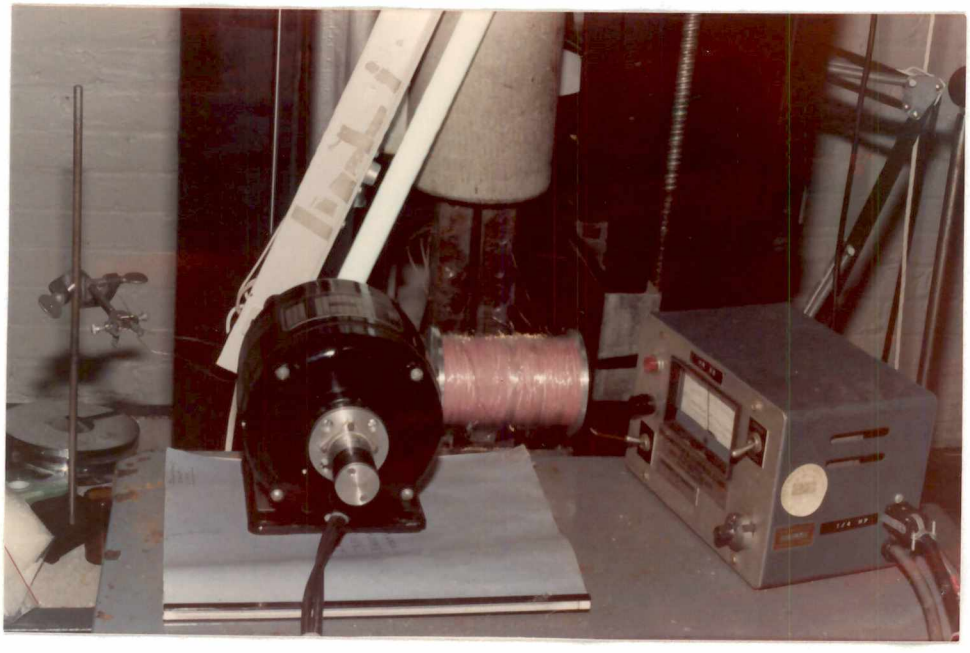


Figure 3.1. Schematic diagram of equipment.



a. An overview of the experimental set-up.



b. Close-up of the isothermal chamber and take-up apparatus.

Figure 3.2. Experimental set-up.

edges of the fiber accurately. Diffused light source also eliminates the problem of getting reflections off the edges of the molten fiber. Incandescent light of a slide projector was used on the same side of camera to illuminate the chamber so that the markings on the chamber could be photographed (to obtain the axial dimension). Slides of a reference steel rod of known diameter were taken at the end of the experiment. The resulting slides were enlarged by a slide projector in order to measure the diameter profile by comparing the extrudate with a reference scale. A typical slide is shown as Figure 3.3. For gravity spinning, one can calculate the apparent elongational viscosity from eqs. [2.2.8] and [2.2.14].

The Instron Capillary Rheometer was used as a precise throughput device. The filling of Instron barrel is very crucial in these high precision elongation experiments as air bubbles trapped in the melt while filling the barrel can either break the spinline or can lead to random fluctuations in throughput rate for a running spinline. With the limited volumetric capacity of Instron barrel, useful running spinline can only be obtained for about 7 to 8 min. with good filling of the barrel at the plunger speed of 0.5 "/min. It takes about 3 to 4 min. to take slides of spinline in 4 to 6 different parts (depending upon the length of spinline). Because of the very narrow depth of field, the camera had to be focused properly each time when a part of the spinline is to be photographed. Attempts were always made to take two sets of slides of spinline.

For gravity spinning, molten filament should elongate under its own weight and quenched filament should be removed with the velocity

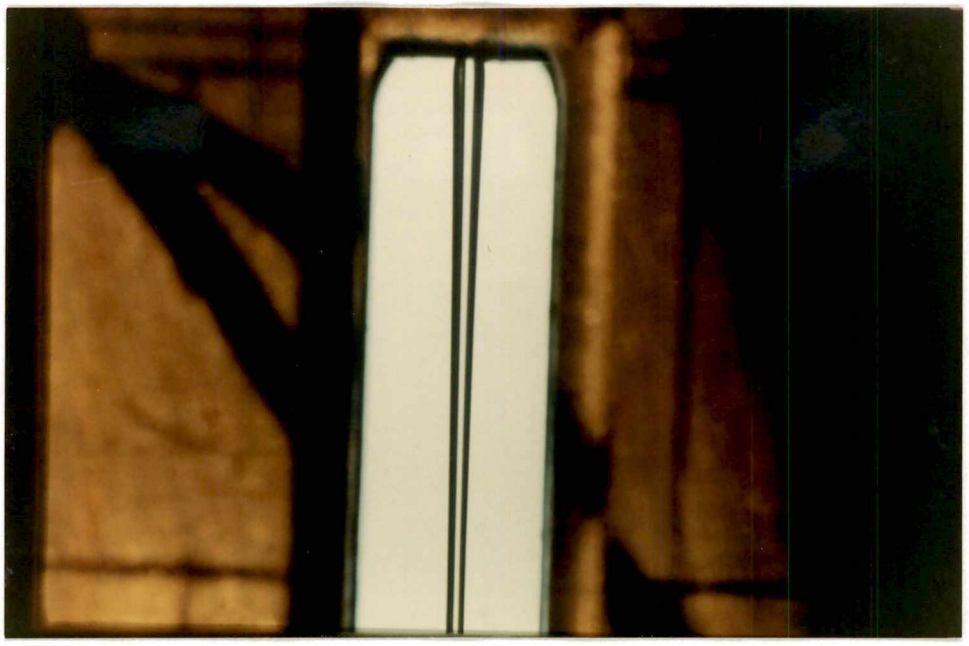


Figure 3.3. A typical slide of a part of the spinline.

with which it enters water bath without applying any take-up force. After starting the spinline with some take-up force (with higher take-up velocity), the take-up velocity was decided by lowering it to the point such that no further reduction was possible without breaking the spinline randomly due to "wiggling" of the spinline and pile-up on the surface of the water bath. However, gravity spinning leads to the wiggling of the spinline, especially of the lower half as filament feels the resistance due to water bath and hence good slides of the lower half with sharp edges of filament were difficult to obtain. Also, it might not be possible to remove the quenched fiber without applying any take-up force, especially for low MFR melts as it might be difficult to decide exact take-up velocity. A tiny force might have to be applied to guide the fiber around the Teflon rod in the water bath and to minimize the problem of the wiggling of spinline to obtain better slides with sharp edges of filament. This may be especially true for the PP-300 MFR samples which has a high viscosity and elasticity since they did not draw down as much (giving lower elongation rates). The lower the draw down ratio, the more difficult it was to take-up the quenched fiber without applying take-up force, in order to minimize the wiggling caused by the resistance felt by the filament while entering the water bath. Attempts were always made to take-up quenched fiber on unused surface of take-up roll as loose aggregate of fibers on take-up roll can change the effective take-up velocity.

CHAPTER 4

PRESENTATION OF SHEAR FLOW DATA

In this chapter the studies of the rheological properties arising in simple shear flow are summarized.

The shear viscosities at low shear rates were measured in a cone-and-plate apparatus (Rheometrics Mechanical Spectrometer) and at high shear rates in a capillary apparatus (the Instron Capillary Rheometer). The first normal stress difference was measured in the cone-and-plate apparatus at low shear rates. For each apparatus there is a lower shear rate limit due to the sensitivity of the load cell or transducer and an upper shear rate limit due to flow instabilities.

The shear viscosity data as a function of shear rate at temperatures of 180 ^{o}C, 190 ^{o}C, and 200 ^{o}C are presented in Figures 4.1, 4.2 and 4.3, respectively. The strong shear thinning nature of these materials is apparent from these figures. Comparison of shear viscosity data of PP-300 MFR with that of remelted web sample prepared from it suggests that significant thermal degradation occured in the screw extruder.

First normal stress difference data as a function of shear rate at temperatures of 180 ^{o}C and 200 ^{o}C are presented in Figures 4.4 and 4.5 respectively. The complete shear viscosity and the first normal stress difference data for various polypropylene melts studied

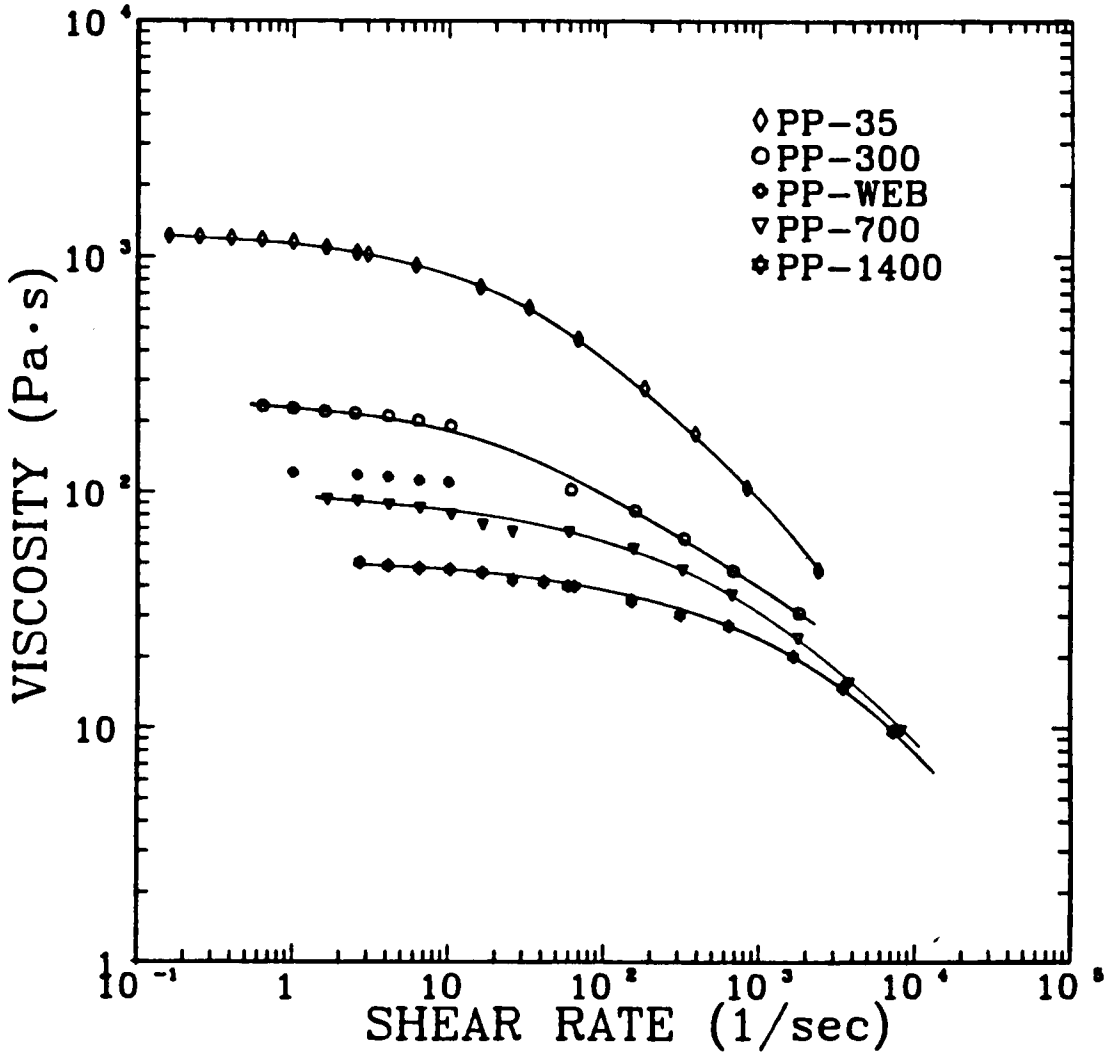


Figure 4.1. Shear viscosity as a function of shear rate for various polypropylene melts at 180 °C.

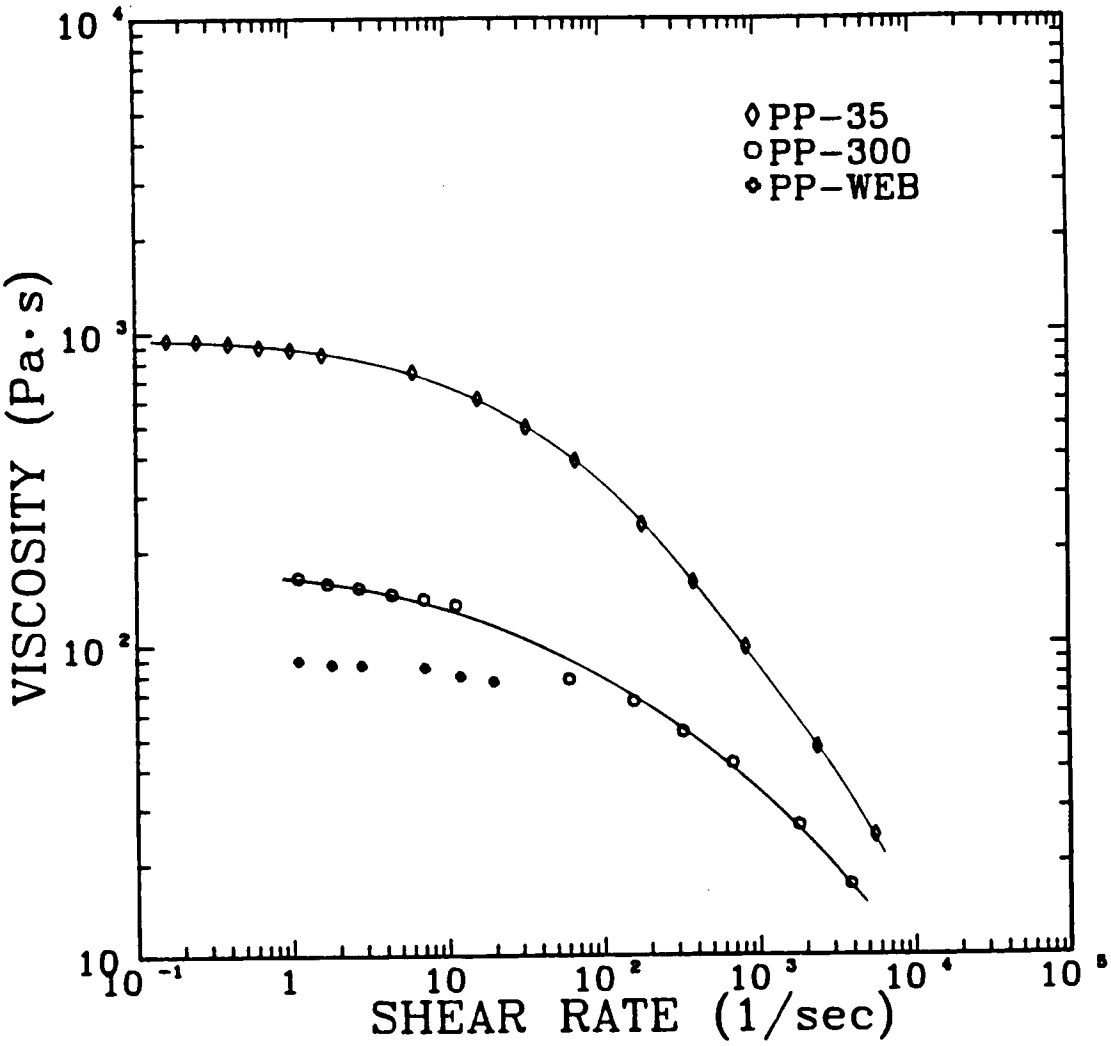


Figure 4.2. Shear viscosity as a function of shear rate for various polypropylene melts at 190 °C.

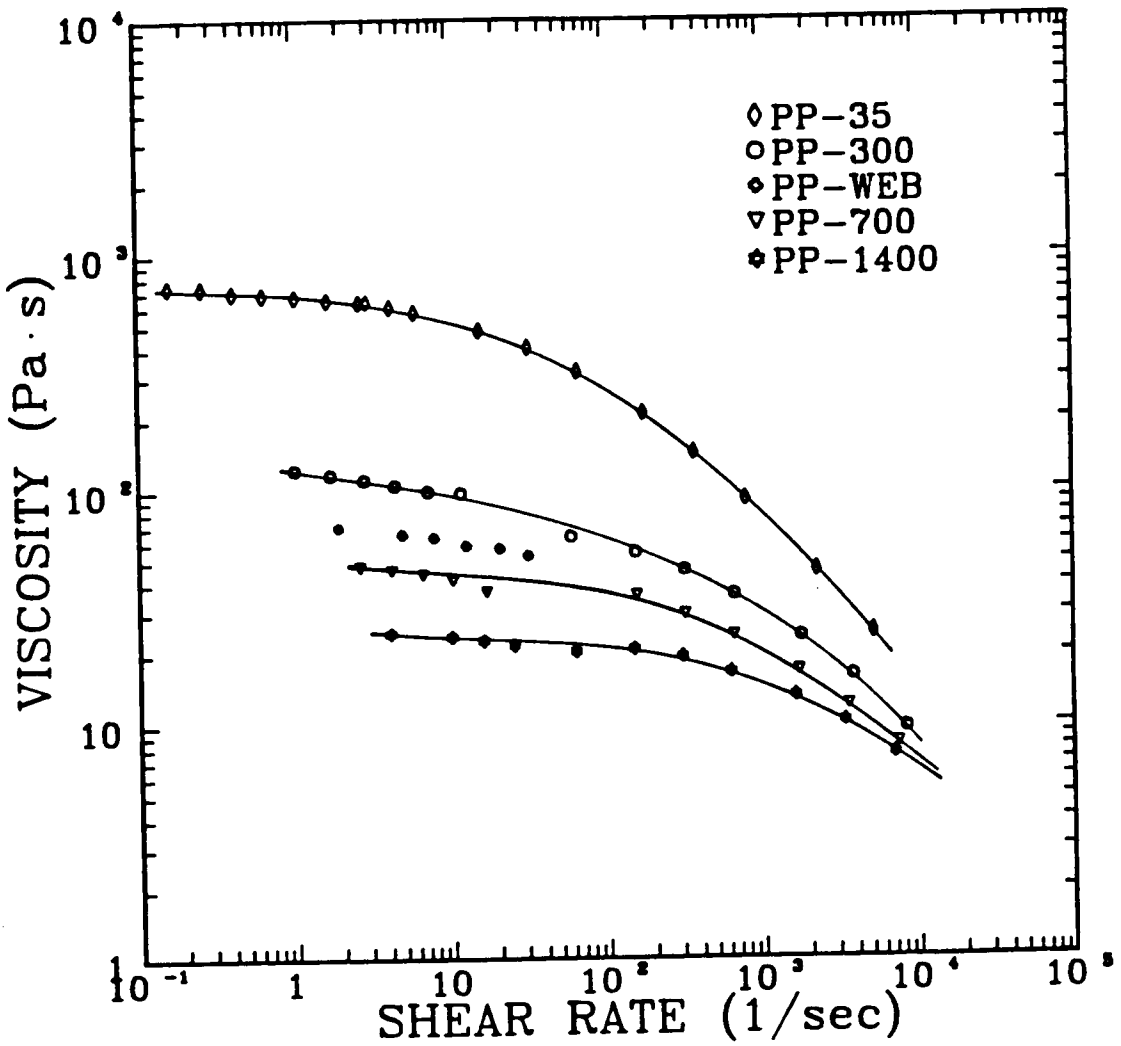


Figure 4.3. Shear viscosity as a function of shear rate for various polypropylene melts at 200 °C.

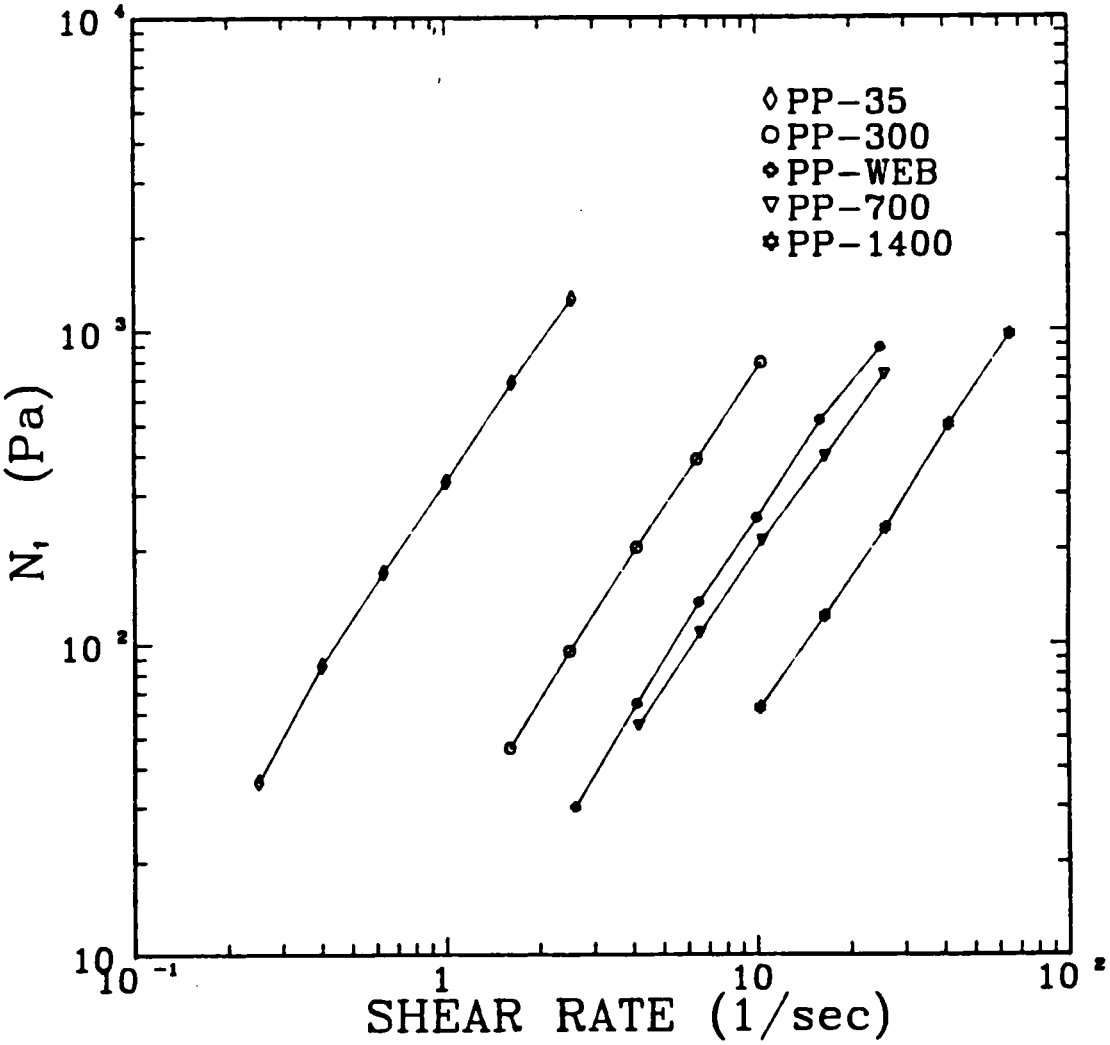


Figure 4.4. First normal stress difference as a function of shear rate for various polypropylene melts at 180 °C.

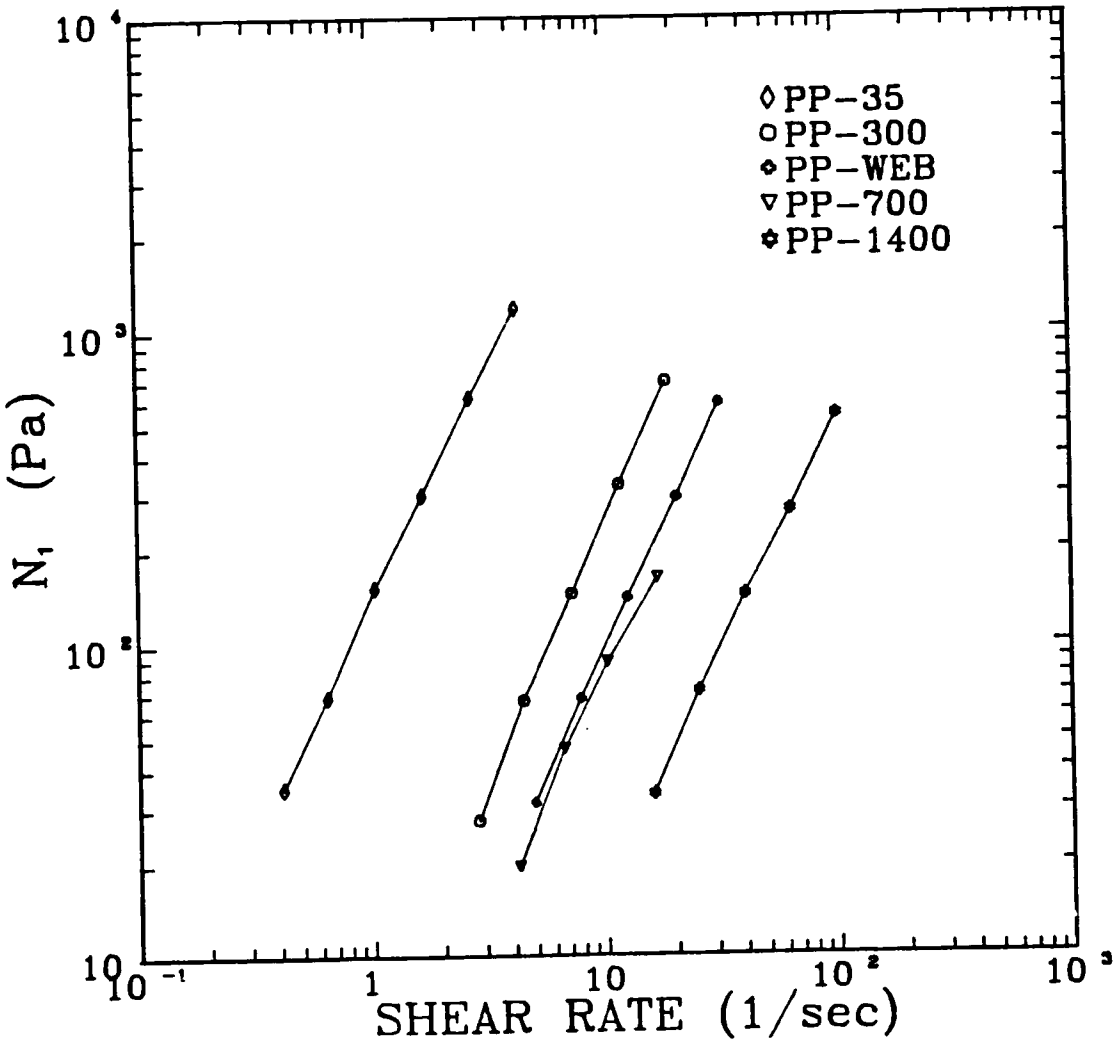


Figure 4.5. First normal stress difference as a function of shear rate for various polypropylene melts at 200 °C.

are tabulated as Appendix-A. The first normal stress difference as a function of shear stress ($N_1(T_{12})$) is independent of temperature for polystyrene as shown by Oda, White and Clark (33). This is supported by data from several investigators. The first normal stress difference as a function of shear rate at three different temperatures for PP-35 MFR is shown in Figure 4.6. When the same data of first normal stress difference are plotted as a function of shear stress, the data fall on a straight line independent of temperature, as shown in Figure 4.7. Oda, White and Clark argued that the slope of this line is only a function of the molecular weight distribution and not the molecular weight. To better represent the variation of the first normal stress difference, we may utilize the empirical power-law relation $N_1 = a\sigma_{12}^{b}$.

The first normal stress difference coefficient ($\Psi_1 = N_1/\dot{\gamma}^2$) can also be computed from these first normal stress difference data and is presented in Figure 4.8 as a function of shear rate for three typical materials at 180 ^{o}C. It can be observed that Ψ_1 is a stronger decreasing function of shear rate than shear viscosity. It is apparent from the Figure 4.8 that Ψ_1 has not reached its Newtonian constant value at the lowest measurable first normal stress difference. The extrapolation of these data to obtain accurate values of zero shear first normal stress difference coefficient ($\Psi_{1(0)}$) would be subjective. The ratio of zero shear first normal stress difference coefficient to zero shear viscosity would give an average value of a zero shear relaxation time. The effective relaxation time (τ) as defined by eq. [2.2.3] is also obtained from

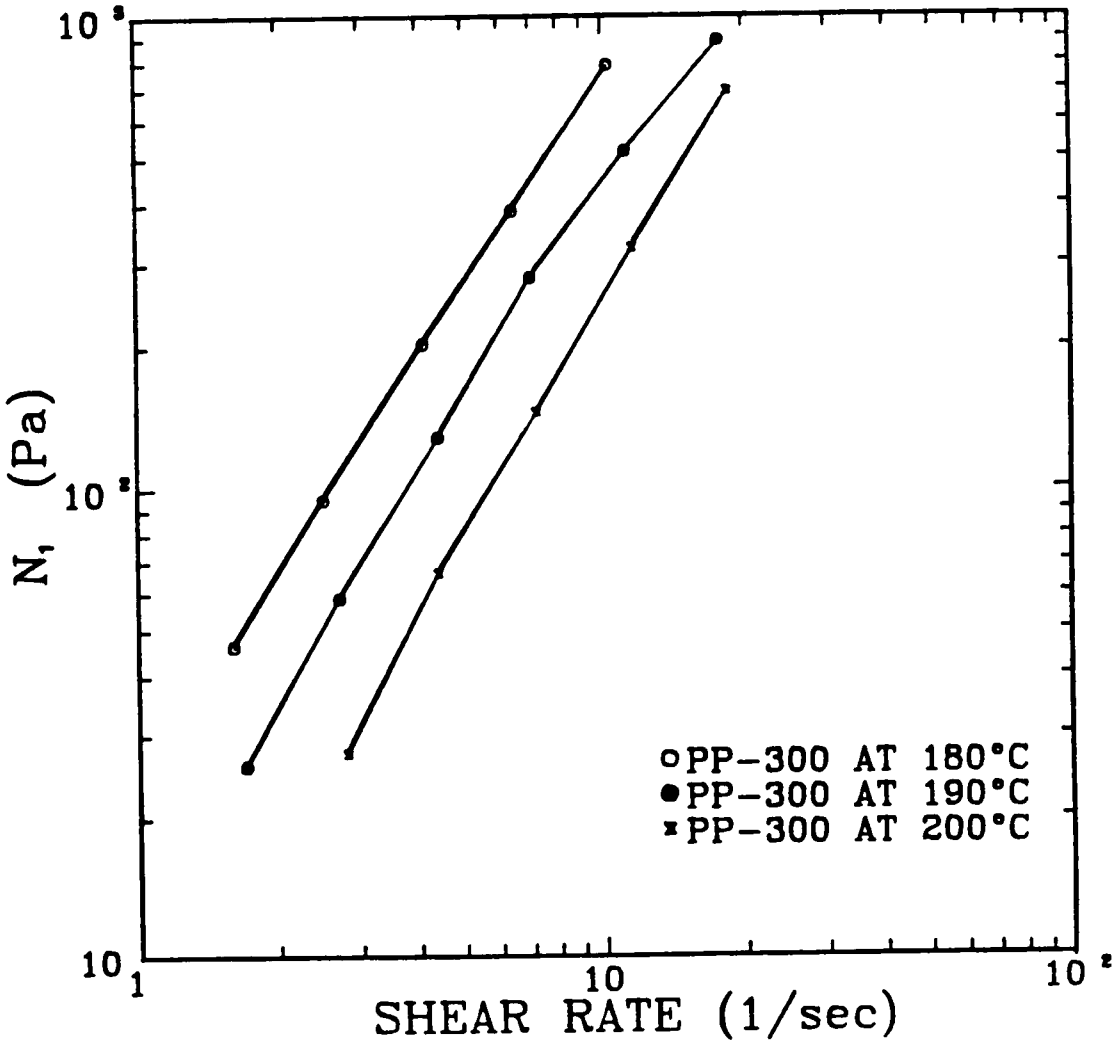


Figure 4.6. First normal stress difference as a function of shear rate for PP-300 MFR at three temperatures.

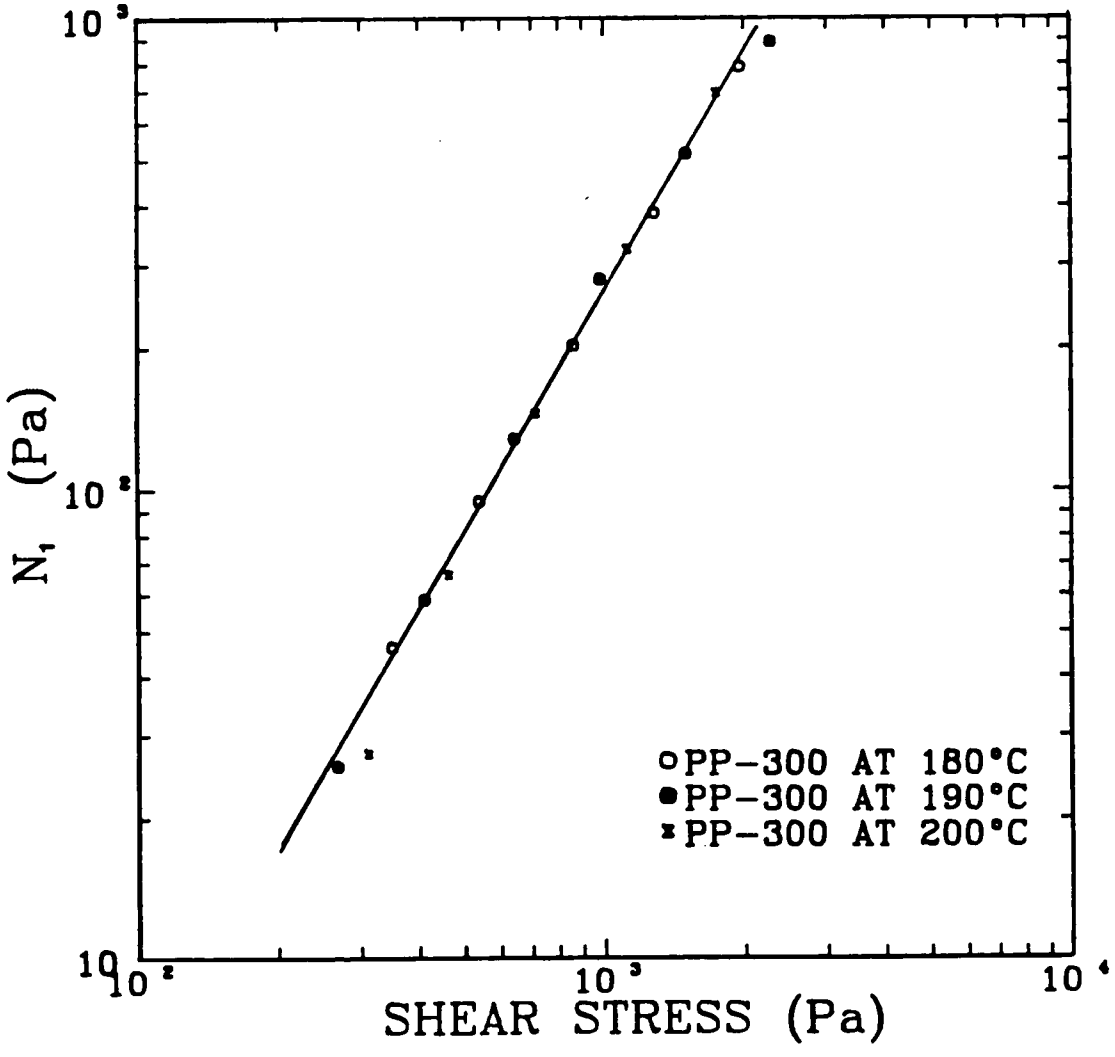


Figure 4.7. First normal stress difference as a function of shear stress for PP-300 MFR for data at three temperatures.

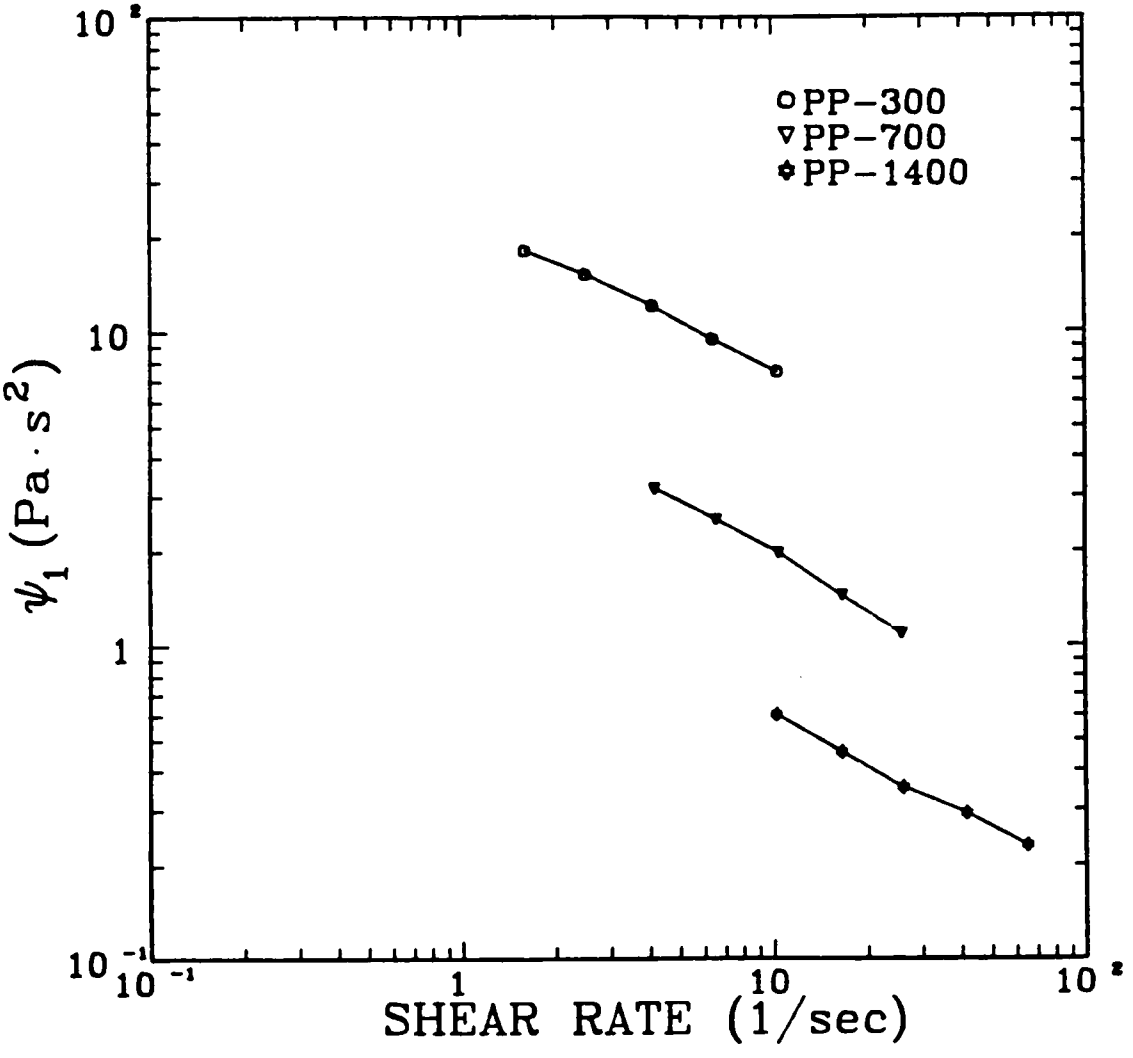


Figure 4.8. First normal stress difference coefficient as a function of shear rate at 180 °C.

the data of the first normal stress difference and the shear viscosity. Hence, the first normal stress difference data in simple shear are quite important to obtain. The effective relaxation time data at a temperature of 180 ^{o}C are shown for the three materials in Figure 4.9. The zero shear relative relaxation time can also be obtained from extrapolation of these data. From Figure 4.9, it is apparent that extrapolation to zero shear would be highly subjective.

The shear viscosity data of a given polymer at different temperatures can be superimposed to obtain master curve by the time-temperature superposition method. The temperature at 180 ^{o}C was chosen as the reference temperature. The master curves for various materials studied are shown in Figure 4.10. The shift factors were calculated using eq. [2.2.5]. The extrapolated zero shear viscosity and the shift factors data for all the materials at the different temperatures are tabulated as Table IV.I. The shift factors (a_T) as a function of the reciprocal of temperature is shown in Figure 4.11. From the slope of this plot, an average energy of activation for flow for the materials studied can be computed using eq. [2.2.5]. The average activation energy for the materials studied is 12.9 Kcal/gmole.

There is an empirical relationship for polymer melts between molecular weight and the zero shear viscosity (η_o); that is, the zero shear viscosity is proportional to some power (often quoted as about 3.5 (45)) of the weight average molecular weight (M_w) above a critical molecular weight. The zero shear viscosity for all materials studied as a function of weight average molecular weight is

Table IV.I :- The zero-shear viscosities and the shift factors at different temperatures for the materials studied.

Temperature ^{o}C	PP-35	PP-300	PP-WEB	PP-700	PP-1400
	η_o (Pa-s)				
180	1250	235	125	95	51
190	950	170	92	-	-
200	740	125	71	49	26
	a_T				
180	1.0	1.0	1.0	1.0	1.0
190	0.76	0.723	0.736	-	-
200	0.592	0.532	0.568	0.516	0.51

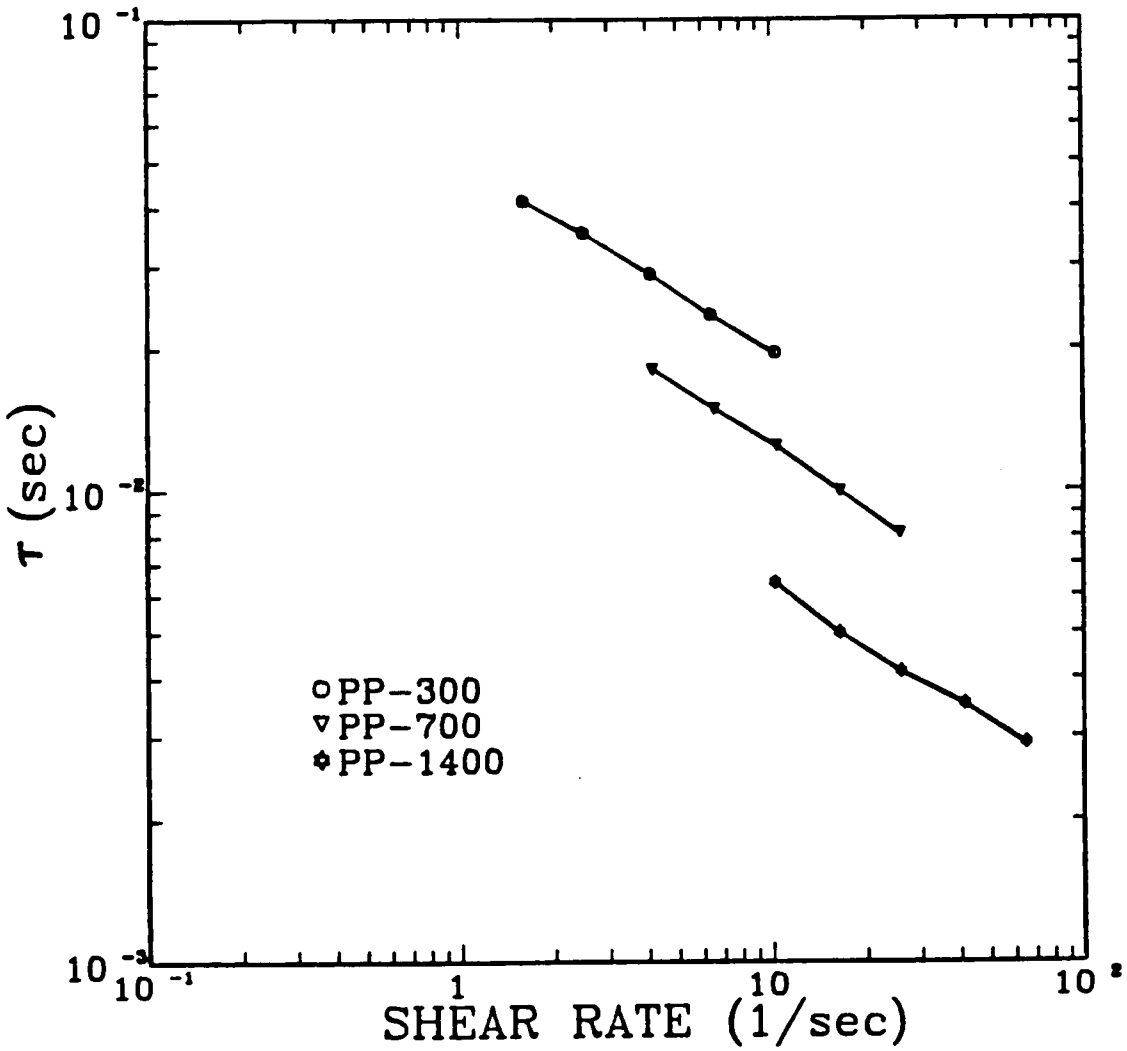


Figure 4.9. Effective relaxation times in shear at 180 °C.

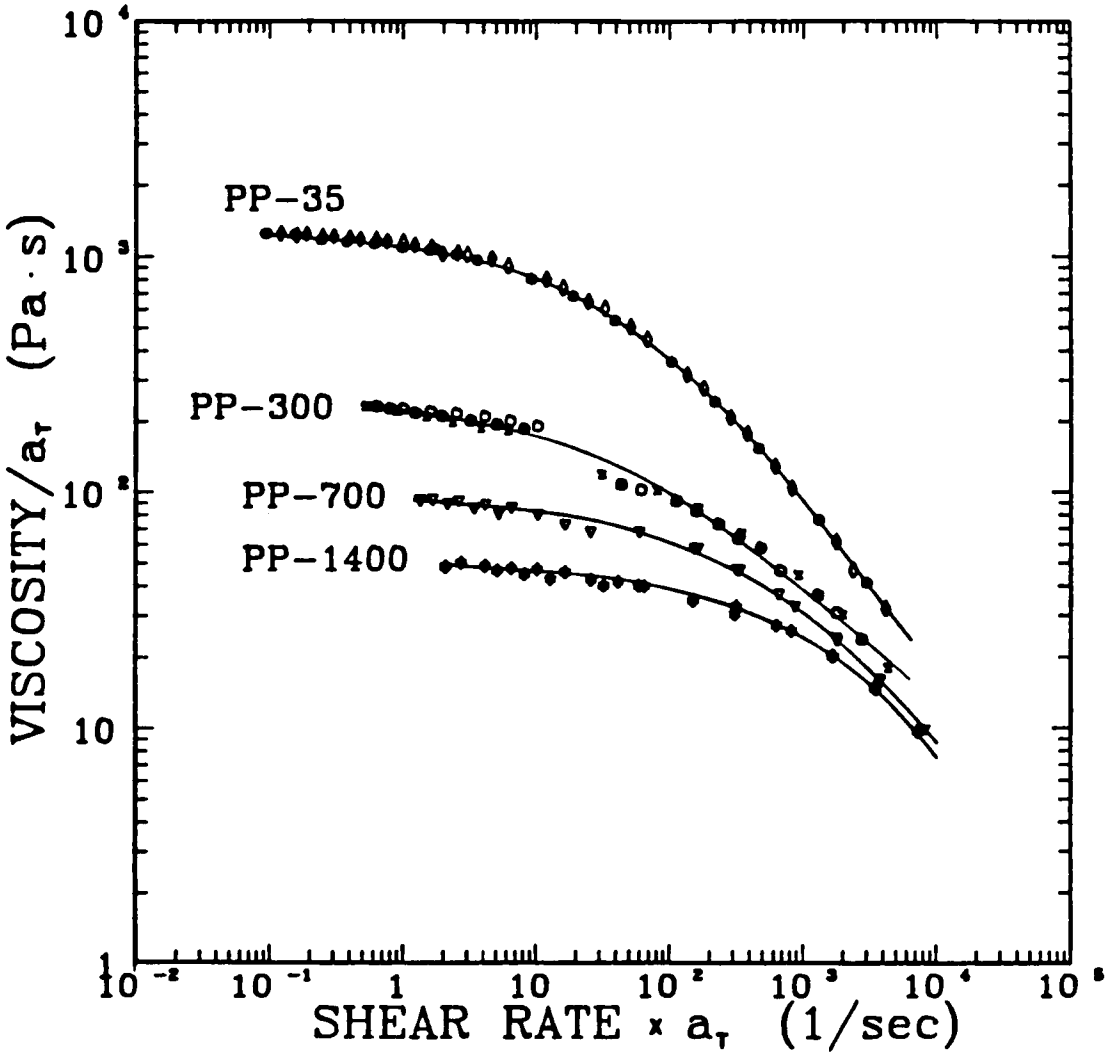


Figure 4.10. Master curves obtained from the data of Figures 4.1, 4.2 and 4.3. Reference Temperature = 180 °C.

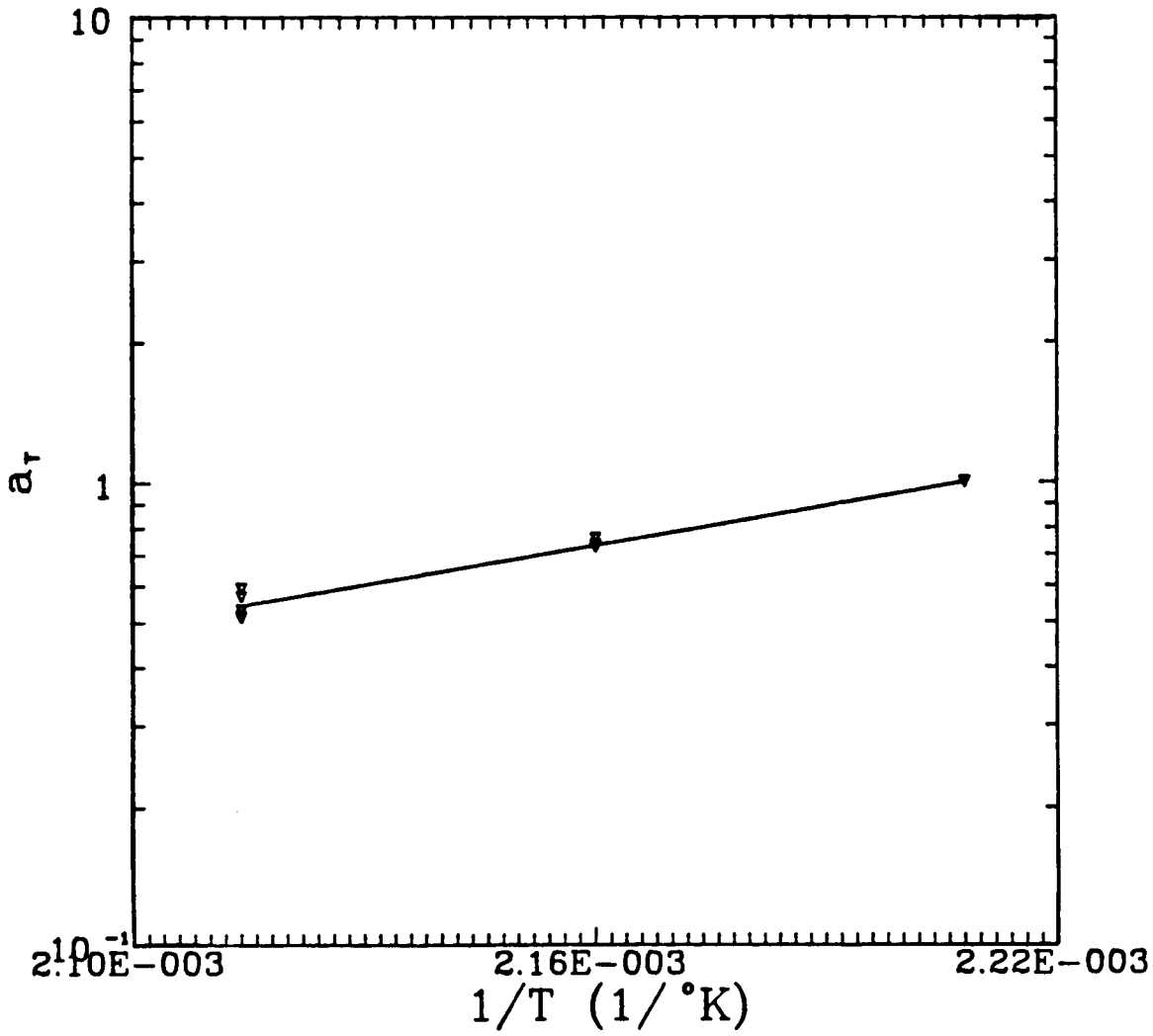


Figure 4.11. Shift factors (a_T) as a function of reciprocal of absolute temperature.

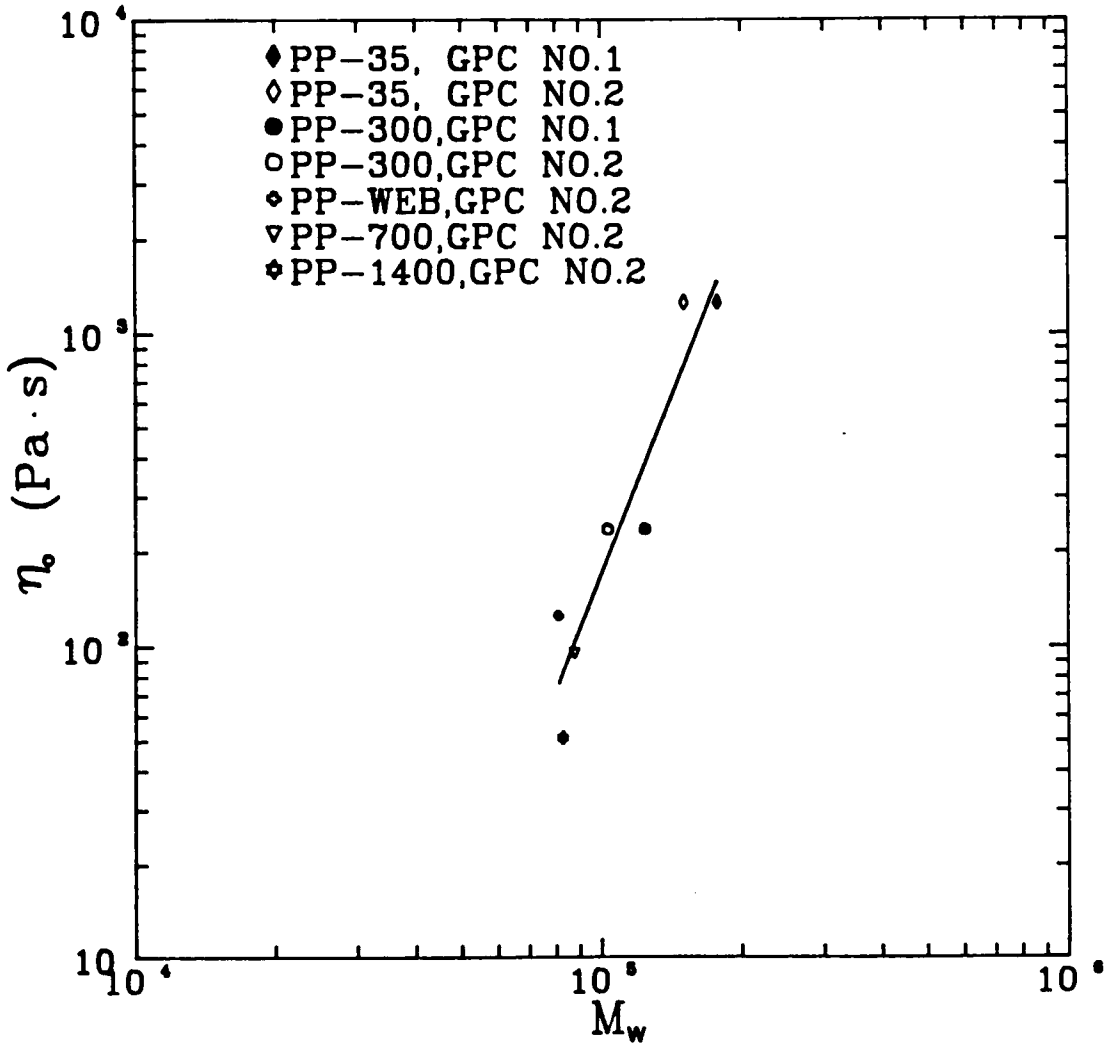


Figure 4.12. Zero-shear viscosities at 180 °C as a function of weight average molecular weight.

shown in Figure 4.12. The weight average molecular weights data were obtained from GPC curves provided by Exxon Chemical Company. The slope of the line is 3.75, which is close to the value of 3.5-3.6 generally reported in the literature.

CHAPTER 5

PRESENTATION OF ELONGATIONAL FLOW DATA

In this chapter the apparent elongational viscosities measured by isothermal gravity spinning experiments will be discussed. The stability of isothermal spinline will also be discussed semi-quantitatively. First, theoretical predictions for Newtonian gravity spinning will be discussed, which will depict salient features of gravity spinning and provide a base case for comparing gravity spinning results for the polymers studied.

5.1 Theoretical Analysis of Newtonian Gravity Spinning

The second order differential equation (see eq. [2.2.11]) for gravity spinning of a Newtonian fluid can be solved numerically using the fourth-order Runge-Kutta method to predict the velocities and elongation rates along the spinline. The initial velocity (U_o) provides one of the two boundary conditions and its value is computed at the point of maximum die-swell diameter obtained experimentally for a given material under specified conditions. The other boundary condition for gravity spinning is zero force (or stress) at the end of the spinline. For Newtonian fluids, this is equivalent to a zero elongation rate at the end of the spinline. The numerical solution requires trial and error: one guesses at the elongation rate at X=0 such that the required boundary condition of zero elongation rate at the end of a spinline of specified length is satisfied. The computer

program for solving this second-order differential equation for Newtonian gravity spinning on an IBM PC is given in Appendix B-1. The program was run using MS FORTRAN compiler on the IBM PC using Wiley scientific subroutine library. The results of this simulation will now be presented.

The velocity profile, the elongation rate, and the stress predicted along the spinline for Newtonian gravity spinning of three Newtonian fluids with viscosities of 235 Pa-s, 95 Pa-s and 51 Pa-s with spinline length of 15.7, 15.52 and 8.83 cm. respectively, are shown as Figures 5.1, 5.2 and 5.3. These viscosities correspond to the zero-shear Newtonian viscosities of PP-300, PP-700 and PP-1400 MFR, respectively at 180 ^{o}C. Note that for the purpose of later comparison, the value of initial velocity is computed at the point of maximum die-swell diameter which is obtained experimentally for a given polymer under the same conditions. Observe that the predicted velocity profiles are sigmodial in shape and the elongation rate (E) and the stress profile go through a maximum along the spinline. In gravity spinning, the force along the spinline decreases continuously to zero. But, initially, the cross-sectional area decreases faster than the force and hence, the stress profile along the spinline goes through a maximum. As the spinline length decreases, this maximum shifts towards the die. The above analysis assumes a stable spinline. As the length of the spinline increases the draw ratio ($DR=U_L/U_o$) increases. The stability analysis for Newtonian gravity spinning predicts that at a critical draw ratio, spinline goes into

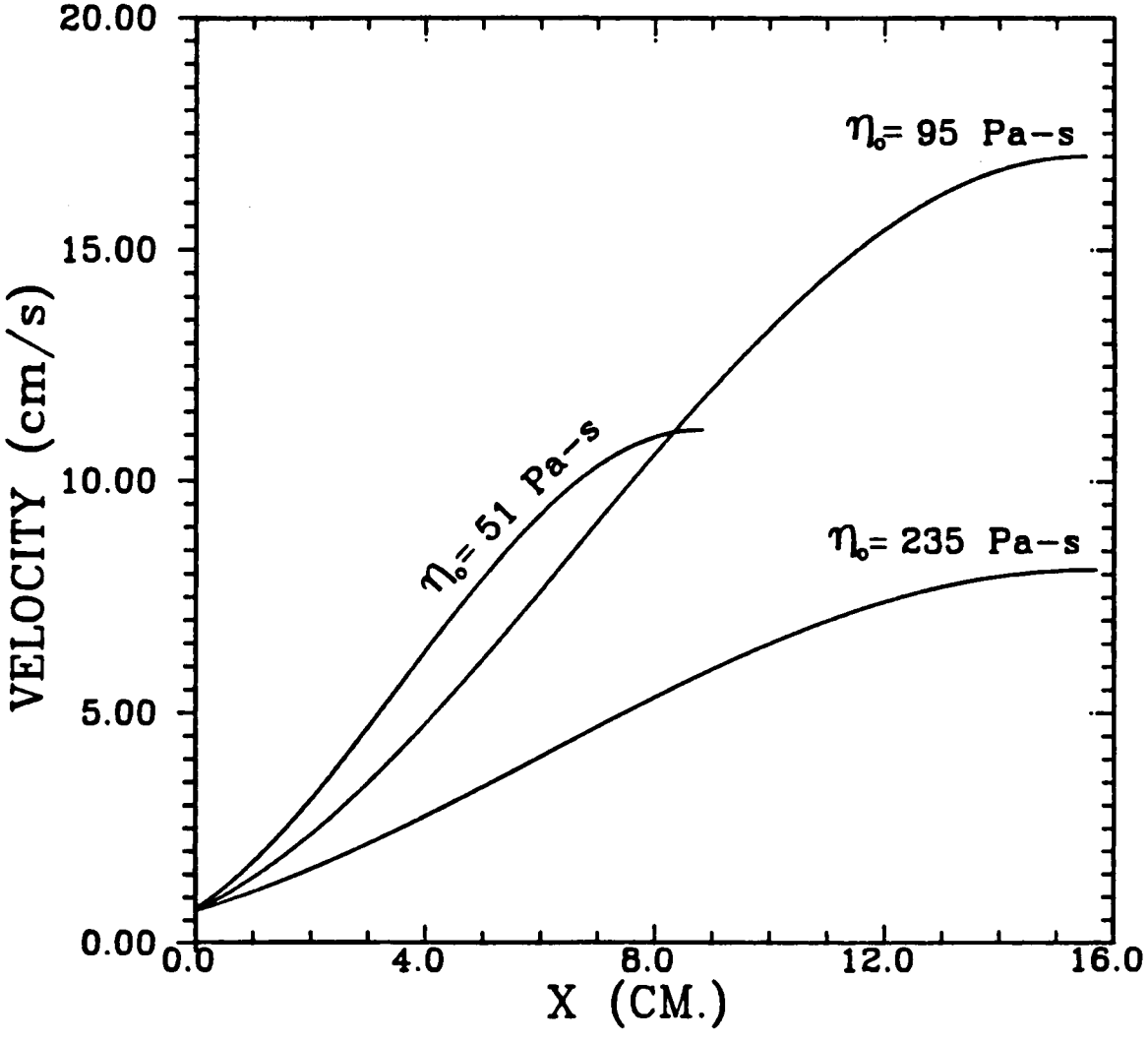


Figure 5.1. Theoretical prediction of the velocity profiles along the spinline for gravity spinning of Newtonian fluids.

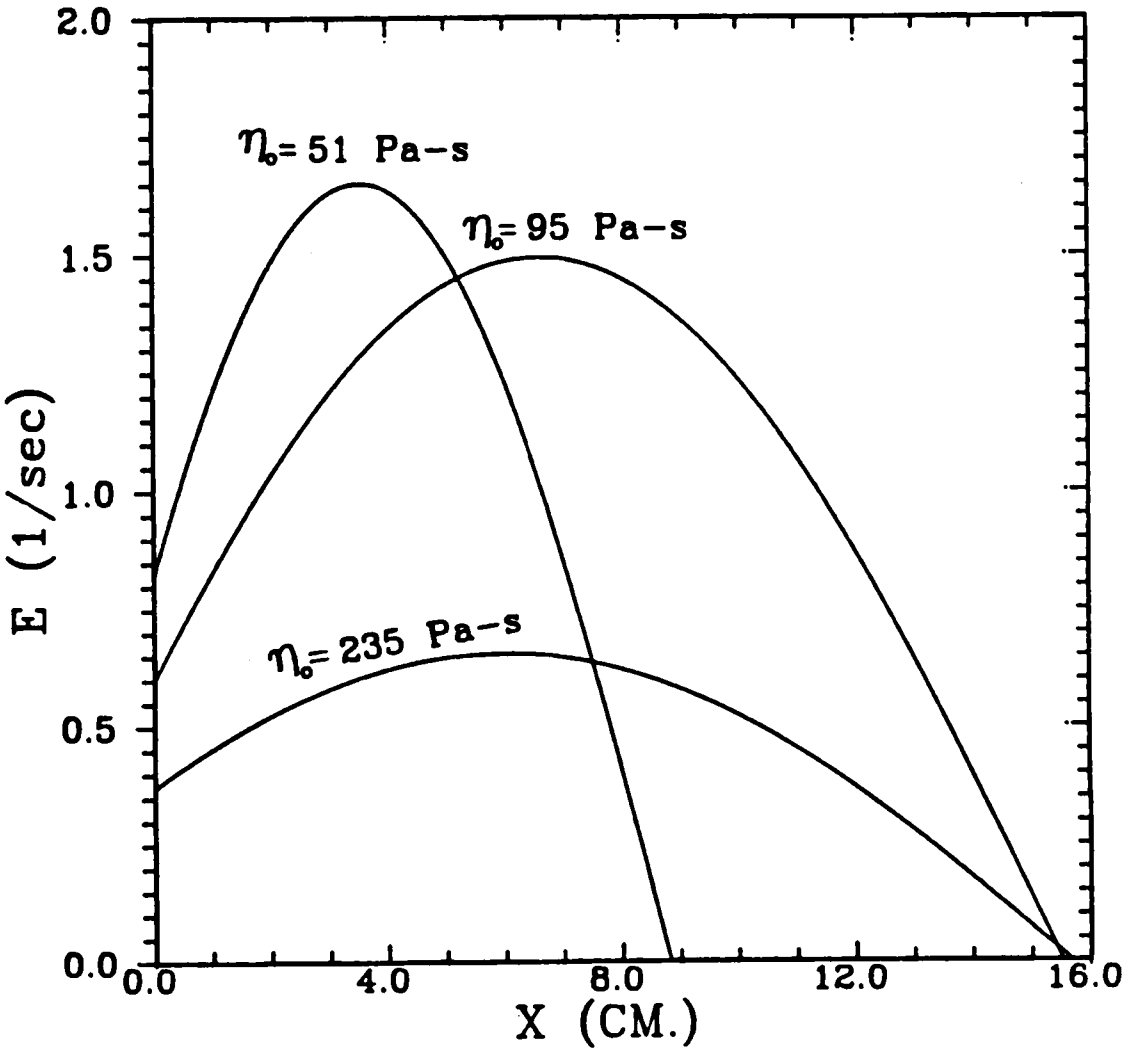


Figure 5.2. Theoretical prediction of the elongation rate profiles along the spinline for Newtonian gravity spinning.

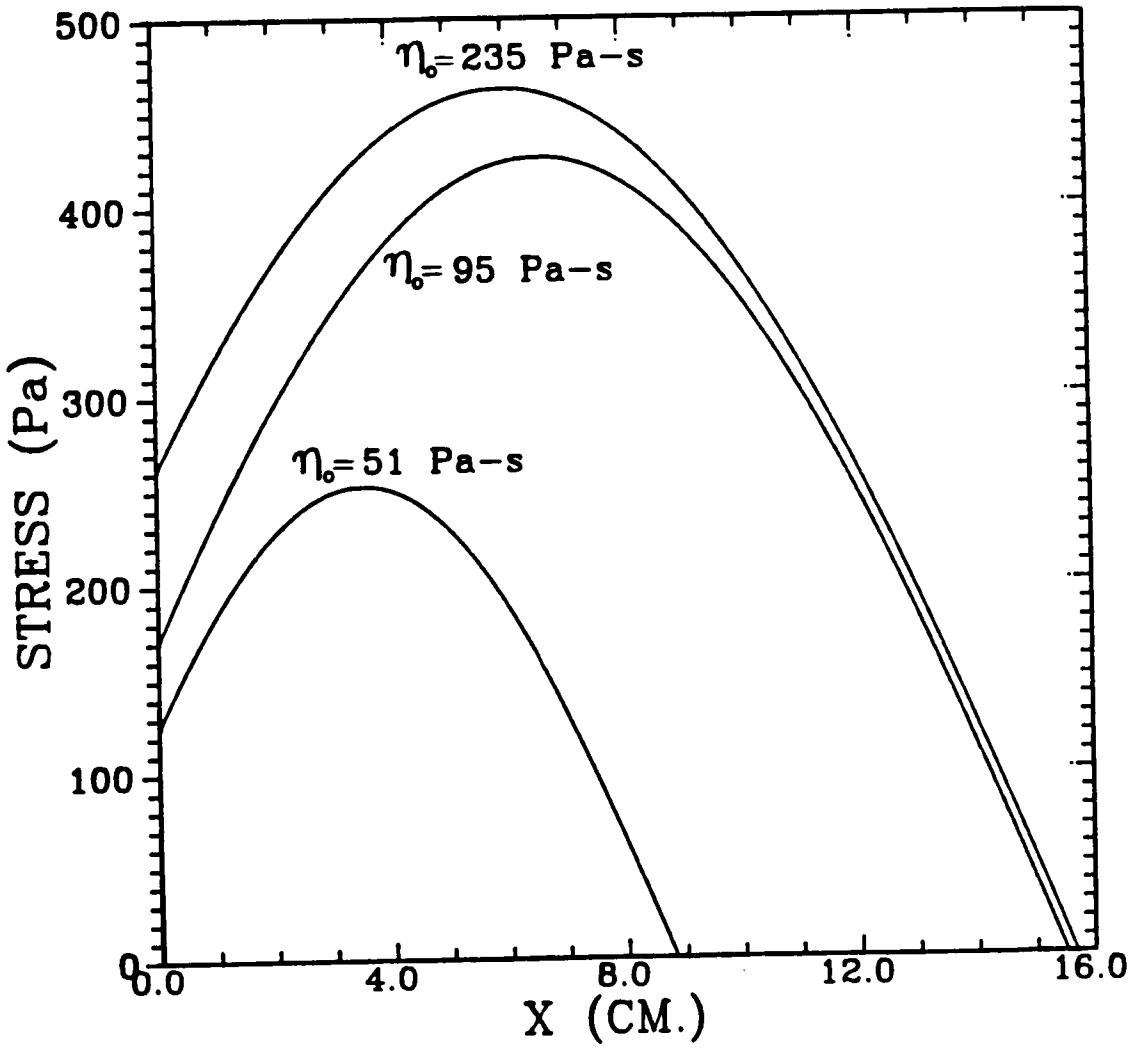


Figure 5.3. Theoretical prediction of the stress profiles along the spinline for Newtonian gravity spinning.

draw resonance, a kind of instability in which periodic variations in diameter occur in the spinline (62,63).

The maximum in stress and elongation rate profile leads to interesting results for gravity spinning of polymer melts as they have finite (but fading) memory and the deformation history becomes important, as will be discussed in the next section.

5.2 Experimental Results

Diameter profile data : Because of all the difficulties mentioned in the experimental section, many attempts to measure diameter profile were unsuccessful due to either breakage of the spinline or to poor slides caused by vibrations of the spinline. Some of the runs had to be discarded because of higher than the required take-up speeds were used, which caused an external take-up forces. Under some conditions, unstable spinline were seen as a result of draw resonance. Those runs with unstable spinline will be discussed later. The most satisfactory diameter data for the stable gravity spinline will now be presented for the various materials studied.

Profiles of the thread diameter measured for PP-300, PP-700 and PP-1400 MFR at 180 ^{0}C (using the photographic technique) are shown in Figure 5.4 and for PP-300 MFR at two different temperatures (180 ^{o}C and 200 ^{o}C) are shown in Figure 5.5. The superposition of diameter profiles for different runs indicates reproducibility of diameter profile data. These diameter profiles have to be differentiated to

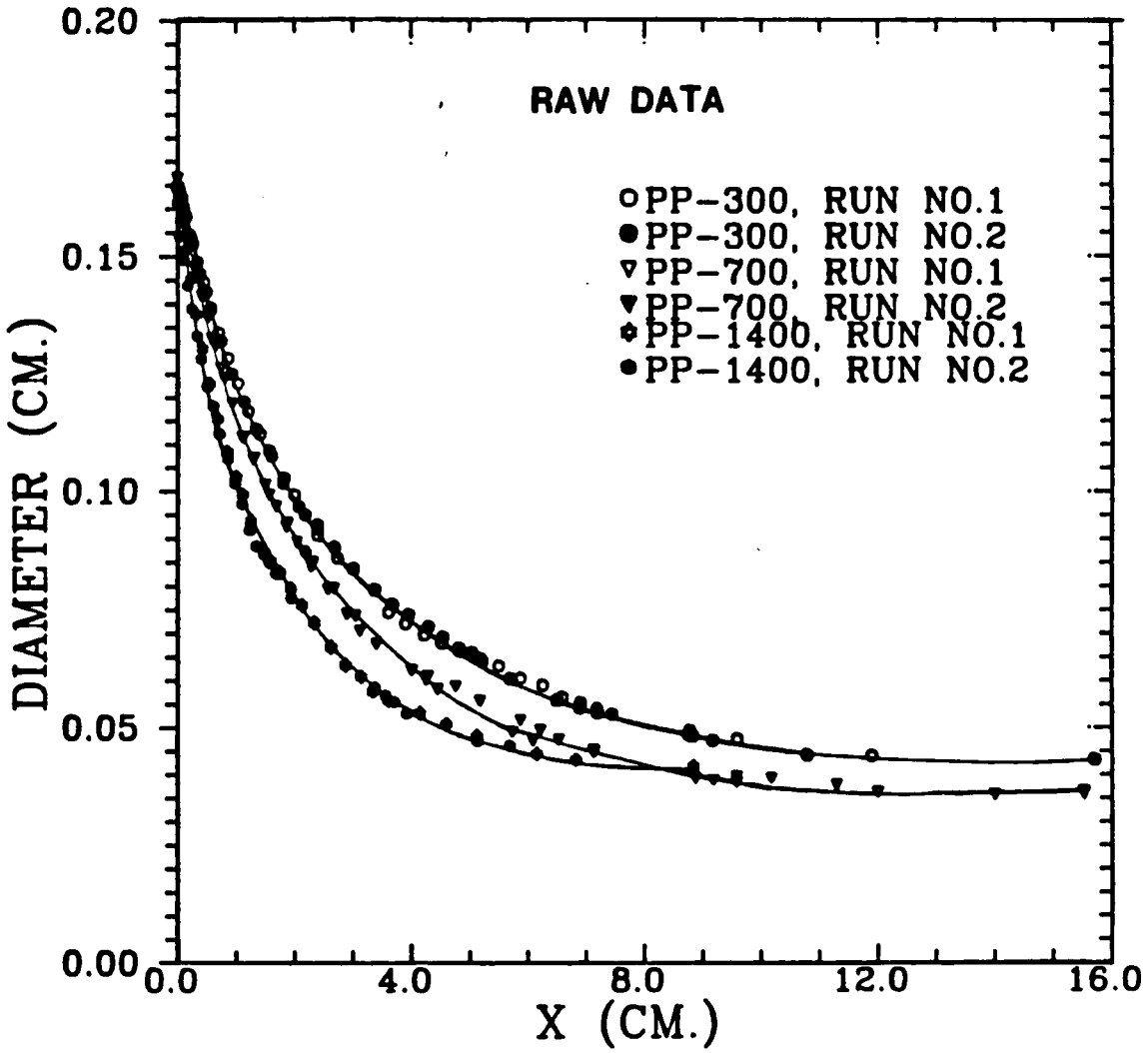


Figure 5.4. Profiles of the thread diameter for various polypropylene melts studied at 180 °C.

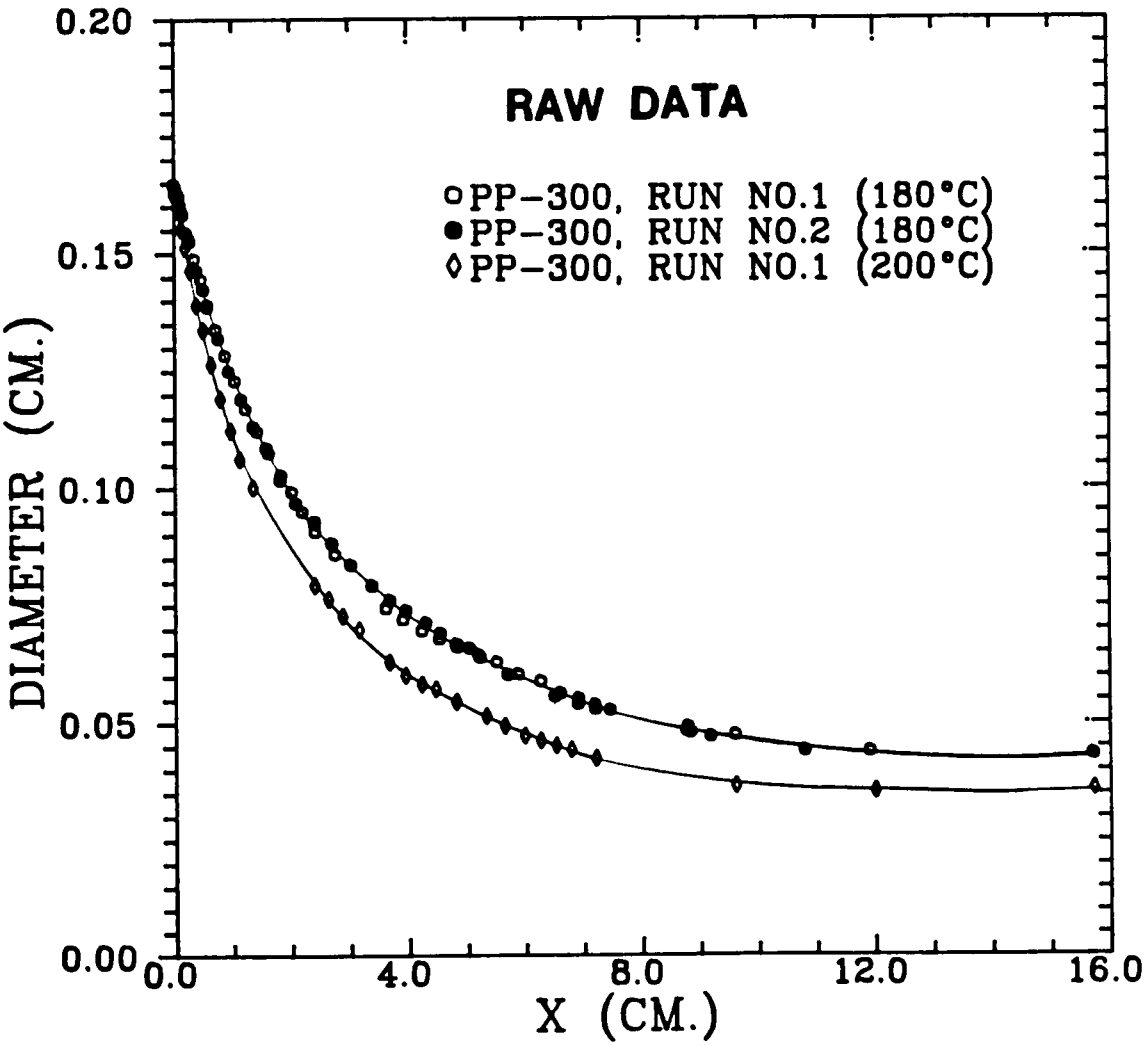


Figure 5.5. Profiles of thread diameter for PP-300 MFR at 180 °C and 200 °C.

obtain elongation rate (E) along the spinline. The measurement of diameter needs to be done with great care, especially since the data will have to be differentiated to obtain the strain rate as a function of distance along the thread. A choice here is whether to smooth the data, for example by fitting a polynomial or not. The values of elongation rate ($E = dV/dX = - 8Q/\pi D^3 * dD/dX$) are very sensitive to the accuracy with which the diameter profile is measured as the gradient of it has to be computed and elongation rate varies with the third power of diameter. In this regard, there has perhaps not been enough attention given in the literature on spinning to the very difficult problem of obtaining accurate filament diameter measurements (64). Note also that most of the diameter change occurs in first 35-40% of the spinline due to the inherent kinematics of gravity spinning resulting from gravity force, which decreases rapidly along the spinline to zero at the end of the spinline. Thus, the diameter change in the lower half of spinline is very small, resulting in lower elongation rates. This coupled with the difficulty of obtaining sharp slides of the lower half of spinline as noted in the experimental section makes it very difficult to obtain accurate measurements of diameter data in the second half of the spinline. These difficulties and some random fluctuations in the throughput rates lead to some scatter in diameter data, especially in the lower half. For these several reasons, data smoothing of some sort was necessary.

A polynomial curve fitting of actual diameter versus axial distance data gave apparently good fits, except towards the end of

the spinline as shown in Figure 5.6. However, these fits resulted in erroneous values for the elongation rates along the spinline, as shown in Figure 5.7. Instead, a polynomial curve fitting of (1/D) versus axial distance data for all the runs gave proper fits and reasonable values of elongation rates. The probable reason for getting such good overall fits is that the small diameters and the small diameter changes in the bottom half of the spinline are magnified by taking the inverse. The polynomial curve fittings of (1/D) versus axial distance data for the runs at 180 ^{o}C are shown in Figure 5.8. The profiles of elongation rates along the spinline obtained for all the runs will be shown in Figure 5.9. Note that as the velocity is proportional to $(1/D)^2$, this procedure is a way of fitting the velocity profile with the equivalent of a higher degree polynomial. The choice of the order of the polynomial would depend upon the data set. The order should be high enough to pick up the trends in a data set, giving an average result without following the scatter in detail. There is a statistical procedure whereby one may test successively increasing orders of polynomials until one reaches a non-significant result (65). Also judgement based on experience and theoretical grounds can lead to the correct choice of the order of the polynomial. In the case of fitting (1/D) versus axial distance data, a minimum of a second degree polynomial would have to be used to give the maximum in the elongation rate profile. Polynomial curve fitting with degree ranging from three to five were used here to smooth the data sets. The correlation coefficient of more than 0.9995 was achieved for all of the curve fittings.

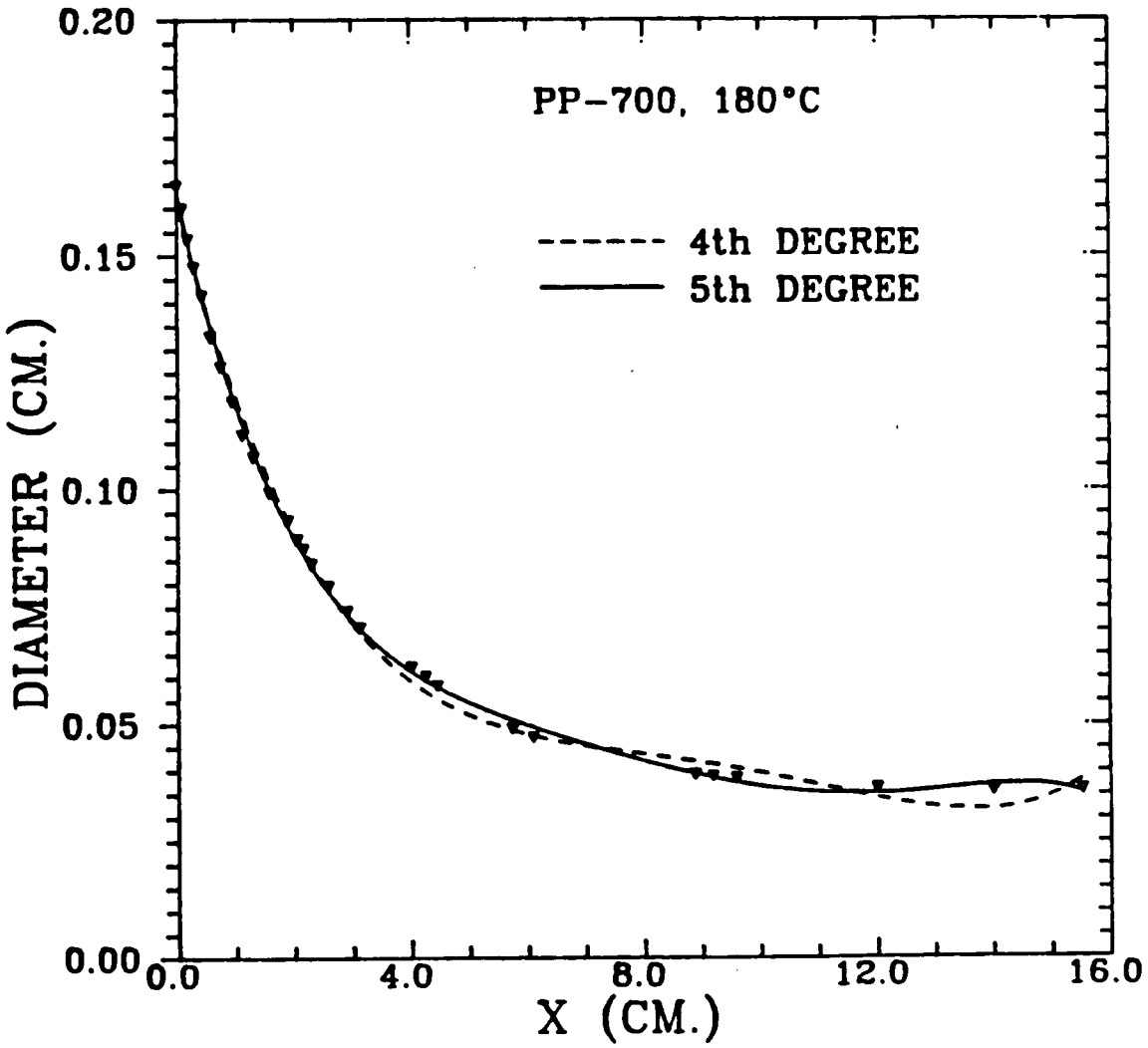


Figure 5.6. Polynomial curve fittings of diameter versus distance data.

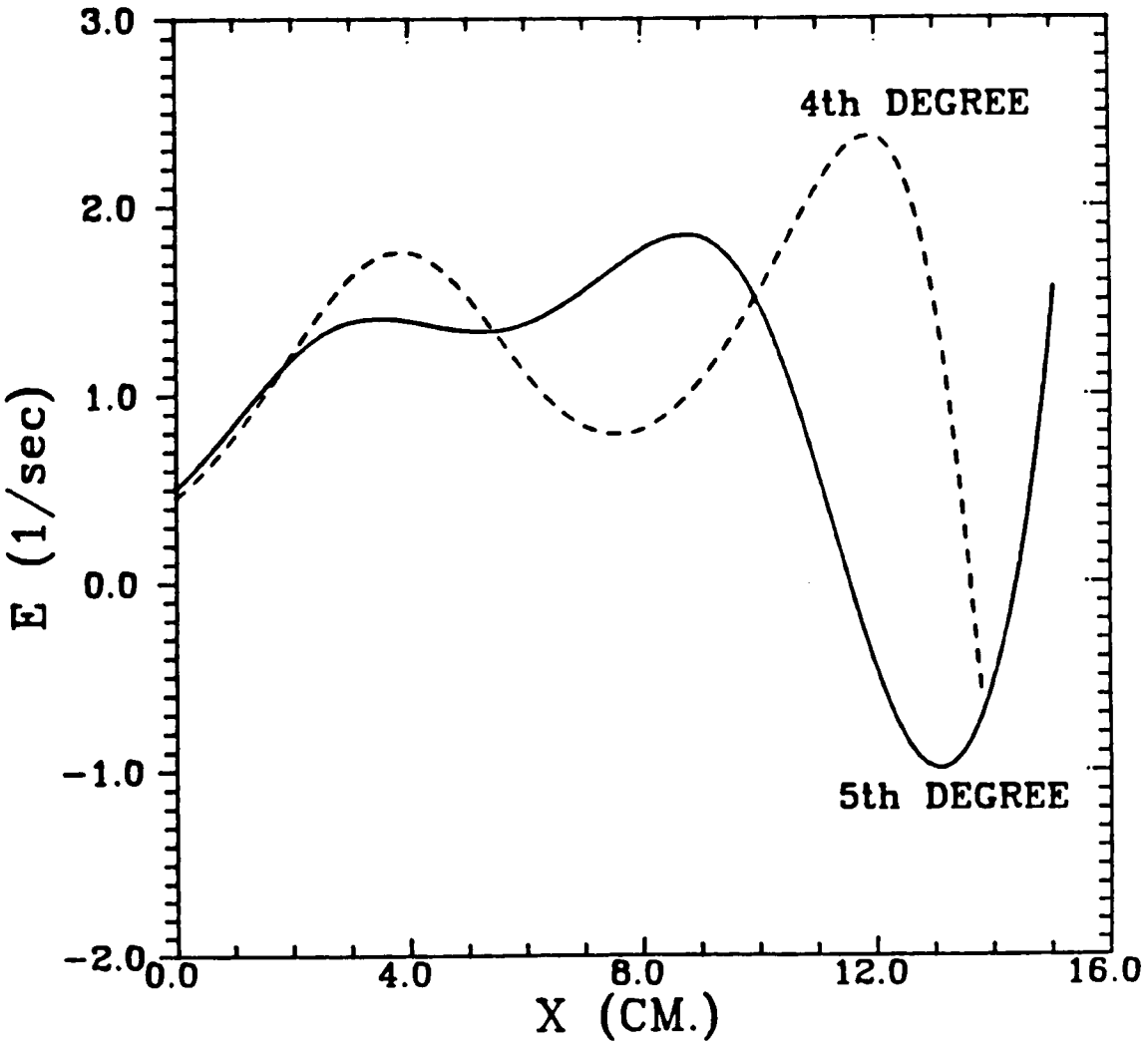


Figure 5.7. Elongation rates along the spinline, computed using polynomial curve fitting of diameter versus distance data of Figure 5.6.

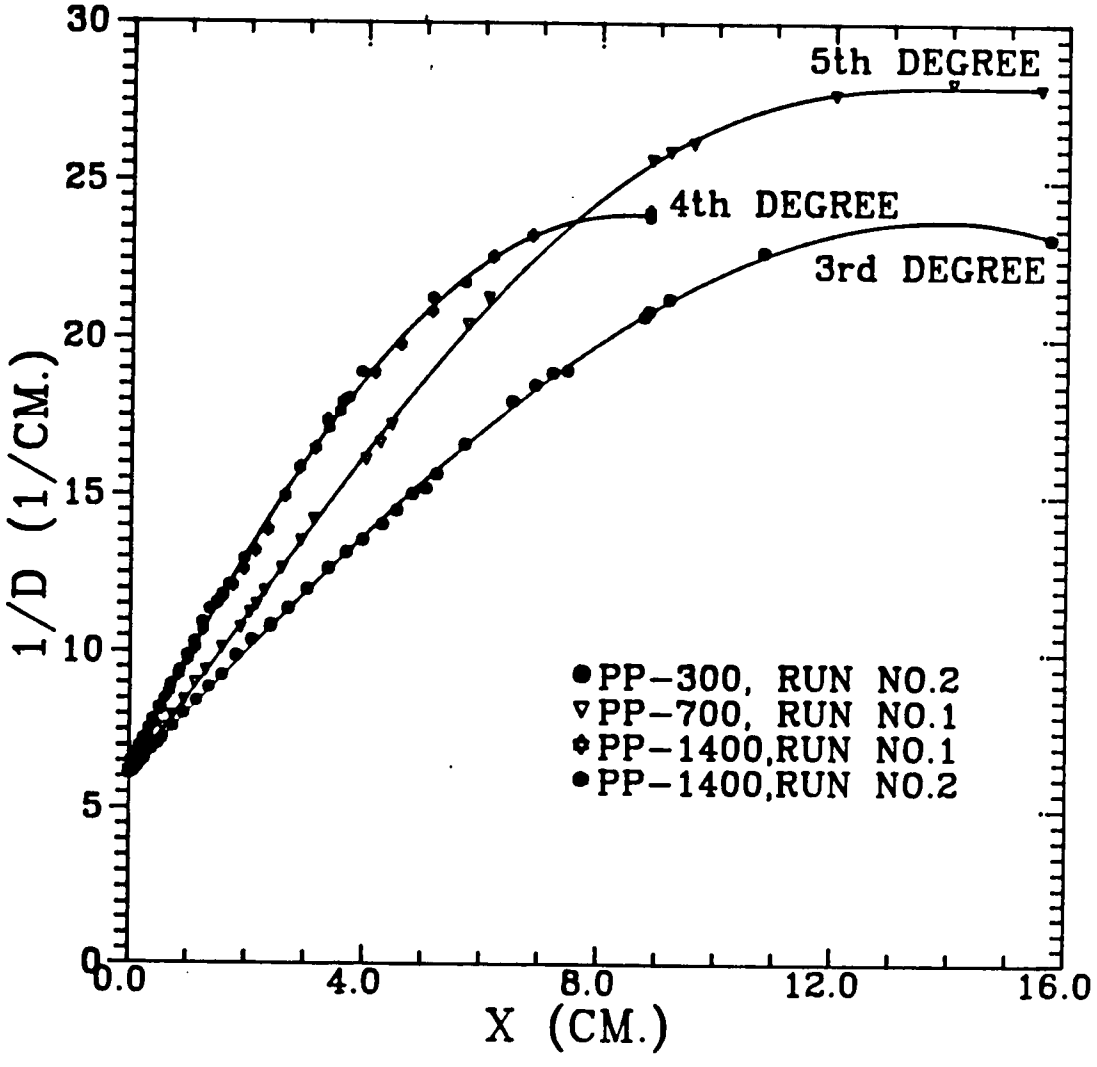


Figure 5.8. The polynomial curve fitting of (1/D) versus distance data for various polypropylenes melts at 180 °C.

Computation of elongation rates, stresses and the apparent elongational viscosity : Once a fitted polynomial is obtained using any suitable statistical package, it can be used to compute elongation rates and the apparent elongational viscosities along the spinline. The elongation rates (E) are computed from differentiating the polynomial curve fitting equation (e.g of fourth degree) as follows:

$$1/D = A + Bx + Cx^2 + Dx^3 + Ex^4$$

$$dD/dx = - D^2 (B + 2Cx + 3Dx^2 + 4Ex^3) \qquad [5.2.1]$$

$$dV/dx = - \frac{8Q}{\pi D^3} \frac{dD}{dx}$$

The stress acting on any cross-section of the thread is obtained from the weight of the hanging spinline below that section which is calculated from integration of diameter profile as shown below :

$$F(x) = \pi g \rho /4 \int_X^L D(x)^2 \, dx \qquad [5.2.2]$$

and

$$\sigma_{11}(x) = 4F(x)/\pi D(x)^2$$

The inertial forces are very small and are neglected in the force balance equation. The forces due to air drag and the surface tension are also neglected in the force balance equation. Hence, the rheological force at any point in the spinline is equal to the gravity force at that point.

After computing elongation rate and stress profile along the spinline, the instantaneous stress/deformation rate ratio can be computed, but as this ratio will depend upon both the deformation rate and history; it is not a parameter of the material which has any fundamental significance. This ratio is termed as the apparent elongational viscosity :

$$\eta_{eapp} = \sigma_{11}(x)/E(x) \qquad [5.2.3]$$

Despite its variable nature, the apparent elongational viscosity represents a convenient comparative parameter in practice, and it is instructive to present results in this format with the understanding that it is a history-dependent and unsteady-state parameter.

The computer program for carrying out computations of elongation rate, stress and the apparent elongational viscosity along the spinline for the fourth degree polynomial curve-fitting is given in Appendix B-2. It is written in Microsoft Advanced BASIC and can be run using Turbo BASIC (or QBASIC) compiler. The integration of diameter profile is carried out numerically by Simpson's rule. The program also calculates the residence time of a fluid element in the

spinline. The results of these computations for different materials studied will now be presented.

The plots of elongation rate and stress profile along the spinline and the plot of apparent elongational viscosities as a function of elongation rate for PP-300, PP-700 and PP-1400 MFR at 180 ^{o}C are shown in Figures 5.9, 5.10 and 5.11, respectively. The elongation rate and the stress profile go through a maximum like Newtonian gravity spinning. As mentioned before, elongation rates towards the end of the spinline were very difficult to measure accurately; and hence are not shown in the figure 5.9. The diameter data and the approximate values of the elongation rates near the end of the spinline do suggest that the elongation rates near the end of the spinline go through a zero and become actually negative (i.e. the velocity is decreasing because of a "swelling" of the spinline). This is more evident in the case of PP-300 MFR, as it is a more elastic material. In gravity spinning, the stress at the end of the spinline is zero. For Newtonian gravity spinning, this also corresponds to a zero elongation rate at the end of the spinline; however, for polymer melts with finite memory, a zero elongation stress at the end requires stress "relaxation" (as in the die-swell) towards the end of the spinline resulting in an increase in thread diameter. This increase in the diameter was difficult to detect in general except that it appeared to be present in the case of PP-300 MFR at 180 ^{o}C.

The plot of the apparent elongational viscosity as a function of the elongation rate (see Figure 5.11) reveals the "hysteresis"

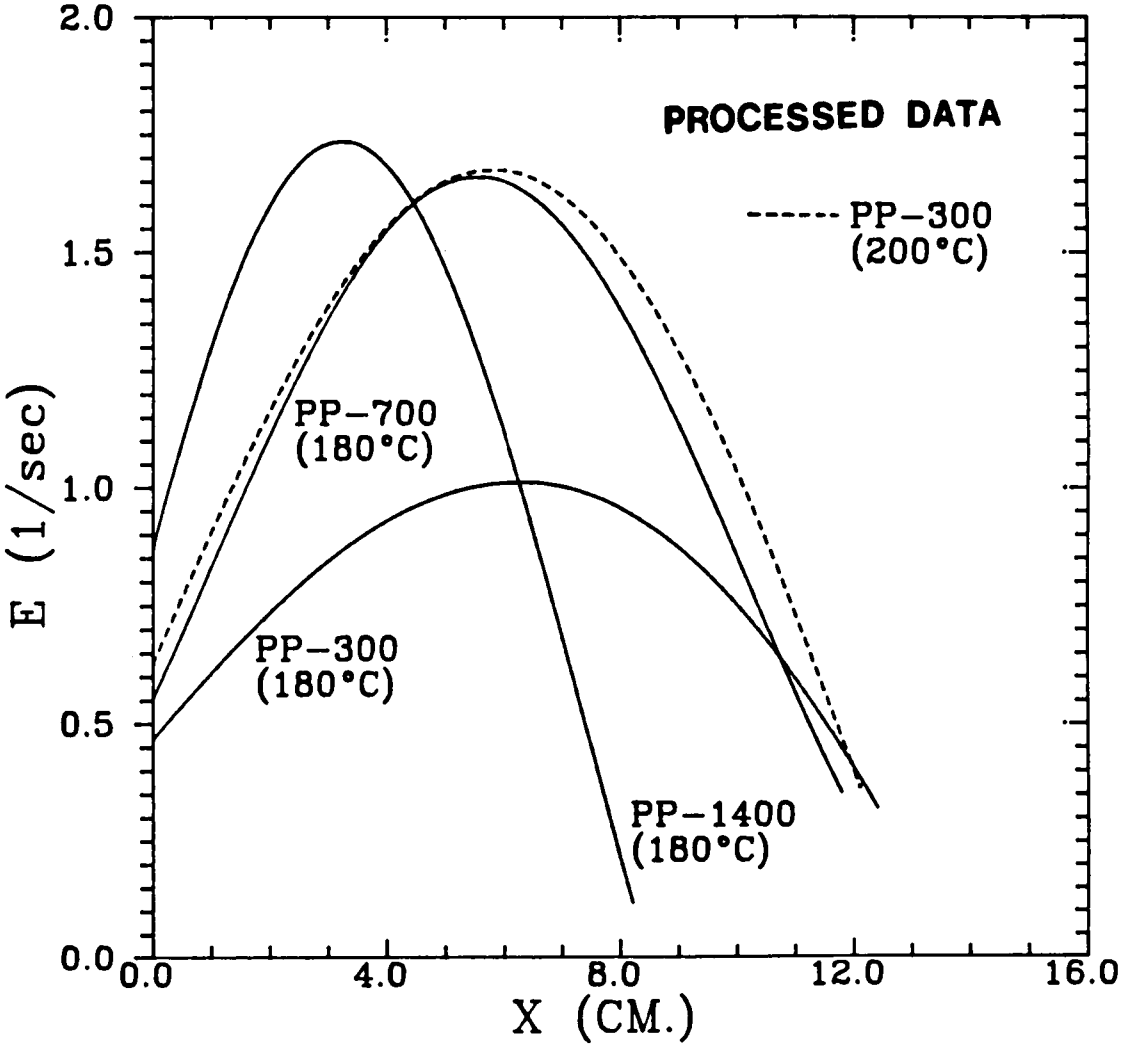


Figure 5.9. Elongation rate profiles along the spinline for various polypropylene melts. Solid lines are the data at 180 °C and the dashed line is data for PP-300 MFR at 200 °C.

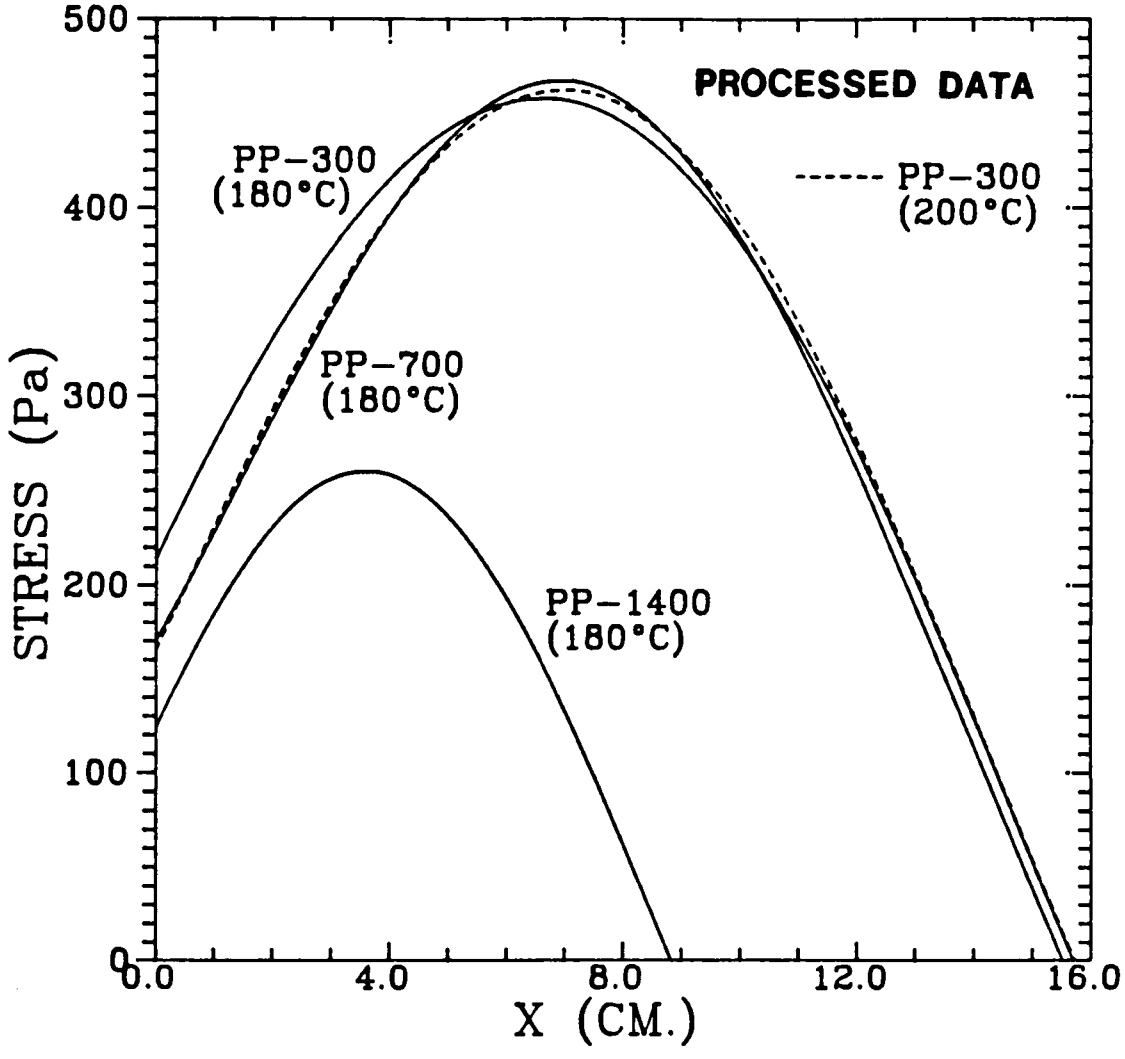


Figure 5.10. Stress profiles along the spinline for various polypropylene melts.

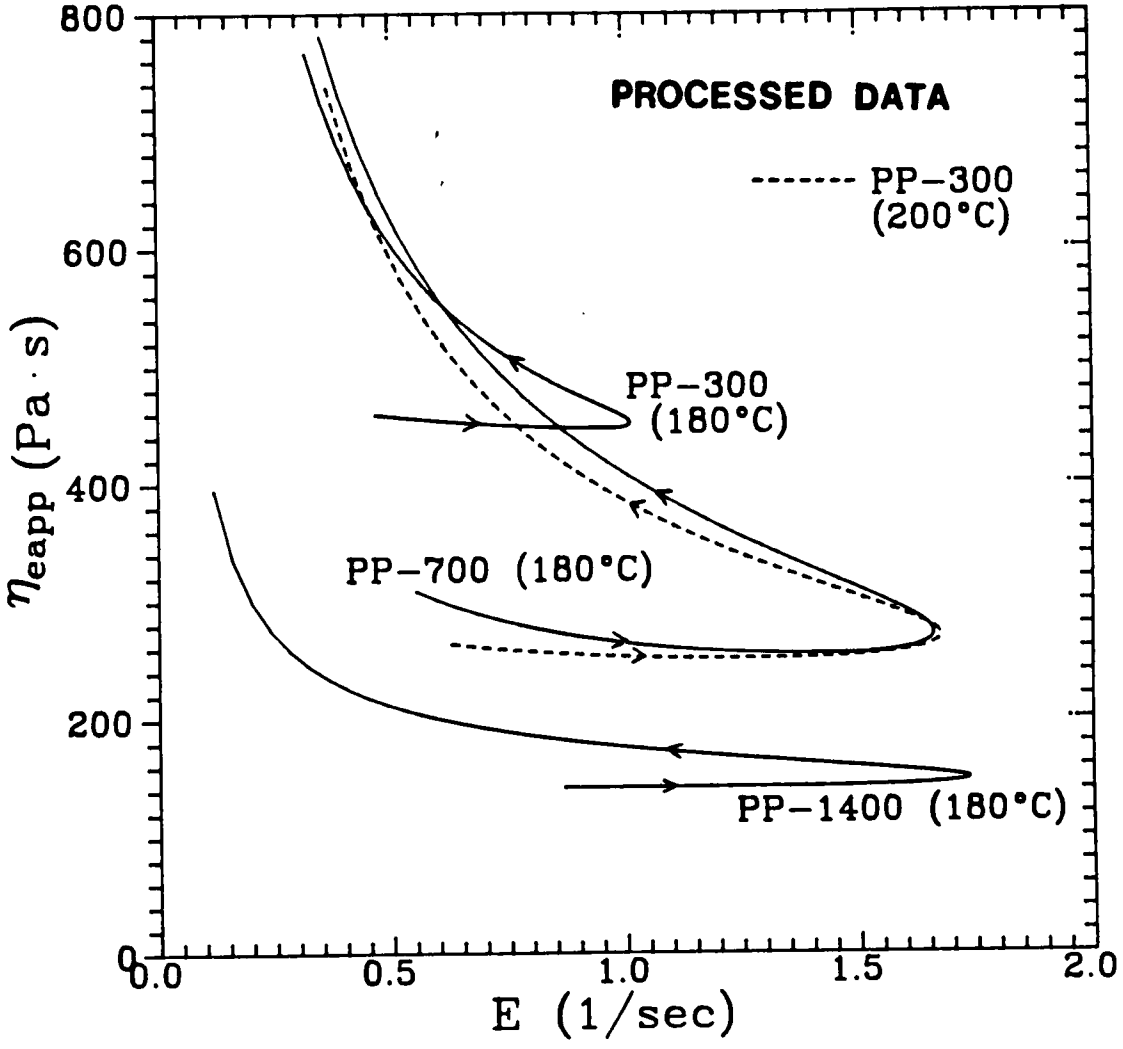


Figure 5.11. The apparent elongational viscosities as a function of the elongation rates for various polypropylene melts. The arrow shows the direction along the spinline.

effect due to the finite memory of polymer melts. This hysteresis is due to the fact that the stress and the elongation rate profile along the spinline go through a maximum, a result peculiar to the gravity spinning. A maximum in stress profile (≈ 450 Pa) occures at about halfway along the spinline and then the stress decreases rapidly to zero. A fluid element experiences such a change in stress very rapidly as its residence time is very small (less than 1 sec.) in the bottom half of the spinline (compared to total residence time of about 3 sec.). Polymer melt with finite (but fading) memory (i.e. having a finite relaxation time) "remembers" its previous deformation and stress history and this results in higher apparent elongational viscosities after the elongation rates go through the maximum along the spinline. The rheological constitutive equations do predict both an increase in diameter towards the end of the spinline and the hysteresis loop in the plot of the apparent elongational viscosity as a function of elongation rate, as will be discussed later. The "width" of the hysteresis loop for gravity spinning depends on the elastic properties (i.e. the average time constant) of the polymer melt with higher the average time constant, wider being the hysteresis loop. In gravity spinning, in principle, there is no external take-up force applied. But as mentioned in the experimental section, it was very difficult to decide on the correct value of the take-up speeds and very small take-up forces might have to be applied to minimize the vibration of the spinline to be able to obtain good slides. The width of the hysteresis loop would be smaller if small external forces (which are not known) are applied

while taking up the quenched fiber and are not accounted for. The hysteresis loop may actually "reverse" itself when somewhat larger take-up forces are applied and are not accounted for. This reverse hysteresis loop was observed in the case of PP-300 MFR when it was taken up with higher speed applying external take-up force. The diameter data for PP-300 MFR at 180 ^{o}C for two runs, one with higher take-up speed and the other with take-up speed lower than the first are shown in Figure 5.12. The plot of the apparent elongation viscosity as a function elongation rate for these two runs is shown in Figure 5.13. The reversal of the hysteresis loop can be observed for the run with higher take-up speed. Even for the run with the lower take-up speed, small take-up force might have been applied and the loop could have been little more wider though it was not possible to reduce take-up speed further without significant vibrations of the spinline which would either break the spinline or make it impossible to obtain good slides with sharper edges of filament. It is impossible to measure such small take-up forces, but if they are somehow guessed and accounted for, it would give "usual" hysteresis loops with a loop width wider than the one with the zero stress at the end of the spinline. These wider loops for non-zero stress boundary condition can be observed if the water bath is kept at a known distance below the end of the isothermal chamber and only the isothermal part of the spinline is considered. The weight of the nonisothermal "hanging" thread would provide the known force (provided the correct take-up speed is used, which is less difficult to achieve at higher take-up speeds) and hence the known non-zero

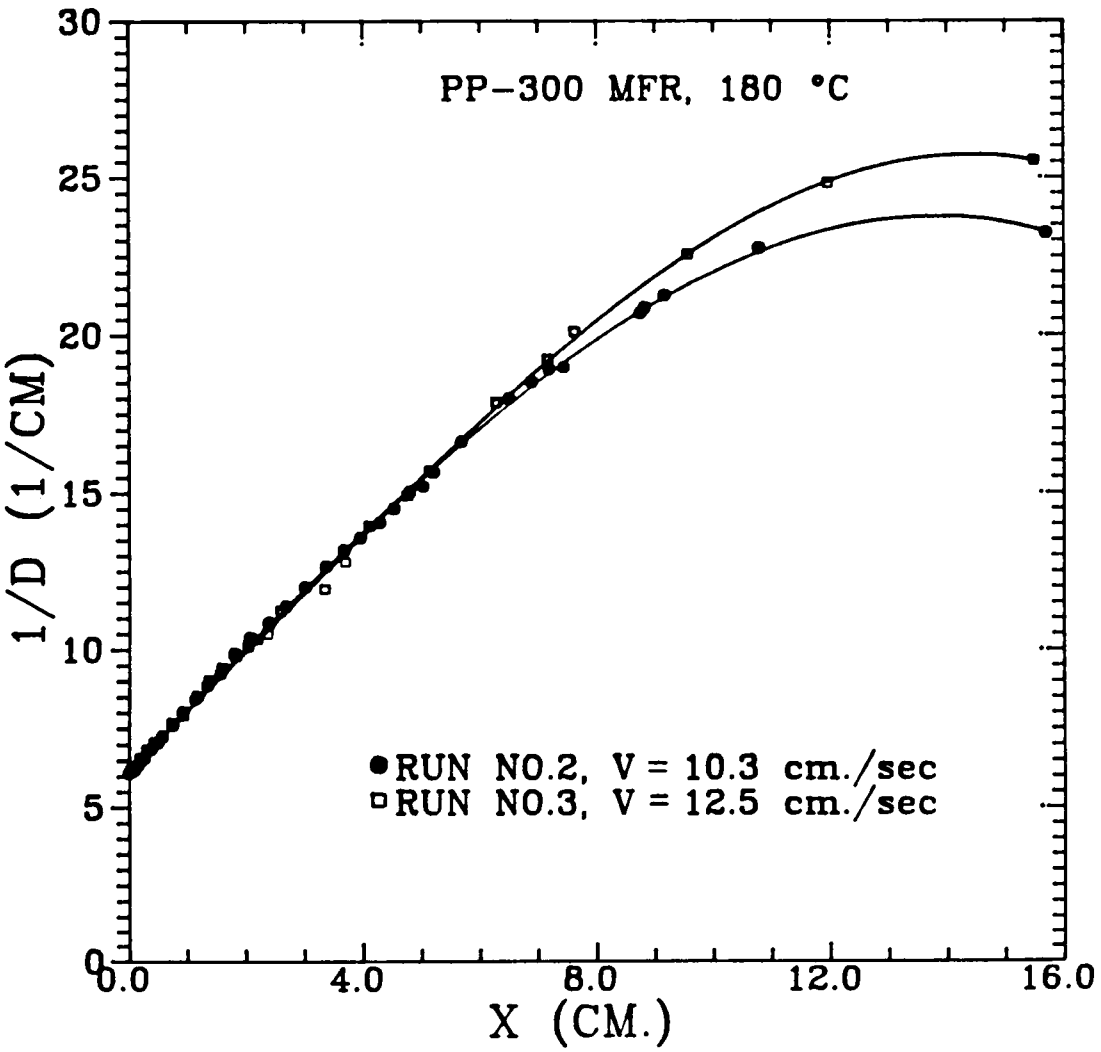


Figure 5.12. The curve fitted profiles of thread diameter for PP-300 MFR at 180 °C at two different take-up velocities.

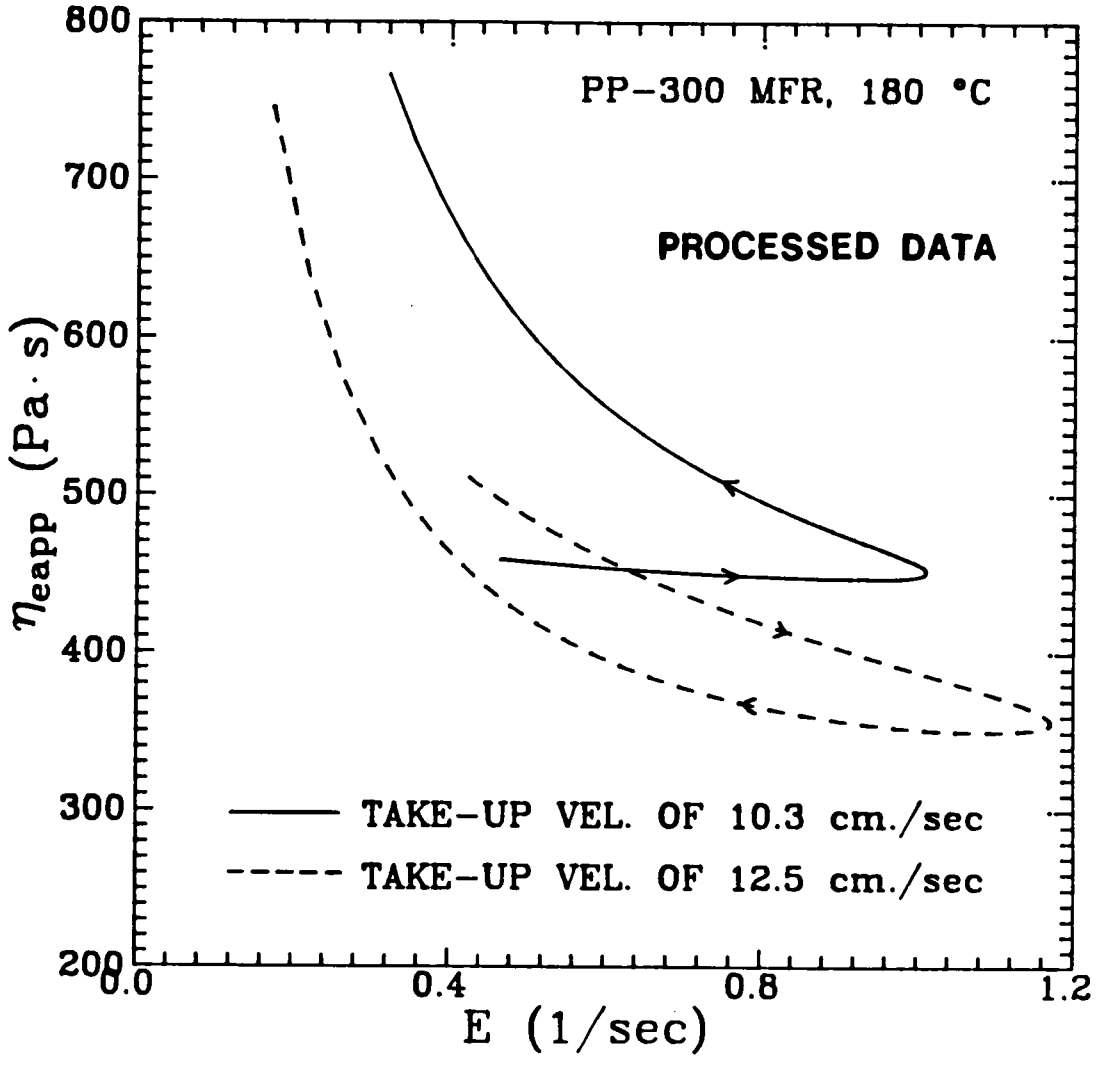


Figure 5.13. The apparent elongational viscosity as a function of elongation rate for PP-300 MFR at 180 °C for the runs shown in Figure 5.12 (without taking into account a small applied take-up force).

stress boundary condition at the end of isothermal spinline of interest. A gravity spinning run (no. 4) like this with L=17.6 cm. (of which the length of the isothermal part was ≈ 13 cm. due to the end of the chamber being open to atmosphere and the remaining was nonisothermal part), was carried out for PP-300 MFR at 180 ^{o}C. The diameter data for this run is shown in Figure 5.14 and is compared with the diameter data for the run no. 2 (L=15.7 cm.) for the same material at 180 ^{o}C. A plot of the apparent elongational viscosity as a function of the elongation rate, computed approximately for this run, is shown in Figure 5.15 and the data are compared with those for run no. 2. It can be observed that the width of the hysteresis loop is wider than that for the run no. 2 and higher elongation rates are obtained.

As will be shown later, the rheological models can predict the "reverse" hysteresis loop, when a non-zero stress condition is used at the end of the spinline and the corresponding take-up force is subtracted from the stress profile prediction of it (which was not accounted for in the gravity spinning data analysis). The model would also predict wider loops than the one obtained without take-up force when a non-zero stress boundary condition is used; in such a case it is the spinline with a known external take-up force. In fact, as the more and more take-up force is applied and accounted for, the hysteresis loop would become wider and wider and when the external force is sufficient (such that the elongation rates would continue increasing rather than going through a maximum), the hysteresis loop would disappear. All these considerations again

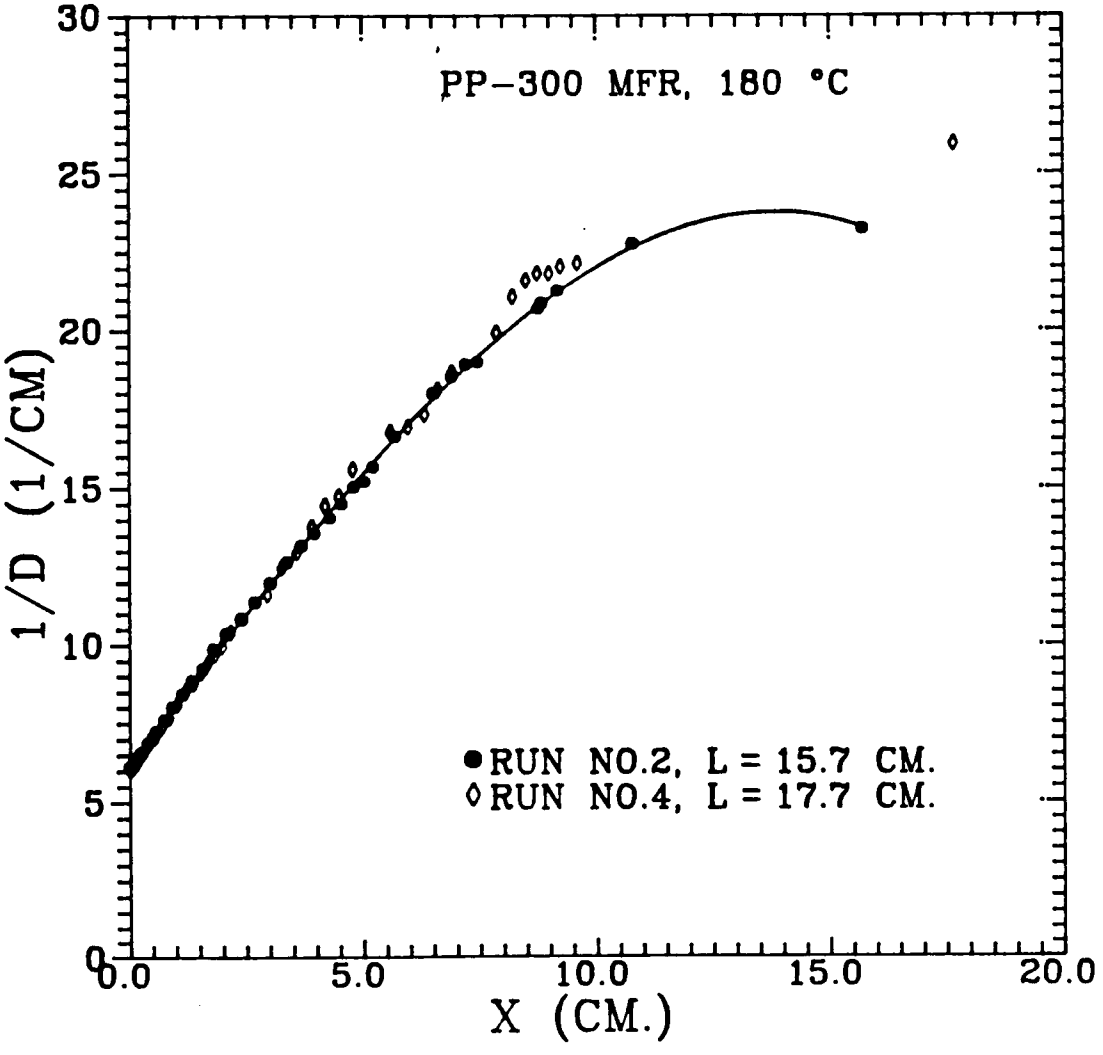


Figure 5.14. Profiles of thread diameter for PP-300 MFR at 180 °C for two different spinline length.

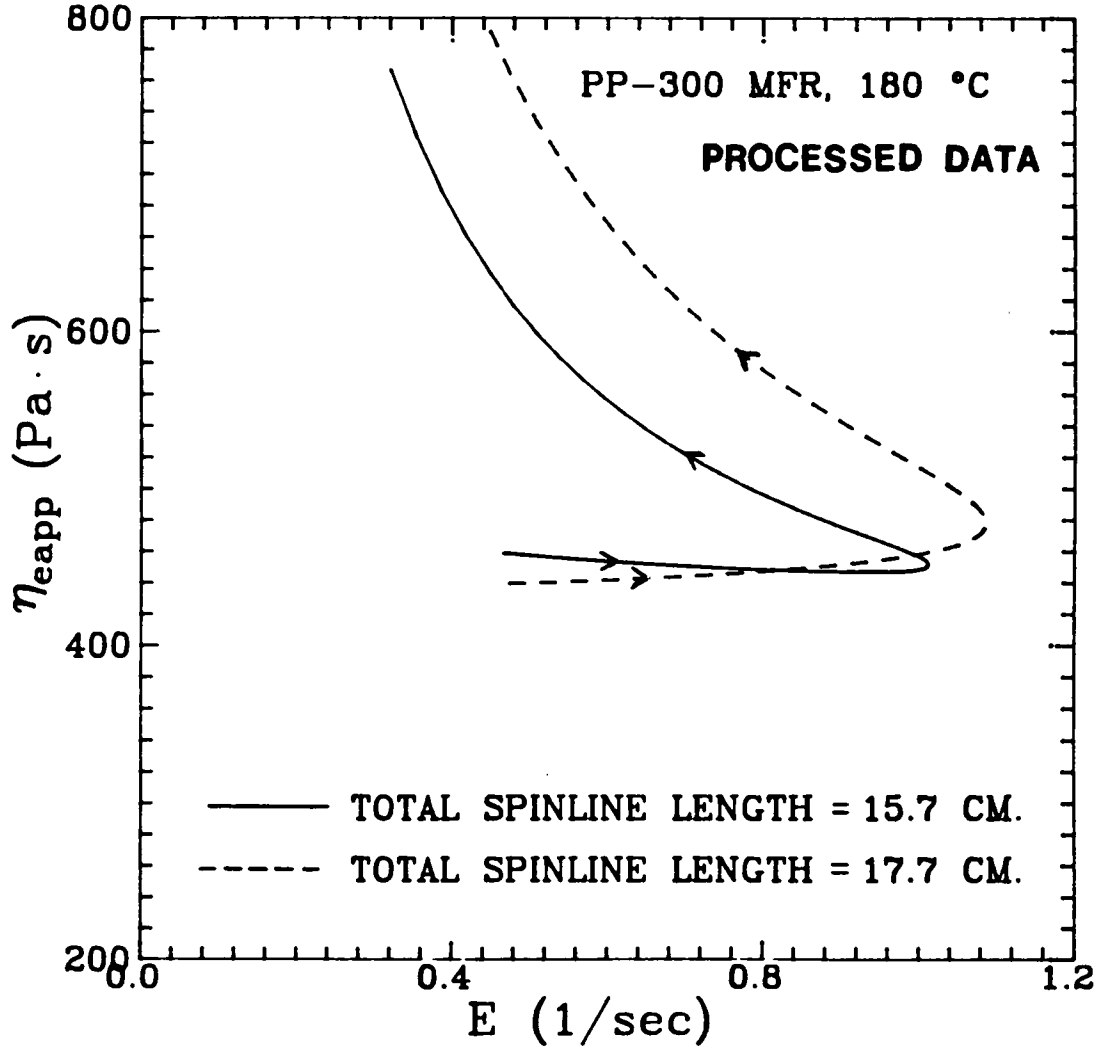


Figure 5.15. The apparent elongational viscosities as a function of elongation rates for PP-300 MFR at 180 °C for two different spinline length.

emphasize the fact that the apparent elongational viscosity is a history dependent and an unsteady-state parameter and the viscosity data analysis for such experiments must be done with a constitutive equation. Such analysis of these spinning experiments will be presented in the next chapter.

The data presented in the above sections were for stable gravity spinning experiments. The instabilies observed for gravity spinning under certain conditions will now be discussed semi-quantitatively .

Spinline instablity during isothermal gravity spinning : A form of spinline instability known as draw resonance, in which periodic variations in diameter occur in the spinline, was observed for all the materials studied under cetain conditions. This spinline instability is different from small random fluctuations in diameter profile along the spinline, caused by fluctuations in throughput rate and probably in take-up speed. Draw resonance shows regular diameter variations which occur when draw ratio (V_L/V_o) exceeds a critical value.

In the case of gravity spinning, the draw ratio is determined by the spinline length, temperature and the throughput rate. Since only two isothermal chambers (of lengths about 8.9 cm. and 15.6 cm.) were used, systematic variations in the spinline length were not possible to determine the exact critical draw ratio at the onset of draw resonance at a given temperature and throughput rate. The temperatures were always set at either 180 ^{o}C or 200 ^{o}C. The Instron

cross head speed (C.H.S.) was normally set at 0.5 "/min. It was also set at 0.2 "/min (one notch lower) for some runs, to study the effect of throughput rate on the spinline stabilty. The C.H.S. also can only be set at discrete values.

Because of the discreteness in the delivery rate and also in the length of the chamber, it was not possible to determine the exact critical draw ratio at the onset of draw resonance under various conditions. All the observed draw ratios are therefore above the incipient (or onset) values; the observed values and the associated experimental conditions are tabulated in the Table V.I. Note that the tabulated values of draw ratios are approximate as it was difficult to decide the take-up velocity for unstable spinline. The experimental draw ratios are based on the velocity in the die.

It can be observed that for the two chambers used, it was not possible to obtain stable spinline for PP-1400 MFR at 200 ^{o}C at a C.H.S. of 0.5 "/min. For the long chamber (L = 15.6 cm.), draw resonance was observed for PP-700 MFR at 200 ^{o}C and for PP-1400 MFR at 180 ^{o}C at a C.H.S. of 0.5 "/min. The stability theory of isothermal spinning is well developed for Newtonian fluids (62,63,66). The isothermal, Newtonian stability theory predicts draw resonance when the draw ratio exceeds 20.2 for conditions in which gravity, surface tension, inertia and air drag are unimportant (a constant force spinline), and the experiments of Donnelly and Weinberger (68) seem generally to confirm this value. Denn et. al. (62) have analyzed the stability of continuous isothermal drawing of Newtonian fluids, taking inertial, surface tension, and gravitational

Table V.I :- Conditions under which draw resonance was observed.

Material	Temp. (°C)	Die diam. (Inch.)	Length of chamber (cm.)	V_0 (cm./sec)	Approx. draw ratio	Re/Fr
PP-300	200	0.058	8.9	0.354	19	44
PP-300	200	0.077	8.9	0.502	-	31
PP-700	200	0.058	15.6	0.885	-	138
PP-1400	180	0.058	15.6	0.885	26	135
PP-1400	200	0.058	8.9	0.885	17	85

effects into account. The general observation is that the gravity enhances the stability of the spinline i.e. draw resonance sets in at the higher values of critical draw ratios than for the constant force spinline.

The plot of $D_R^{1/2}$ as a function of Re/Fr for Re=Re/We=0 as computed theoretically for Newtonian fluids is shown as Figure 5.16. The solid lines are the calculations of Denn et al. and dashed lines are the calculations of Shah and Pearson. Values of the ratio of Reynolds number to Froude number ($Re=\rho Lv_o/3\eta_o$ and $Fr=v_o^2/gL$) for the conditions under which draw resonance was observed are tabulated in Table V.I (using the zero-shear viscosities). The approximate draw ratios at which draw resonance was observed are also shown in Figure 5.16 as a function of computed values of Re/Fr. The dashed lines on the left of the figure are the asymptotic predictions for constant force spinline for different values of the power law index. From the plot it is apparent that the materials showed draw resonance at quite lower values of draw ratios than the Newtonian predictions. Although, no stability theory exists for gravity spinning of non-Newtonian fluids, inspection of the asymptotes at the left suggests that the observed lower values are not unreasonable. Draw ratio values for stable spinlines will always be lower than those observed for unstable spinlines and are not shown here. Nam and Bogue (77) observed that the polypropylene melts exhibiting draw resonance broke by ductile failure at higher draw ratios in the spinning experiments.

In the melt blown process, hot air jets are used to blow the fibers on to a collector screen. Although, the force field in

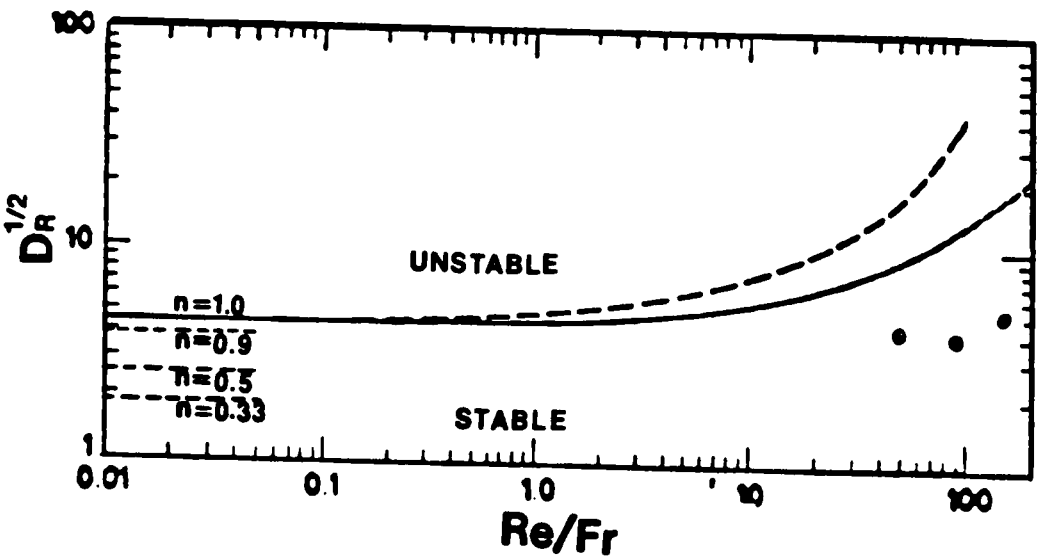


Figure 5.16. Plot of $D_R^{1/2}$ as a function of Re/Fr for Re=Re/We=0. The solid line is calculations of Denn et al. and the dashed line is the calculations of Shah and Pearson, as reproduced in Denn et al. (62).

gravity spinning is not the same as that due to the air jets in the melt blown process, it is probably not unreasonable to assume that an instability analogous to draw resonance will occure in the second case as well. If the average diameter of the web fibers is taken to be 5 μm., a calculation based on mass balance (with 380 μm. dia. holes with 0.4 g/min/hole throughput rate) suggests that if a single fiber is to draw down to the final diameter of 5 μm., its final velocity would be more than sonic. Since this is not possible, some sort of breakage must be occuring in between the die and the collector.

CHAPTER 6

MODELLING OF SHEAR FLOW AND ELONGATIONAL FLOW DATA

In this chapter the analysis of shear flow and elongational flow data using the Bogue-White (BW) model and the Phan-Thien and Tanner (PTT) model will be discussed. The shear flow data will be analyzed first and the model parameters obtained from analyzing the shear flow data will also be used to predict the elongational flow data.

6.1 Modelling of Shear Flow Data

The shear flow data for the various materials studied at different temperatures are presented in chapter IV. The strong shear thinning nature of these materials is apparent from these data. Note that the average relaxation time in shear cannot be obtained accurately as the extrapolation of the the first normal stress difference coefficient data to zero shear rate would be highly subjective. The analysis of shear viscosity and the first normal stress difference data using the Bogue-White model will be discussed now.

The Bogue-White model predictions for the shear viscosity and the first normal stress difference coefficient as a function of shear rate are given as follows:

$$\tau_{neff(i)} = \frac{\tau_{n(i)}}{1 + (a\tau_{n(i)}\dot{\gamma})^{0.75}} \qquad [6.1.1a]$$

$$\eta(\dot{\gamma}) = \sum_{i=1}^{n} G_{(i)}\tau_{neff(i)} \qquad [6.1.1b]$$

$$\Psi_1(\dot{\gamma}) = \sum_{i=1}^{n} 2G_{(i)}\tau_{neff(i)}^2 \qquad [6.1.1c]$$

where "a" is a thinning parameters and $G_{(i)}$ and $\tau_{n(i)}$ are the relaxation modulus and the relaxation time respectively for each mode of linear viscoelastic spectrum. The linear viscoelastic spectrum data for these materials could not be obtained experimentally due to lack of dynamic measurements facility in cone-and-plate rheometer.

The steady shear flow data can be used to obtain values (or value) of the relaxation time and modulus as well as a "thinning parameter" as will be done here using the Bogue-White model. The Bogue-White model requires atleast two pairs of values of the relaxation time and modulus to be able to best fit both the shear viscosity and the normal stress data with a single value of thinning parameter "a" (20). Also it is very difficult to obtain more than two pairs of τ's and G's using the steady shear data. The Bogue-White model is used here to extract two pairs of τ's and G's as well as the thinning paramter "a" by fitting the steady shear data. The value of G_1 was set at 2E04 Pa and even than sets of values of these five parameters were obtained by fitting the shear data using a least

square fitting method. The values of relaxation spectrum parameters had to satisfy the known zero shear viscosity value ($\eta_o = G_1\tau_1 + G_2\tau_2$) and had to give resonable value of zero shear first normal stress difference coefficient ($\Psi_{1(o)} = 2G_1\tau_1^2 + 2G_2\tau_2^2$) as it could not be obtained unambiguously. The sets with same or nearly same values of thinning paramter "a", best fitting the shear viscosity and the first normal stress difference coefficient data individually, were chosen for the various materials studied. Note that one pair of G's and τ's (with G_1 = 2E04 Pa and corresponding very low value of τ_1) gives almost Newtonian contribution and the other pair contributing to thinning behavior in shear.

The fitting of shear viscosity data using the Bogue-White model for PP-300 MFR at both 180 ^oC and 200 ^oC and for PP-700 and PP-1400 MFR at 180 ^oC is given in Figures 6.1 and 6.2, respectively. The fitting of the first normal stress difference coefficient data using the BW model for PP-300, PP-700 and PP-1400 MFR at 180 ^oC is shown in Figure 6.3. Note that two sets of G's and τ's used for each material give almost identical prediction of shear viscosities but their prediction of the first normal stress difference coefficients are quite different. This again emphasizes the importance of the normal stress data.

The predictions of the PTT model for the shear viscosity and the first and second normal stress difference data as a function of shear rate (26) are given as follows :

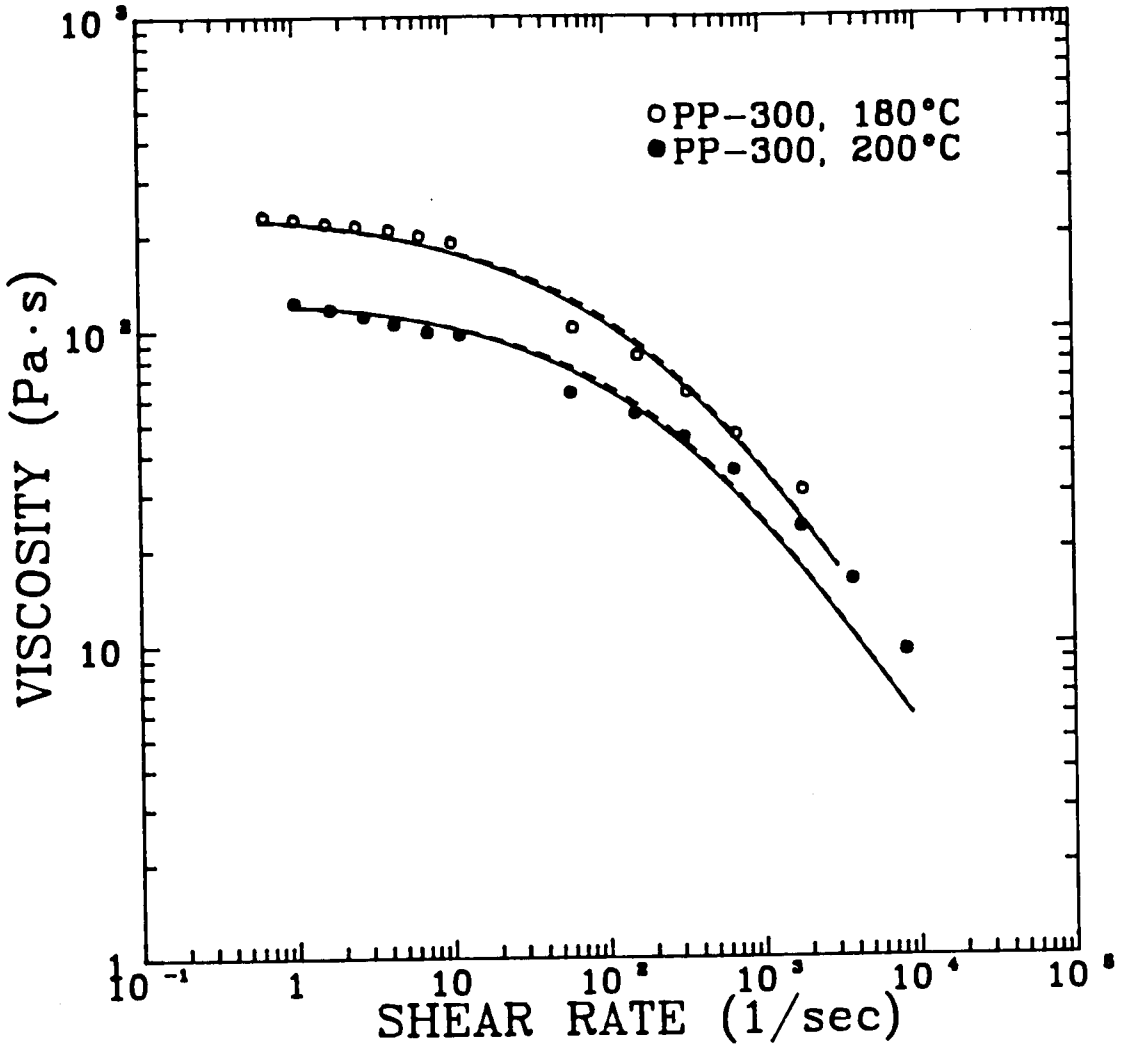


Figure 6.1. Fitting of shear viscosity data for PP-300 MFR using the Bogue-White model.

PP-300 MFR, 180 °C
——— τ_1=0.0076 sec., G_2=592.9 Pa, τ_2=0.14 sec., a=0.74.
------ τ_1=0.0088 sec., G_2=226.9 Pa, τ_2=0.26 sec., a=0.74.

PP-300 MFR, 200 °C
——— τ_1=0.0037 sec., G_2=1133 Pa, τ_2=0.045 sec., a=0.92.
------ τ_1=0.0046 sec., G_2=412.5 Pa, τ_2=0.08 sec., a=0.92.

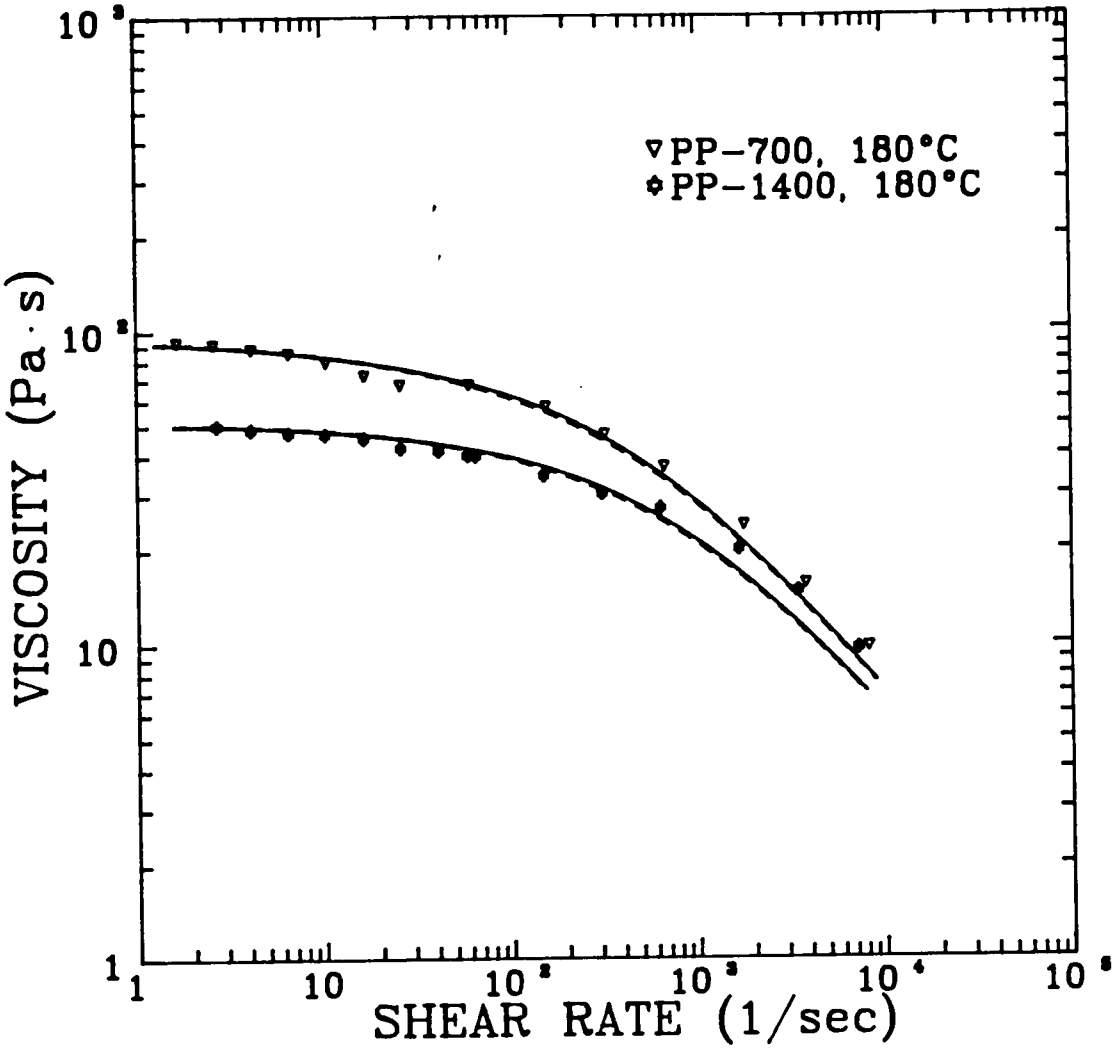


Figure 6.2. Fitting of shear viscosity data for PP-700 MFR and PP-1400 MFR at 180 °C using the Bogue-White model.

PP-700 MFR, 180 °C
——— τ_1=0.0039 sec., G_2=100 Pa, τ_2=0.17 sec., a=0.57.
------ τ_1=0.0036 sec., G_2=255.6 Pa, τ_2=0.09 sec., a=0.57.

PP-1400 MFR, 180 °C
——— τ_1=0.0023 sec., G_2=59.5 Pa, τ_2=0.084 sec., a=0.55.
------ τ_1=0.0021 sec., G_2=300 Pa, τ_2=0.03 sec., a=0.55.

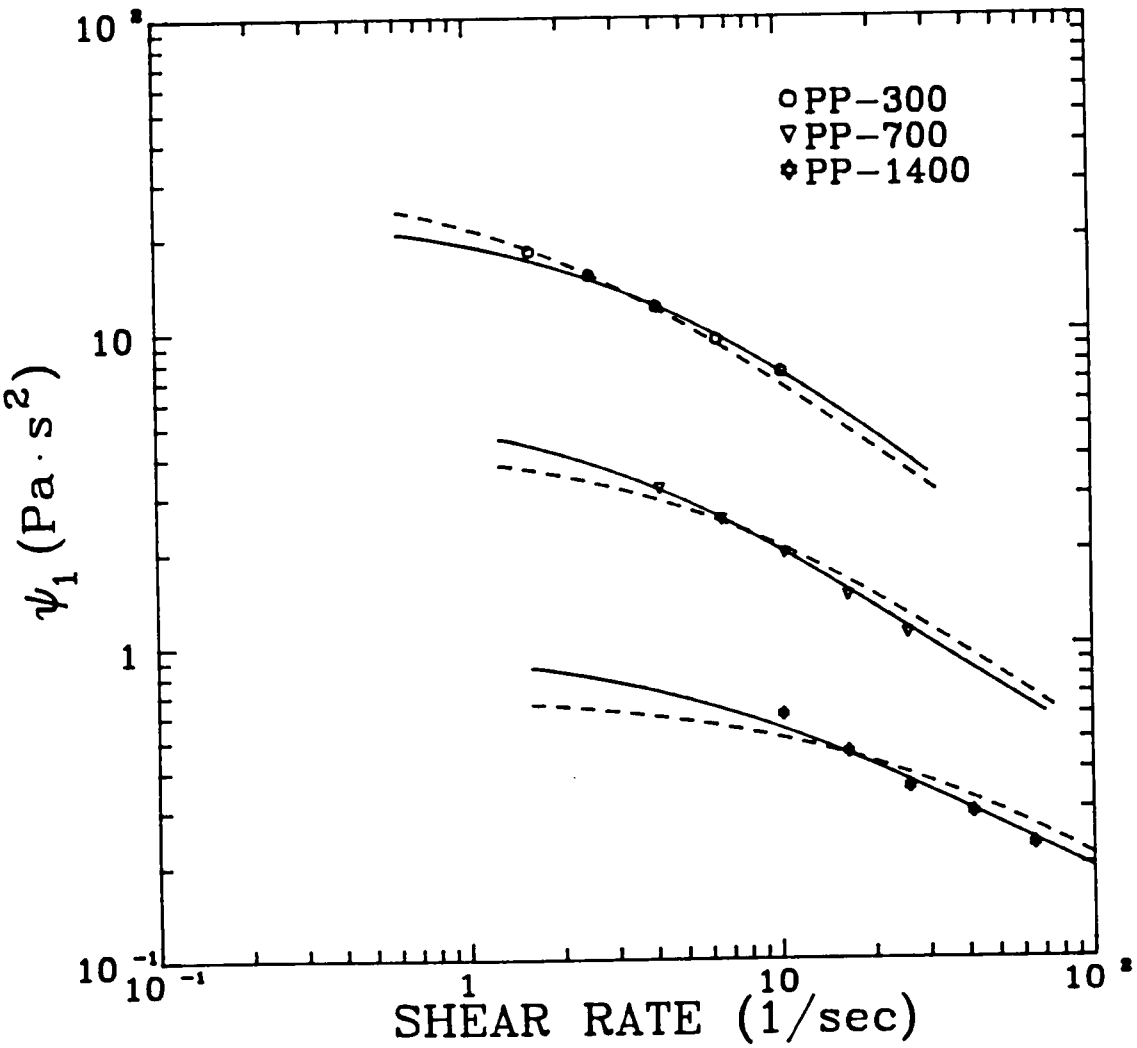


Figure 6.3. Fitting of the first normal stress difference coefficient data using the Bogue-White model (using the same model parameters as used for fitting the shear viscosity data).

$$\eta = \sum_{i=1}^{n} \frac{G_i \tau_i}{1 + \xi(2-\xi)\tau_i^2 \dot{\gamma}^2} + O(\varepsilon) \qquad [6.1.2a]$$

$$N_1 = 2 \sum_{i=1}^{n} \frac{G_1 \tau_1^2 \dot{\gamma}^2}{1 + \xi(2-\xi)\tau_i^2 \dot{\gamma}^2} + O(\varepsilon) \qquad [6.1.2b]$$

$$N_2 = -\xi/2 \, N_1 \qquad [6.1.2c]$$

The equation [6.1.2c] is an exact result but equations [6.1.2a] and [6.1.2b] are perturbation results which are valid only at low shear rates. The PTT model in this form predicts an asymptotic slope of -2.0 in the plot of viscosity versus shear rate, while the experimentally observed value is about -0.75 to -0.8. Hence, the PTT model would give poor fits of the shear viscosity data at very high shear rates. However, the above predictions are based on a perturbation scheme in ε and may be valid only at lower values of the shear rate. Phan-Thien and Tanner have used these predictions only up to shear rates of 100 sec^{-1} for low density polyethylene at 150 ^{o}C (25,26). They also reported that the shear flow predictions were insentitive to the values of ε ranging from 0.01 to 0.001. The literature values of ε, obtained from elongational data, are of the order of 0.01 but as will be seen in the next section, values of ε of the order of 1.0 are necessary to fit the gravity spinning data of the present work. The value of the paramter ξ can be found from the ratio of the second to the first normal stress differences. This ratio for polymer melts and solutions usually lies between

-0.2 to -0.3 (31,32). Due to the lack of second normal stress difference data for the materials studied, ξ=0.4 (corresponding to -0.2 in the normal stress ratio) will be taken in all subsequent calculations. Since explicit equations to predict the steady shear data over the entire range of shear rates are not available in the literature, the fitting of shear data using the PTT model will not be presented.

The Bogue-White model parameters (two G's, two τ's and a thinning paramter "a"), obtained by fitting the steady shear data will be used in a preliminary treatment of the elongational flow data in the next section.

6.2 Theoretical Simulation of Gravity Spinning Experiments

As mentioned before, the elongational deformation in isothermal gravity spinning experiments is history dependent and the instantaneous stress/deformation rate ratio, termed the apparent elongational viscosity, depends upon both the deformation rate and history. Hence, the analysis of apparent viscosity data for gravity spinning experiments must be made in terms of a suitable constitutive equation. Such an analysis will now be discussed.

The constitutive equation used to describe the rheological behavior of a viscoelastic liquid is the key to any analysis of how the material flows. Constitutive equations, both in differential form and integral form, can be used for the interpretation of spinning data. For integral models, a calculation of the stress evolution requires a knowledge of the kinematics upstream and into

the nozzle, or spinneret; spinneret kinematics are very complex and can only be crudely approximated (69,70). A problem in applying integral equations in process design is that the material being deformed will seldom begin the deformation process of interest in its "virgin" (stress-free) state, and the upstream deformation history will seldom be known accurately. Even then a computer program was written to predict stress profile for Newtonian gravity spinning, using known kinematics and using a convected Maxwell model in the integral form (known as the Lodge model). Relaxation time values approaching zero were chosen to simulate Newtonian behavior. But even in this simple Newtonian case, using known kinematics (predicted by theory of Newtonian gravity spinning) with no trial and error, simulation takes an enormous amount of computing time on an IBM PC for predicting stress profiles along the spinline. The prediction of stress using such integral constitutive equation requires a double integration to be performed and hence requires a large amount of computing time. The theoretical simulation of gravity spinning, requiring trial and error in terms of guessing kinematics and matching the stresses predicted by the force balance equation to that predicted by an integral form of constitutive equation with unknown kinematics in the spinneret was felt to be intractable.

Derivative type constitutive equations circumvent many of these difficulties, since the material memory is introduced in a manner dependent only on the local values of stress, deformation rate, and the derivatives of these quantities. Using the differential models, the simulation of gravity spinning experiments requires, a numerical

solution of first order ordinary differential equations (see Appendix-C). For example, using one value of the relaxation time and the modulus, three differential equations are to be solved numerically: one for total stress σ_{11} (differential force balance equation), and the other two for the extra stress tensors T_{11} and T_{22} (the differential constitutive equation). These differential equations can easily be solved using a fourth-order Runge-Kutta method with much less computing time. The solution of these differential equation requires initial data for the filament velocity if the fluid is inelastic; if the fluid is viscoelastic then it is also necessary to specify the ratio of the axial to the radial extra stresses and the fraction of the axial stress that is contained in each mode of the viscoelastic spectrum. Here, a knowledge of the kinematics upstream into the spinneret is not required but a substitute difficulty is that the solution of the differential equations requires boundary conditions on the viscous stresses T_{11} and T_{22} at an arbitrary initial plane (usually taken as the plane of maximum die-swell). The total stress σ_{11} ($\sigma_{11} = T_{11} - T_{22}$) is chosen for a given simulation, but the exact split into T_{11} and T_{22} is not known apriori and has to be decided arbitrarily. The kinematics upstream into the spinneret would presumably decide this split-up. Note that this problem does not arise with Newtonian liquids, because viscous stresses for Newtonian liquids are exactly related to velocity gradients and $T_{22} = -1/3\ \sigma_{11}$ holds true all along the spinline. Keunnings et al. (71) analyzed the profile development in continuous isothermal drawing and found that for an upper-

convected Maxwell model and the Phan-Thien and Tanner model, this ratio lies between -0.5 to 0.0. But, as will be shown later, this problem is insignificant for less elastic liquids with very low values of relaxation time. Even for relatively more elastic liquids (e.g. PP-300 MFR) the model predictions for the extreme values of this ratio are identical except in the initial part of the spinline near the die. Hence, the model predictions are insentitive to any particular value of the ratio chosen. Differential models have also the advantage of requiring much less computing time than integral models and thus have been used commonly for the simulation of melt spinning experiments.

The Bogue-White model and the Phan-Thien and Tanner model (PTT model), both in differential form have been used here to analyze the gravity spinning data. The constitutive equations for these models are presented in Chapter 2. The appropriate differential equations for the simulation of gravity spinning can be obtained by evaluating the Oldroyd convected time derivatives for the appropriate kinematics and are given in Appendix-C, along with the force balance equation in differential form. All these differential equations are asymptotic (or thin filament) equations that assume a radially uniform axial velocity profile; the asymptotic equations are applicable only downstream of the spinneret, after rearrangement of the laminar profile in the spinneret hole. Most authors have assumed that the asymptotic equations can be applied starting at the point of maximum extrudate swell; profile developments studies in melt spinning tend to support this assumption(72). The same assumption is also used

here and the velocity at the point of maximum die-swell will be used as a initial condition for the simulation. The ratio of T_{11}/T_{22} is assumed to be zero for most of the simulations, although its value is varied for the simulation of PP-300 MFR, which is a more elastic melt. The computer programs for the simulation of gravity spinning experiments on an IBM PC are given in Appendix B-3 and B-4, for one G, one τ case and for two G's and two τ's case, respectively. The programs are written in BASIC and were run using Turbo Basic Compiler. The theoretical simulation of the gravity spinning experiments for the materials studied will now be presented.

Prediction of elongational flow data from shear data : One of the central questions that has been of interest to rheologists is the extent to which measurements made in shear are relevant to extensional flow when linear relaxation spectrum data are not available. The steady shear data are analyzed using the Bogue-White model in the previous section. The parameters extracted by fitting steady shear viscosity and normal stress data using the Bogue-White model will be used here to predict the apparent elongational viscosities as a function of elongation rates. The initial stress σ_{11} is varied such that the predicted spinline length (using $\sigma_{11} = 0$ as the boundary condition) comes out to be correct. The results of these simulations for PP-300, PP-700 and PP-1400 MFR at 180 ^{o}C are shown in Figure 6.4 in the form of plot of the apparent elongational viscosity as a function of the elongation rate and the results are

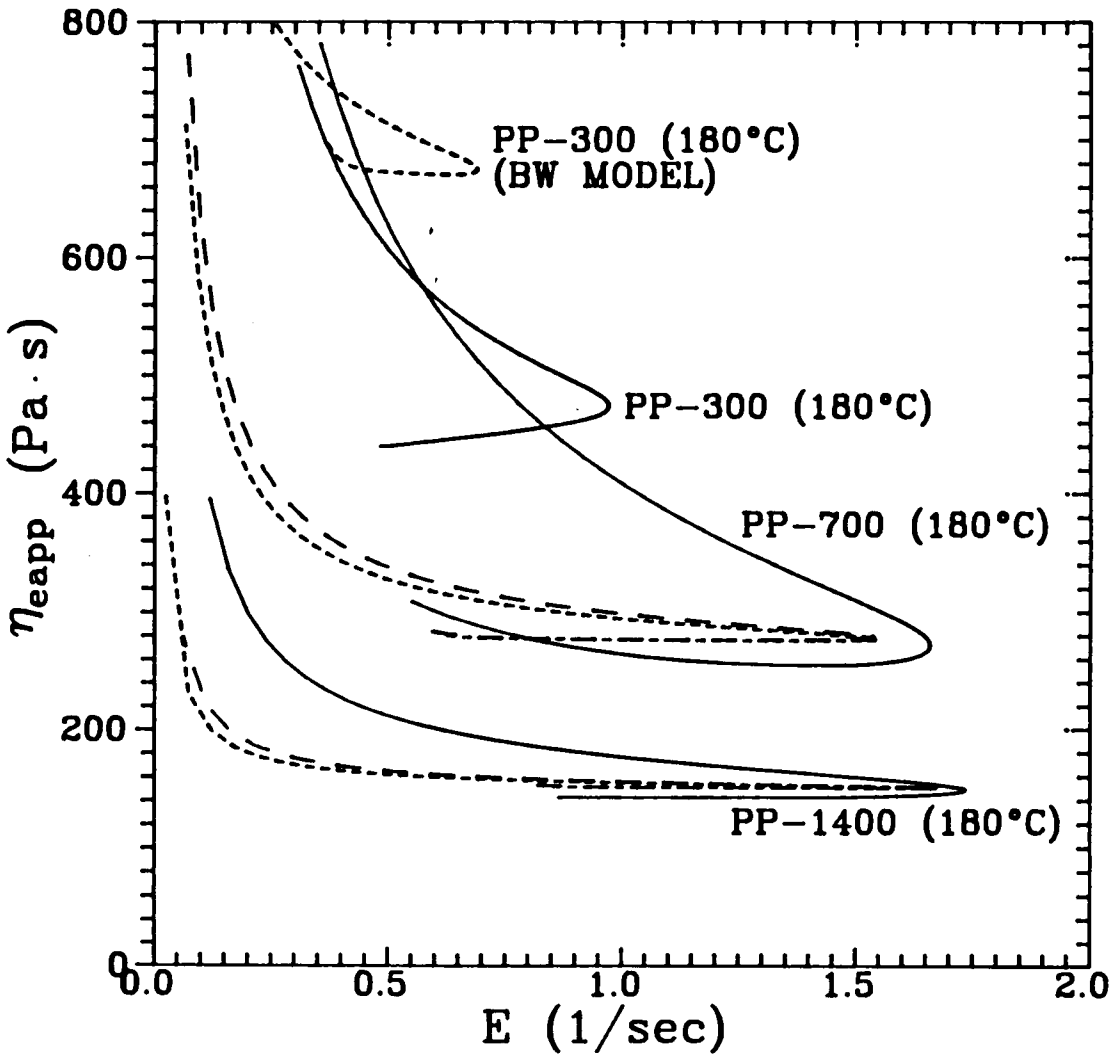


Figure 6.4. Predictions of the apparent elongational viscosities as a function of the elongational rates using the BW model using the model parameters obtained from the shear data.

PP-300 MFR, 180 °C.
------- τ_1=0.0088 sec., G_2=226.9 Pa, τ_2=0.26 sec., a=.74.

PP-700 MFR, 180 °C.
-------- τ_1=0.0036 sec., G_2=255.6 Pa, τ_2=0.09 sec., a=.57.
———— τ_1=0.0039 sec., G_2=100.0 Pa, τ_2=0.17 sec., a=.57.

PP-1400 MFR, 180 °C.
------- τ_1=0.0021 sec., G_2=300.0 Pa, τ_2=0.03 sec., a=.55.
————— τ_1=0.0021 sec., G_2=59.5 Pa, τ_2=0.084 sec., a=.55.

compared with the experimental data. Observe that the width of the hysteresis loop predicted is much smaller than the experimental values. Note also that the width of the hysteresis loop depends upon an average relaxation time; the higher the relaxation time, the wider the loop is. Hence, the results of the simulation suggest the need for using a higher value for the average relaxation time. This need to use higher values of an average relaxation time in elongational flow experiments has been observed by various researchers previously also (72,73,74). Denn et al. (75) have claimed that the need to have higher value of an average relaxation time is a consequence of the use of a single relaxation time model and the shear data can be used to predict the elongational flow data provided that the full spectral data on the melt are available. But there is no detailed experimental study to back up this assertion. In practice, the full spectral data on polymer melts are rarely available. In the absence of full spectral data in the present work, we must try to use those available from shear experiments. The two G's and two τ's extracted from the shear data using the Bogue-White model could not predict the elongational flow data quantitatively and the results suggest the need for using a higher value of the average relaxation time. The PTT model also required higher values of an average relaxation time to quantitatively fit the elongation data as will be shown in the next section. Hence the conclusion seems to be independent of a particular model. The higher value of an average relaxation time will now be used to fit the elongational flow data.

Modelling of the elongational flow data using one G and one τ : The Bogue-White model and the PTT model, using one G and one τ, will now be used to fit the elongational flow data. As noted in the previous section a higher value of the average relaxation time τ must be used to fit the elongational flow data quantitatively. The values of τ would be decided based on overall fits of the stress profiles, velocity profiles and the apparent elongational viscosity data as a function of elongation rate. Note that due to the difficulties mentioned in the experimental section, extremely accurate diameter data in the bottom half of the spinline could not be obtained and hence experimentally obtained values of elongation rates and the apparent elongation viscosities in this part of the spinline should be viewed with caution. Many of the features of the simulation will now be demonstrated for PP-700 MFR.

The predictions of the Bogue-White model in the form of plot of the apparent elongational viscosities as a function of elongation rates for PP-700 MFR at 180 ^{o}C for three different values of τ are shown in Figure 6.5. The plots of the stress profiles and the velocity profiles along the spinline for PP-700 MFR at 180 ^{o}C for the same values of τ are given as Figures 6.6 and 6.7, respectively. Note that the value of G's are computed using the condition that the product of G and τ must give the known zero shear viscosity and the same value of thinning parameter "a" is used as obtained by fitting the shear data. The ratio of T_{11}/T_{22} was assumed to be 0.0 for this case. The simulation involves specifying initial velocity, taken at the point of maximum die-swell, as obtained experimentally. The

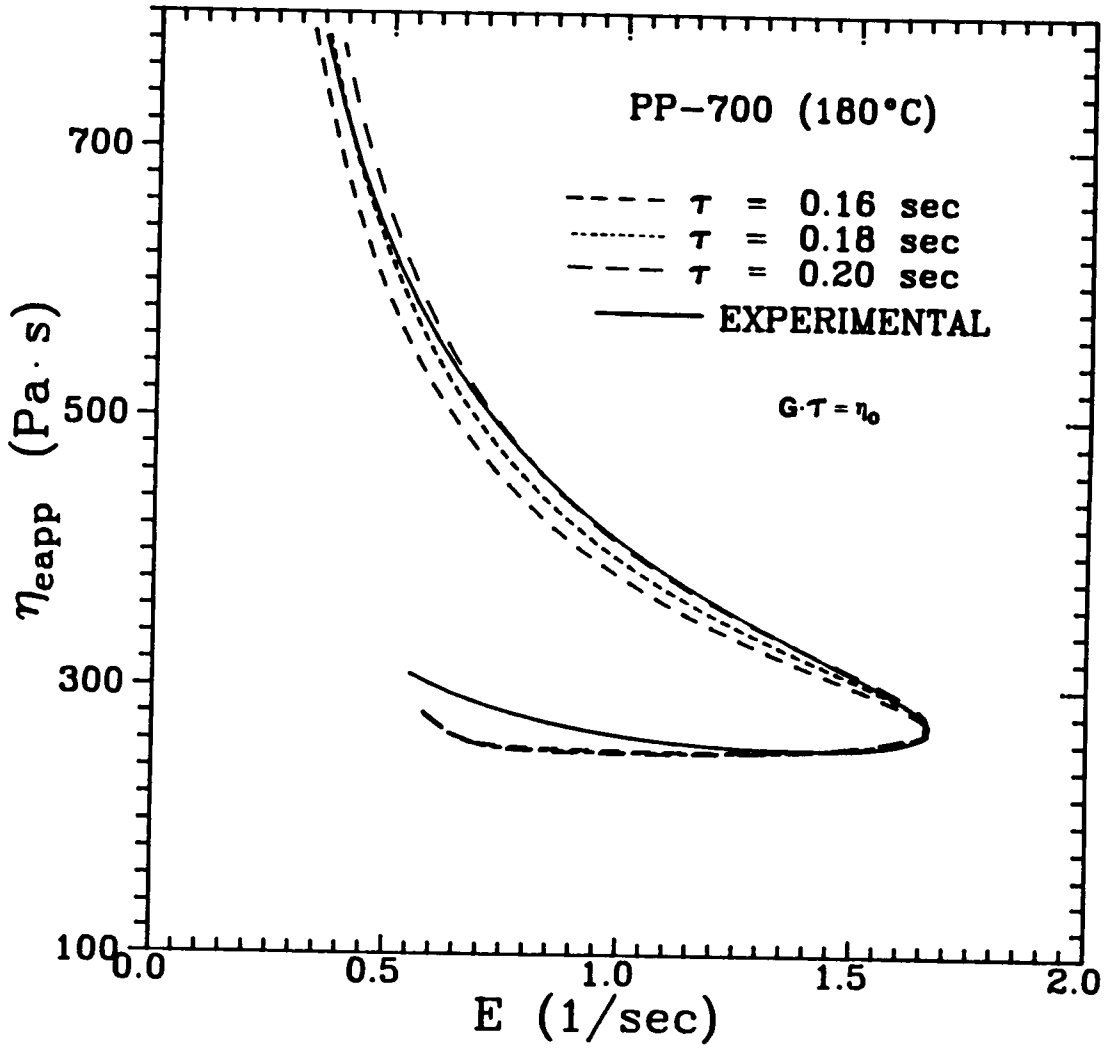


Figure 6.5. Comparison of the experimental data for PP-700 MFR at 180 ^{o}C with predictions of the BW model using three different values of average relaxation times and a=0.57.

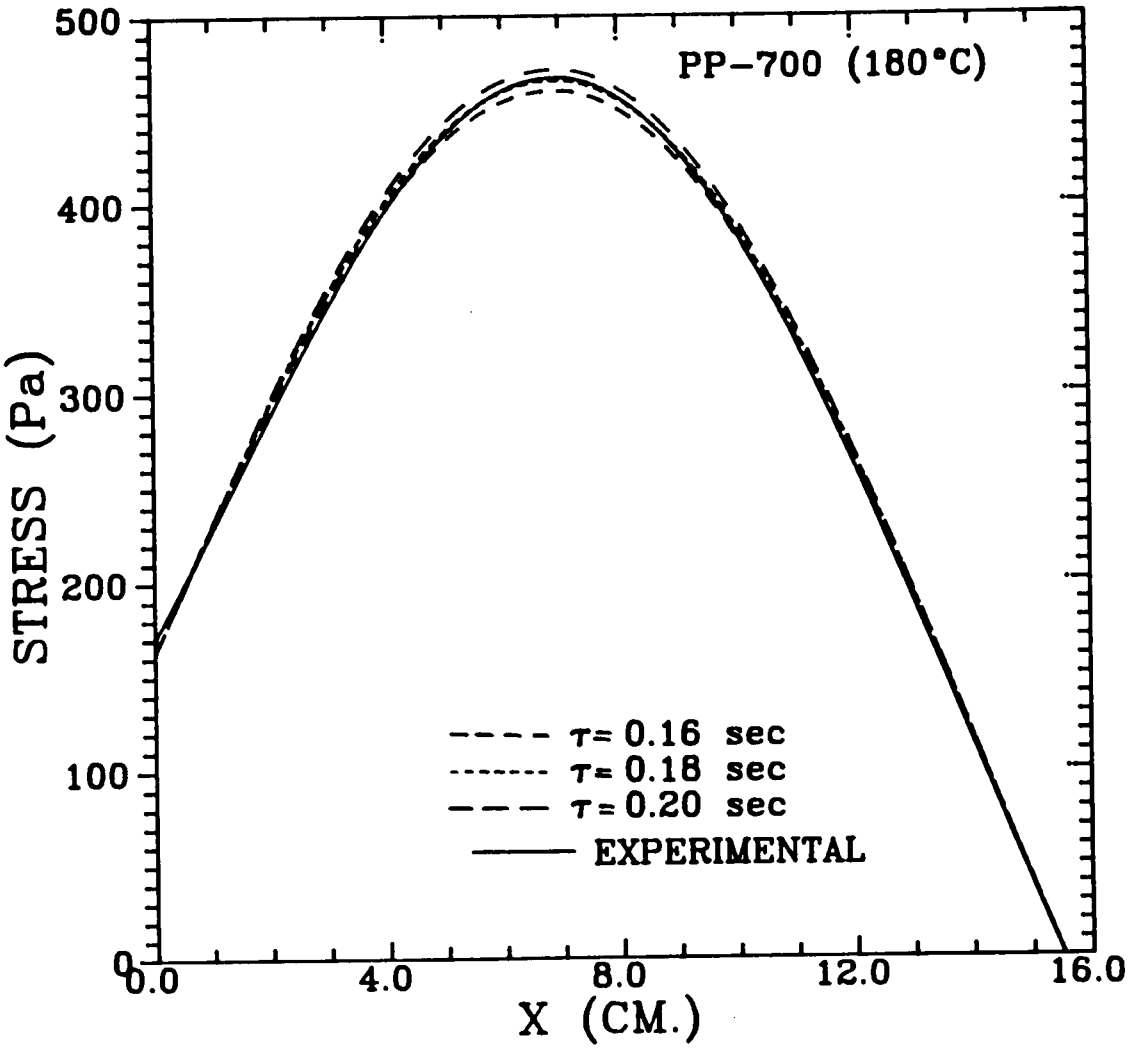


Figure 6.6. Comparison of the experimental data for PP-700 MFR at 180 °C with predictions of the BW model using three different values of average relaxation times and a=0.57.

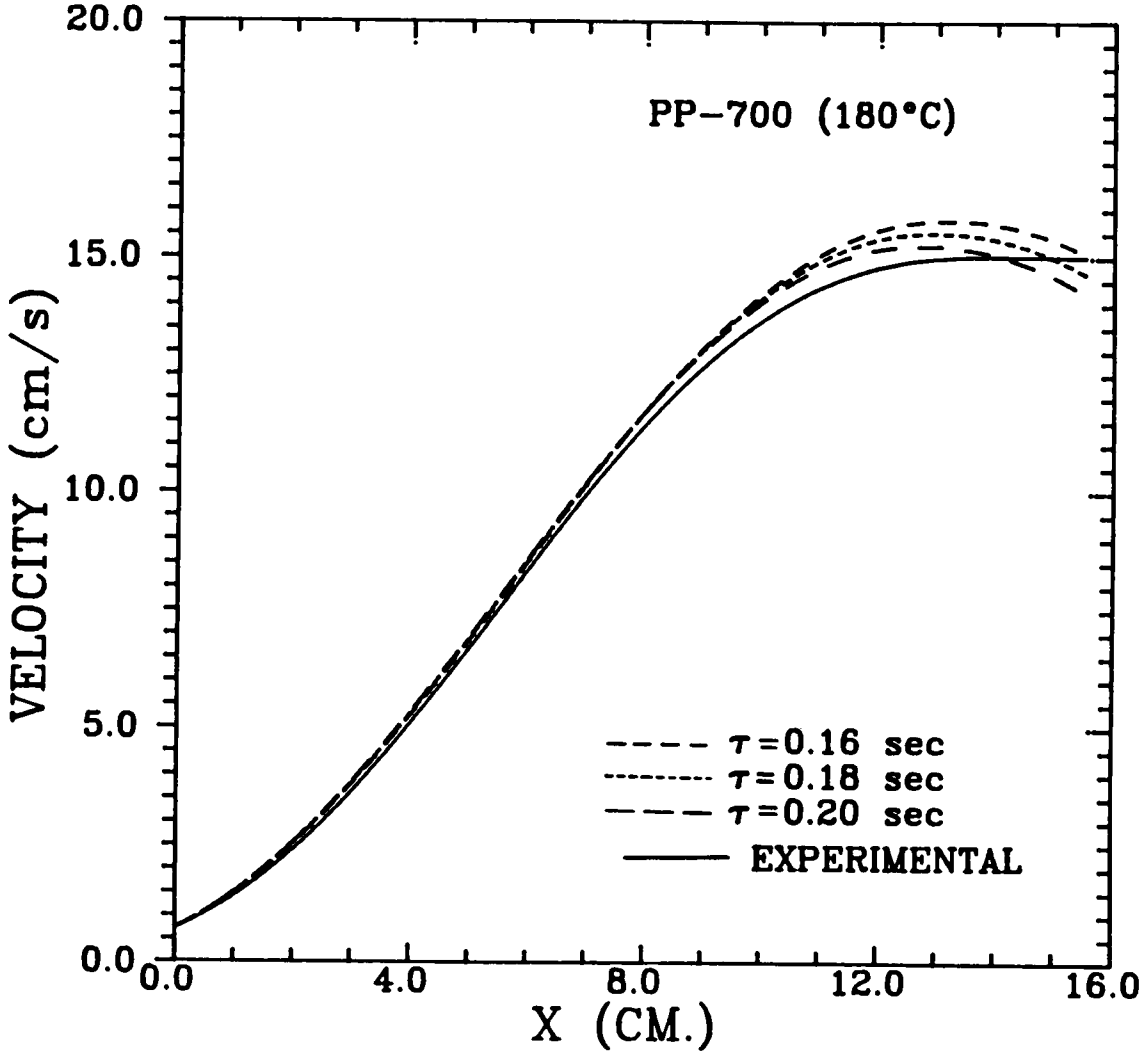


Figure 6.7. Comparison of the experimental data for PP-700 MFR at 180 °C with predictions of the BW model using three different values of average relaxation times and a=0.57.

initial total stress value is varied until desired spinline length is predicted using a zero stress boundary condition. Observe that the model does an excellent job of fitting the elongational data quantitatively. Also observe that out of three values of τ, the value of τ=0.18 sec does the best overall fitting of the elongational data. Note that the elongation rates and hence the apparent elongational viscosities are very sensitive to the accuracy with which the diameter profile is measured. Hence the plot of the apparent elongational viscosity as a function of the elongation rate with a given width of hysteresis loop is a very sensitive way of plotting the fiber spinning data. Higher drawdown ratio was achieved in the case of PP-700 MFR at 180 ^{o}C and the data were most accurate as higher values of elongational rates were achieved; hence the quenched fiber could be removed from the water bath at a desirable take-up velocity apparently without applying a take-up force.

After deciding on an average relaxation time τ=0.18 sec., based on an over-all fits of the elongational data using the BW model, the same value of τ was used for the predictions of the elongational data using the PTT model and the convected Maxwell model. The predictions of the various models as well as the predictions assuming the Newtonian behavior are compared in Figures 6.8 to 6.12 in the form of plots of the apparent elongational viscosity as a function of the elongation rate, the stress profile, the velocity profile, the elongation rate profile and the apparent elongational viscosity profile along the spinline, respectively. Many features of the gravity spinning experiments can be observed in these plots. At the

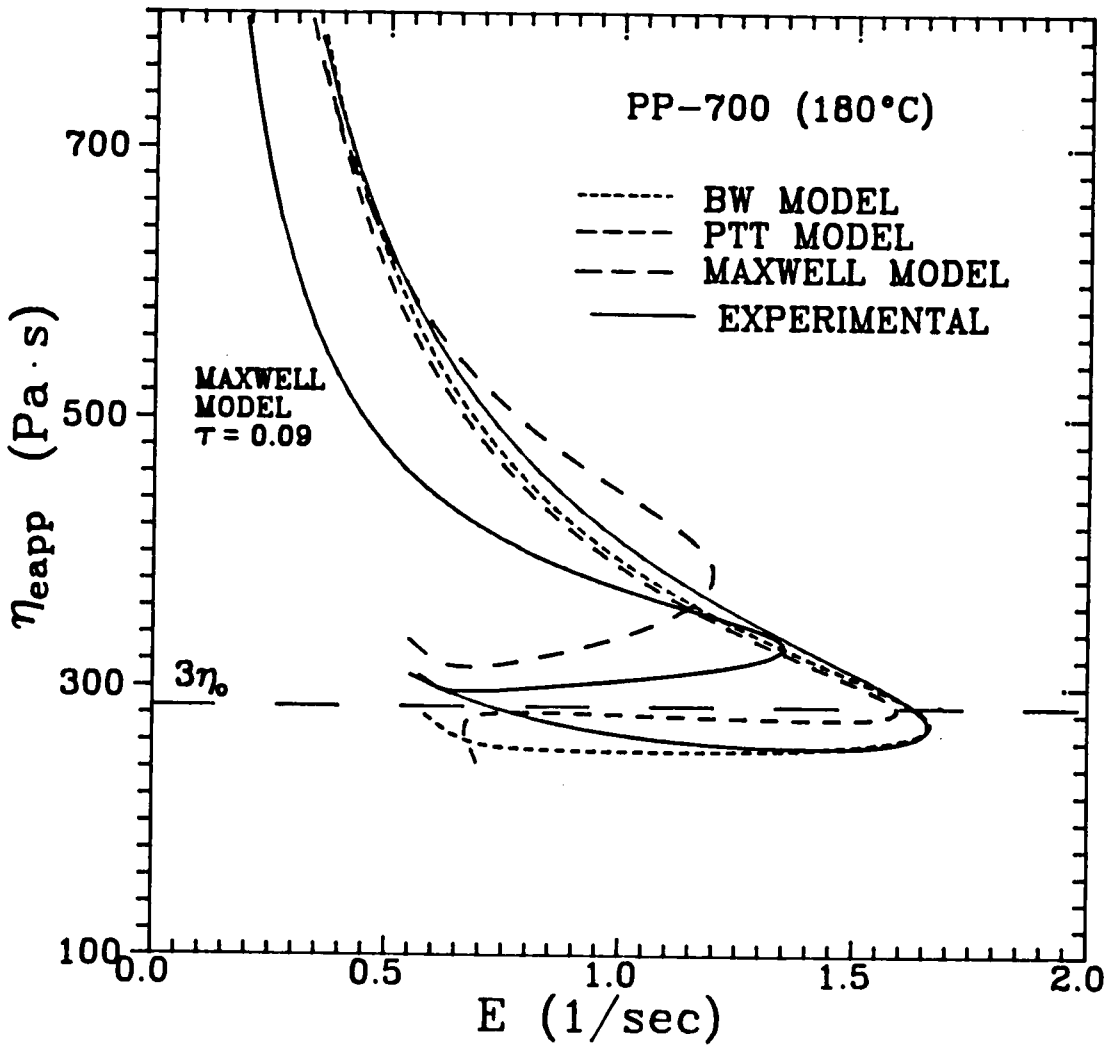


Figure 6.8. Comparison of the experimental data for PP-700 MFR at 180 ^{o}C with the predictions of various models using τ=0.18 sec. Model prediction for the Maxwell model with τ=0.09 sec. is also shown as solid line.

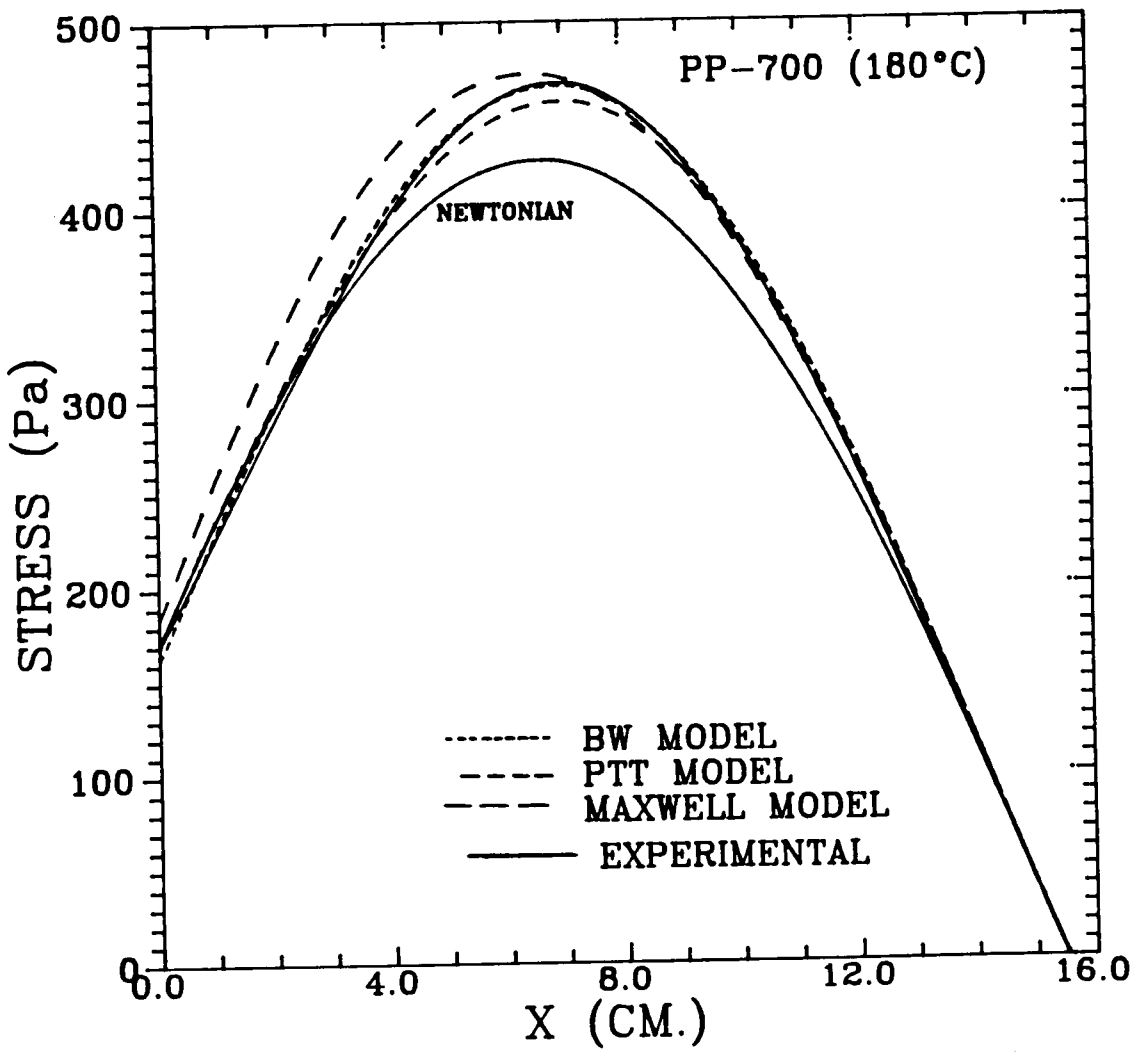


Figure 6.9. Comparison of the experimental data for PP-700 MFR at 180 °C with the predictions of various models using τ=0.18 sec. and with the prediction assuming Newtonian behavior.

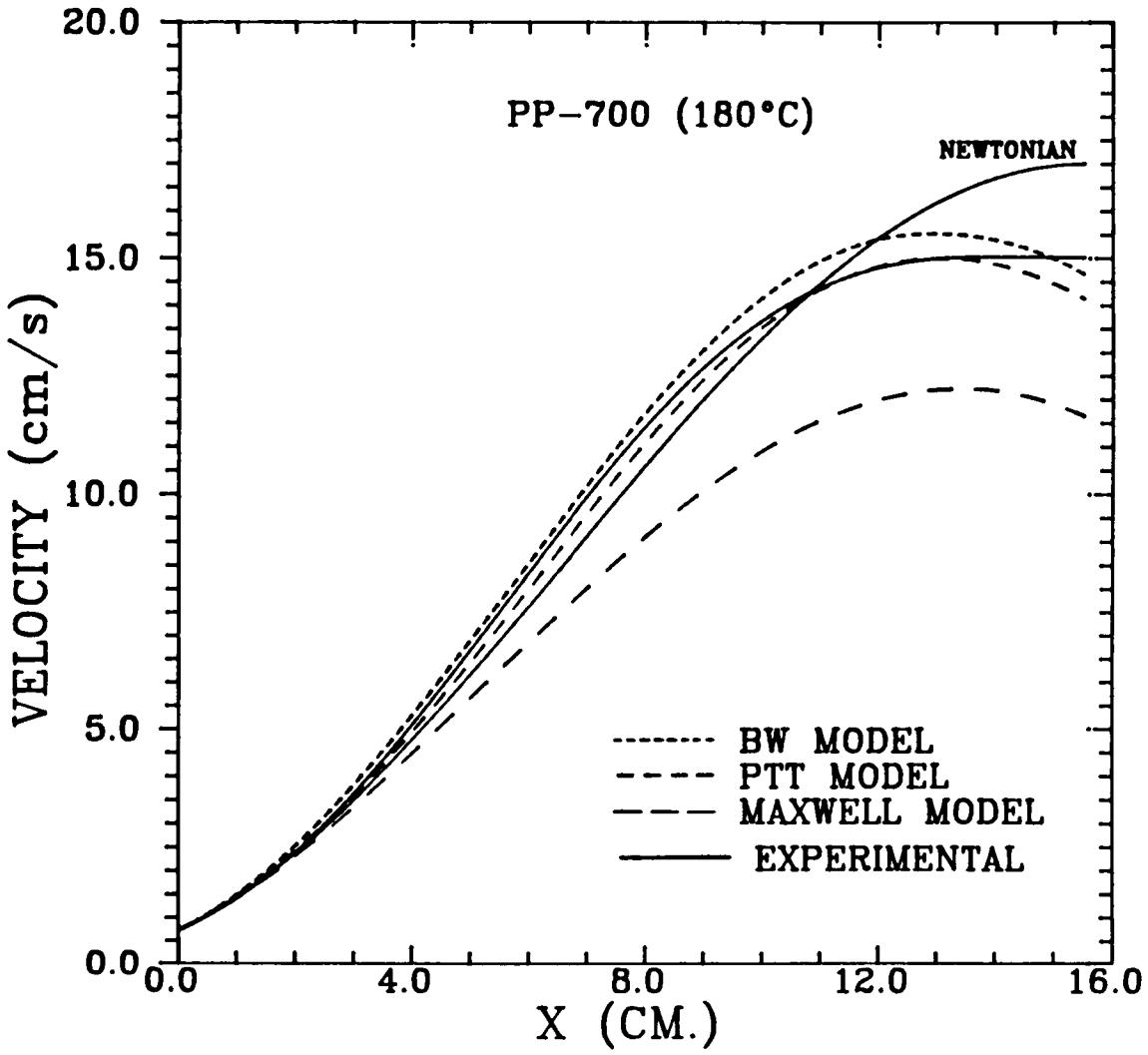


Figure 6.10. Comparison of the experimental data for PP-700 MFR at 180 °C with the predictions of various models using τ=0.18 sec. and with the prediction assuming Newtonian behavior.

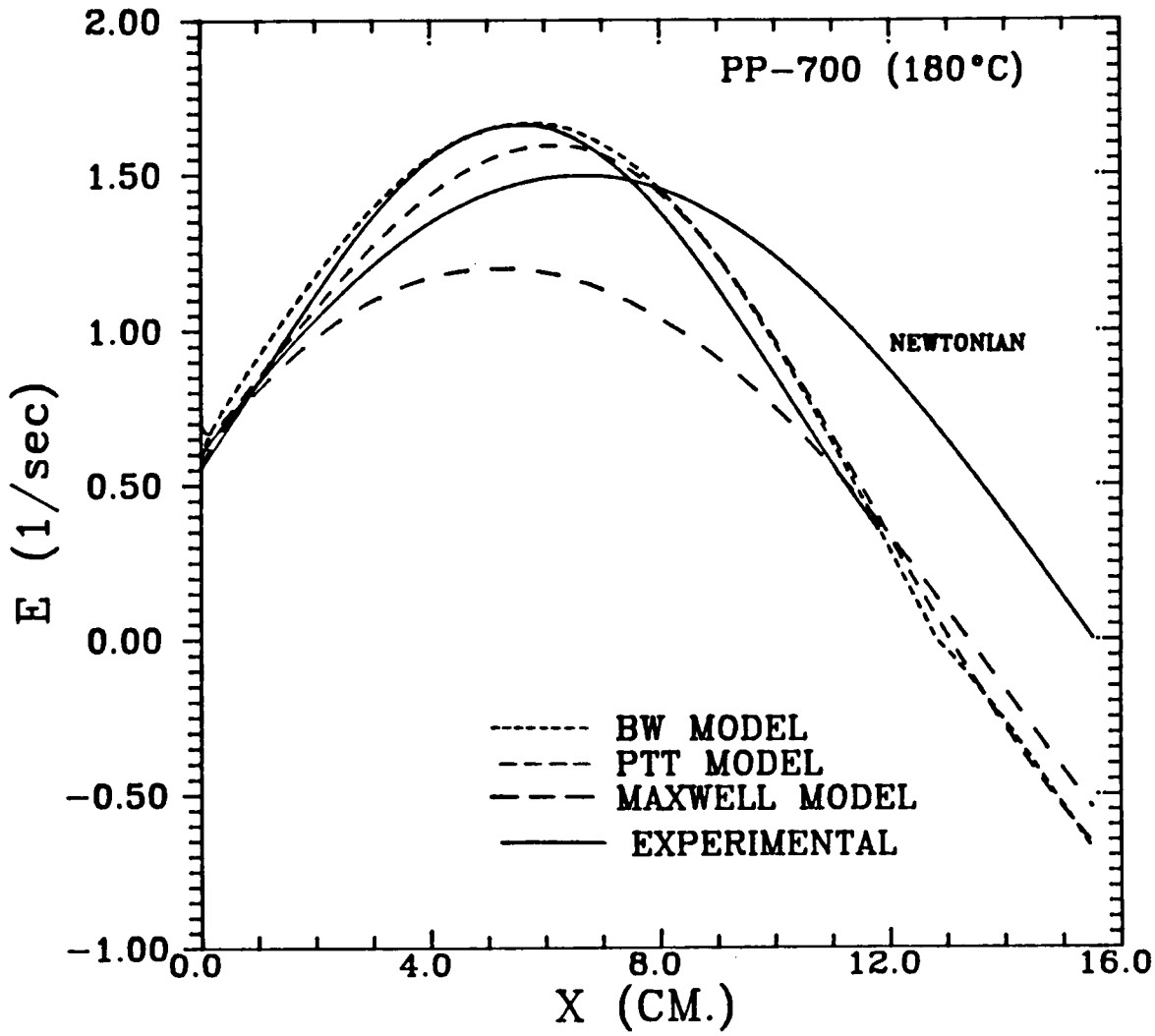


Figure 6.11. Comparison of the experimental data for PP-700 MFR at 180 °C with the predictions of various models using τ=0.18 sec. and with the prediction assuming Newtonian behavior.

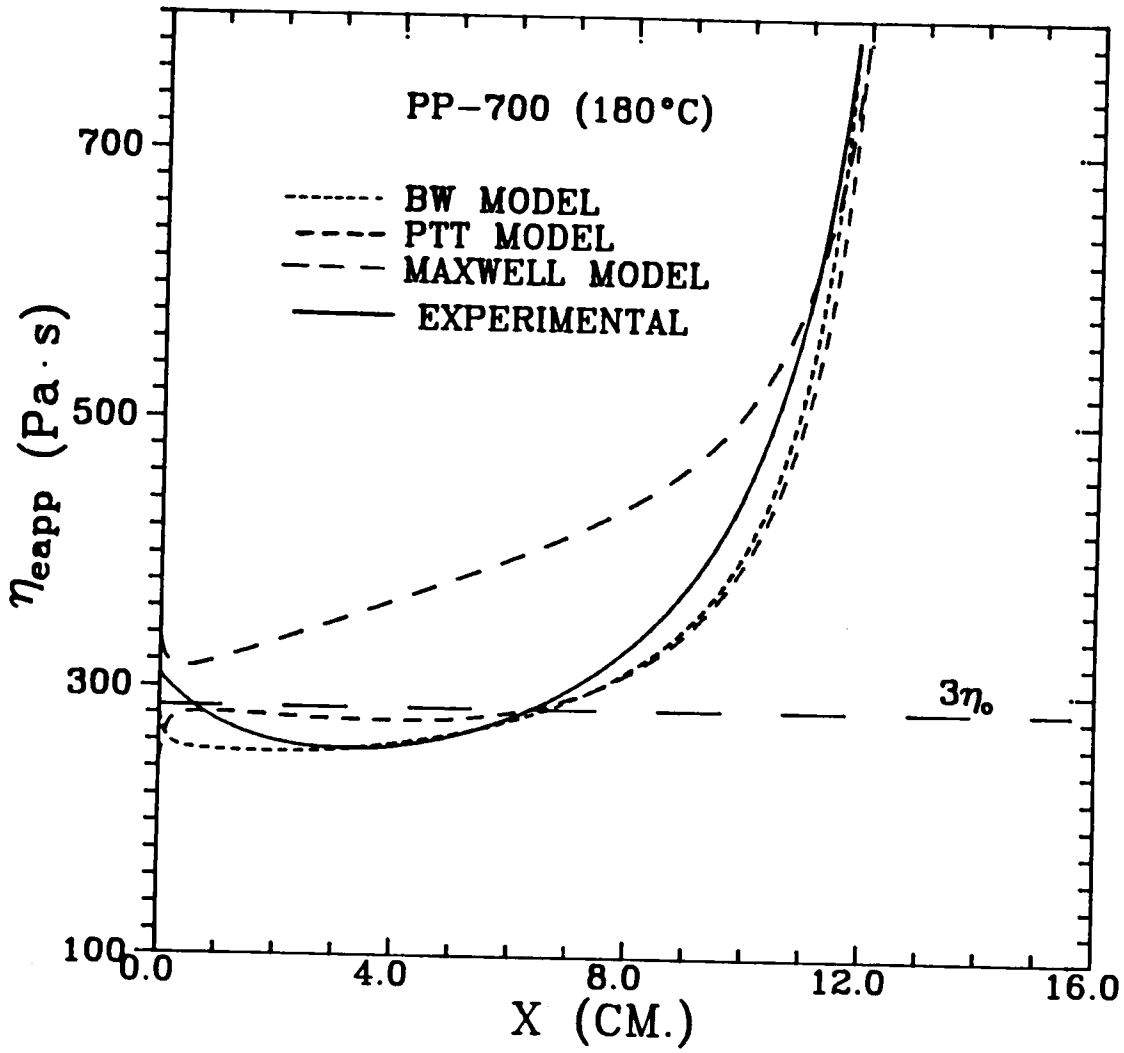


Figure 6.12. Comparison of the experimental data for PP-700 MFR at 180 °C with the predictions of various models using τ=0.18 sec.

outset, it can be observed that the simple one element convected Maxwell model and the Newtonian predictions give poor fits of the experimenatal data; although the convected Maxwell model does predict all the features of the gravity spinning experiments qualitatively. Comparison of the predictions of the convected Maxwell model with the experimental data suggest an elongation thinning model is necessary, e.g. the Bogue-White model which is the convected Maxwell model with the deformation rate dependent relaxation times. Note that the apparent elongational viscosities before the upturn are close to three times the zero shear Newtonian viscosity. The PTT model (=0.4 and ε=0.72) gives reasonable overall fits of the experimental data, although the lower hysteresis width predicted by the PTT model (due to lower effective relaxation time) suggests that an even higher value of the average relaxation time could be used to fit the experimental data. The value of 0.72 used for ε is very high compared to the literature value of 0.015 (25,26) used for polyethylene for a constant force spinline. This high value of ε seems reasonable for gravity spinning experiments as much lower spinline stresses are involved; hence high value of ε is necessary to get required "thinning" in the PTT model (which can be regarded as the convected Maxwell model with the stress dependent relaxation times). It is apparent from Figures 6.4, 6.5 and 6.8 that constitutive equations with finite relaxation times do predict the hysteresis loop; the higher the value of the effective relaxation time, the larger the width. This is due to the finite but fading "memory" of polymeric melts and therefore the stress depends not only

on the instantaneous strain rate but also on the entire deformation history.

The velocity profiles (see Figure 6.10) predicted by these models are sigmoidal in shape and the predicted elongation rates (see Figure 6.11) go through a maximum, as was observed experimentally. The models also predict the decrease in the velocity with a corresponding "swelling" of diameter towards the end of the spinline. This is due to the zero stress boundary condition at the end of the spinline, as mentioned before. The theoretical Newtonian take-up velocity is higher than the experimental value, although the theoretically predicted Newtonian elongation rates were lower than the experimental values in the first half of the spinline. This suggests a material behaving like a thin fluid in the first half of the spinline (giving higher than the Newtonian drawdown prediction) and a material behaving more like an elastic solid (having the apparent viscosity increasing with decreasing elongation rate) in the bottom half of the spinline.

The plot of the apparent elongational viscosity versus spinline distance (see Figure 6.12) shows that the apparent elongational viscosity first decreases but then go on increasing along the spinline (except when it becomes negative due to negative elongation rates very near the end of the spinline). This is a feature of any stable spinline i.e. the apparent elongational viscosity must increase after some point for a spinline to be a stable one. For an unstable gravity spinline, any model predicts a decreasing elongational viscosity along the spinline with increasing elongation

rates until a convergence in computation is no longer attained. The same features were also observed while modelling a constant force spinline (where gravity, drag and inertial forces are neglected) and are also reported in the literature (77).

Since the Bogue-White model and the PTT model gave similar predictions for the gravity spinning experiments, the simpler of the two, the Bogue-White model, will be used for the subsequent computations.

All of the above model predictions were based on a zero stress boundary condition, which must be the case for gravity spinning experiments without a take-up force. For Newtonian behavior, this boundary condition also corresponds to a zero elongation rate at the end of the spinline. The BW model predictions using the zero stress and the zero elongation rate boundary condition for PP-700 MFR at 180 ^{o}C are shown in Figures 6.13 and 6.14. It is apparent from the plots that the predictions using the zero stress boundary condition matches the experimental data much better than the predictions using the zero elongation rate boundary condition. Experimentally, the force at any point in the spinline was computed using the weight of the threadline below that point based on the measured diameter profile. This would result in a zero force and hence a zero stress at the end of the gravity spinline. In the case of polymer melts, a zero stress at the end of the spinline would require stress relaxation, resulting in a negative velocity gradient towards the end of the spinline. The condition of zero elongation rate could be achieved by applying an external take-up force but it would be difficult to ascertain that

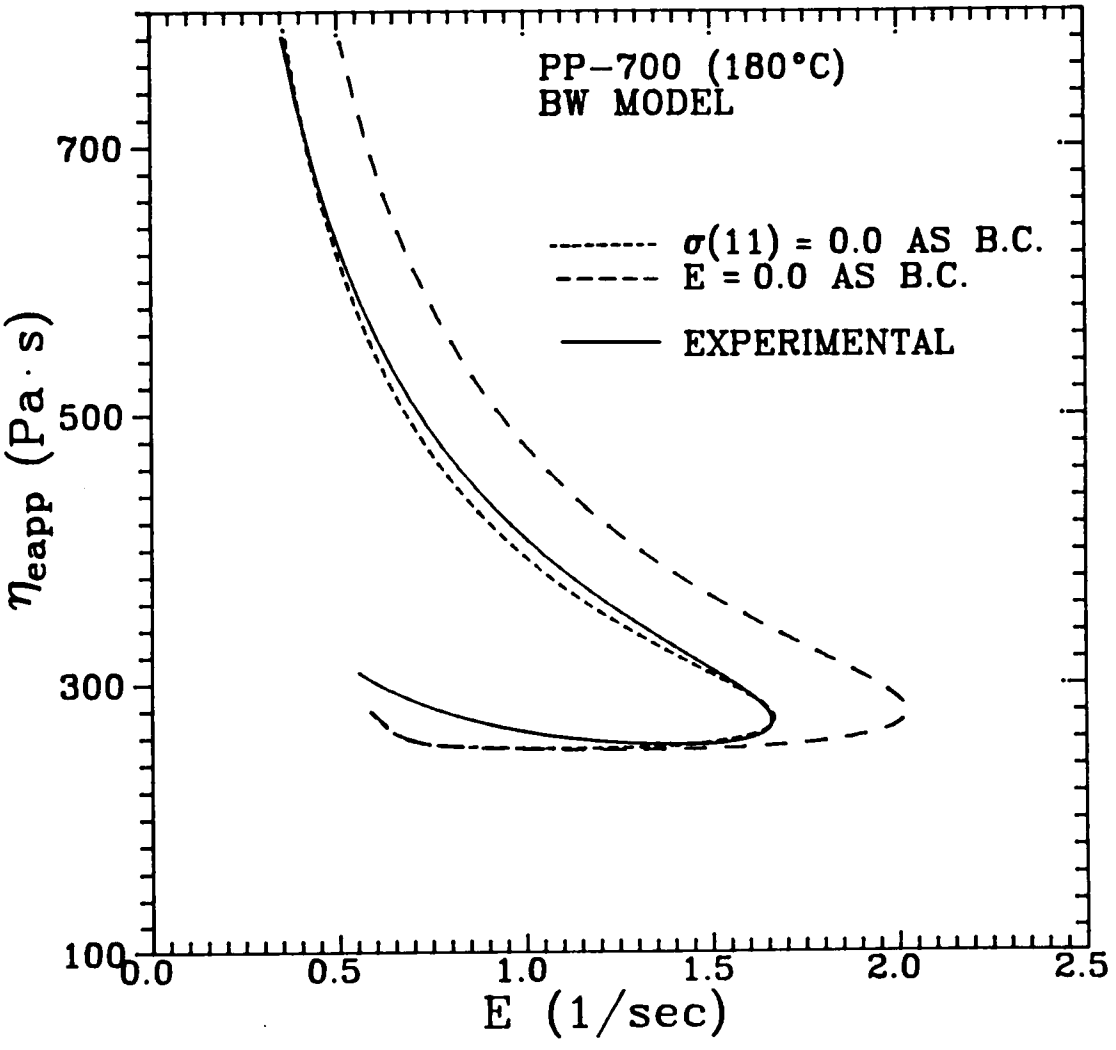


Figure 6.13. Comparison of the experimental data for PP-700 MFR at 180 °C with the BW model predictions using two different boundary conditions.

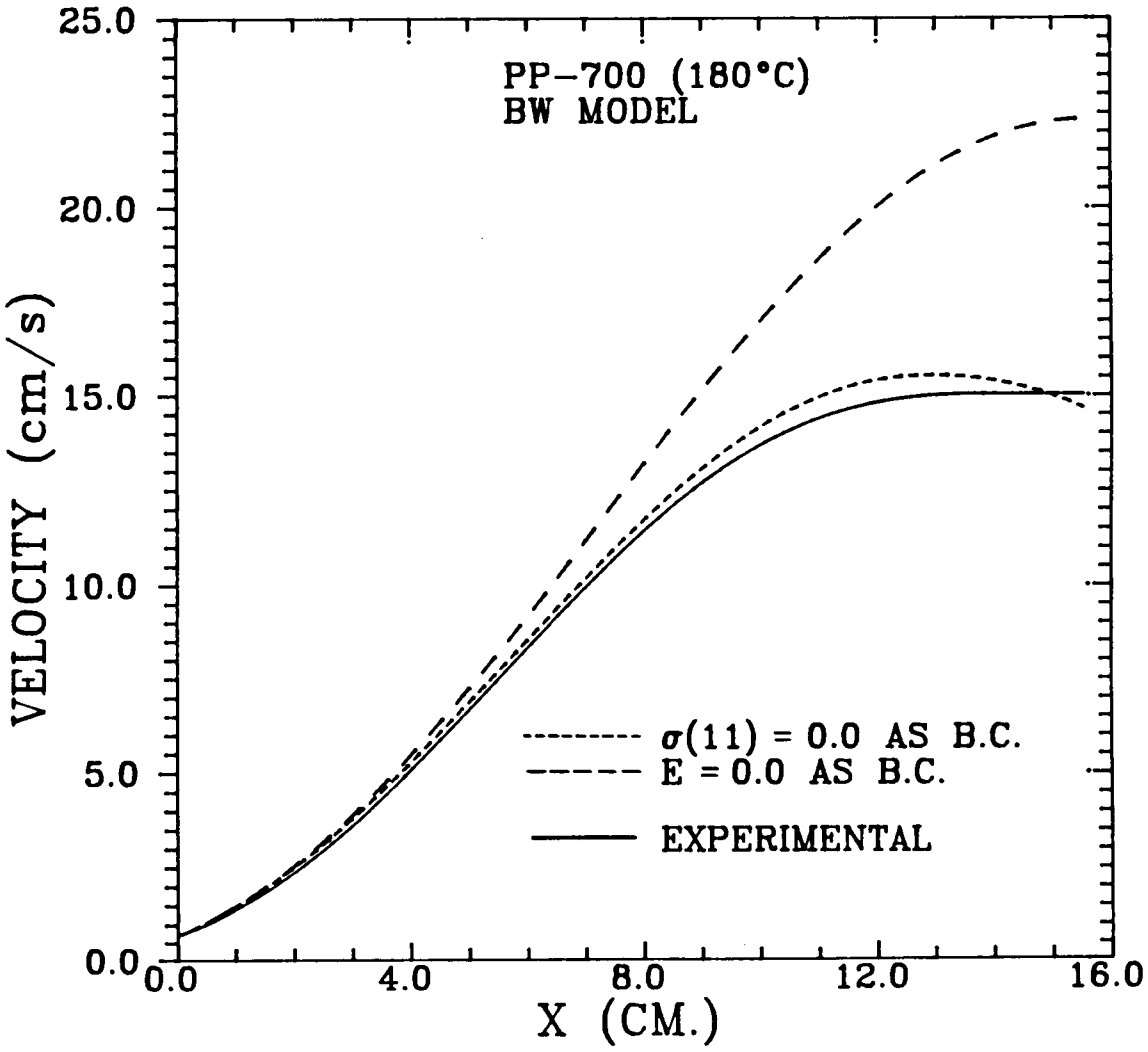


Figure 6.14. Comparison of the experimental data for PP-700 MFR at 180 ^{o}C with the BW model predictions using two different boundary conditions.

this condition is achieved and it would not be possible to measure the associated small take-up force. Experimentally it is possible to achieve a zero stress boundary condition by lowering the take-up velocity until any further reduction causes an accumulation (pile-up) of material on the water bath. However, a spinline running under this condition tends to vibrate significantly and may break.

The predictions of the Bogue-White model (τ=0.08 sec. and a=0.55) in the form of plots of the apparent elongational viscosity versus the elongation rate, the stress profile and the velocity profile for PP-1400 MFR at 180 ^{o}C are shown in Figures 6.15, 6.16 and 6.17, respectively. The model predictions are compared with the experimental data and the Newtonian predictions. Note that the same value of "a" is used as obtained by fitting the shear data. Observe that the apparent elongational viscosity before the upturn is about three times the zero shear viscosity. Comparison of the experimental data with the Newtonian prediction suggest that material behaved close to a Newtonian behavior. Note that (see Figure 6.15) very small take-up force might have been applied resulting in the discrepancies between the model prediction and experimental data in the bottom half of the spinline. Even a tiny take-up forces that may have been applied to minimize vibrations of spinline would have noticeable effects in the bottom half of the spinline where gravity forces due to hanging threadline weight are already small.

If larger take-up forces are applied and are not accounted for, a "reverse" hysteresis loops can be obtained in the plot of the apparent elongational viscosity versus elongation rate as was

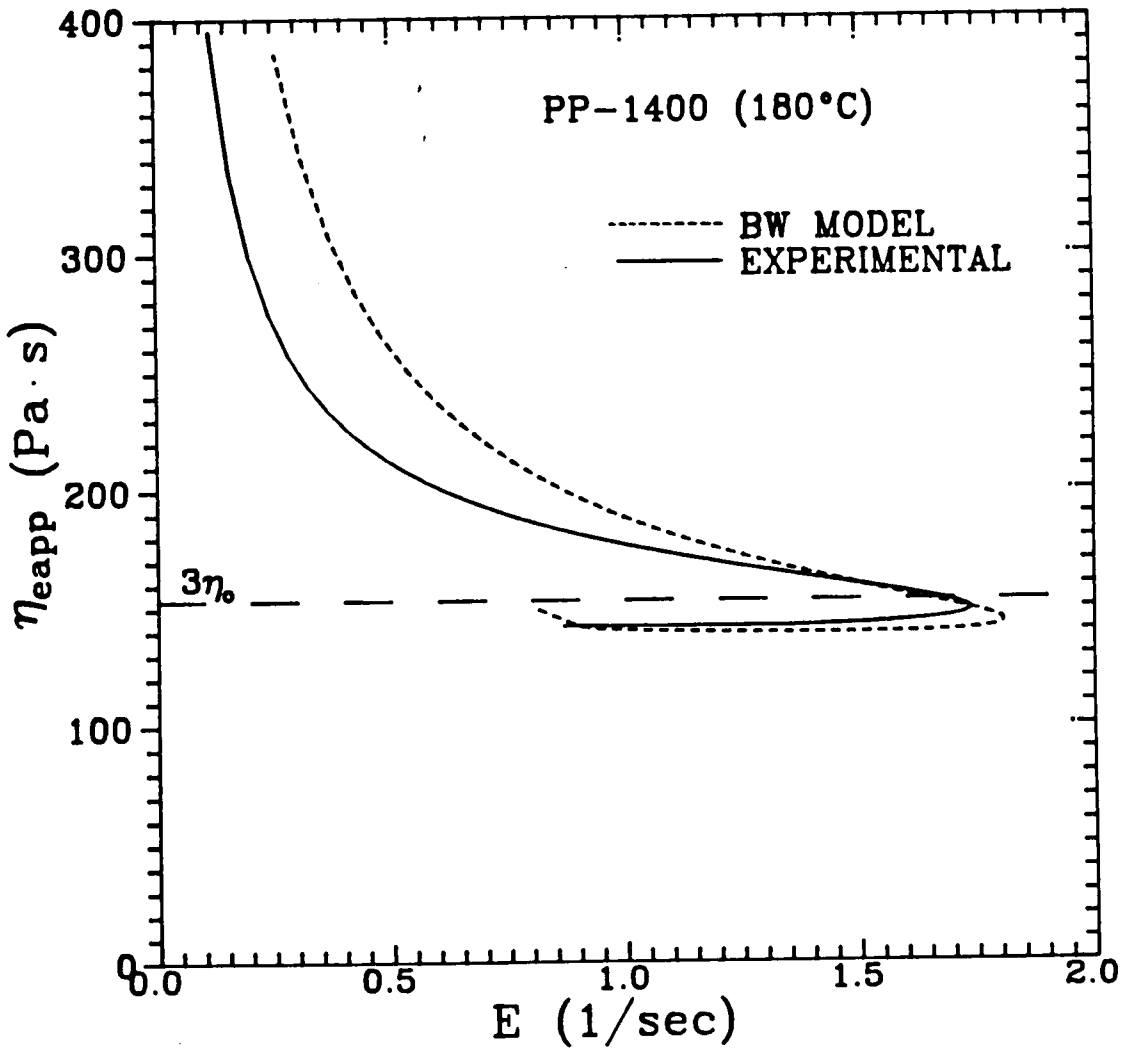


Figure 6.15. Comparison of the experimental data for PP-1400 MFR at 180 °C with the predictions of the BW model using τ=0.08 sec. and a=0.55.

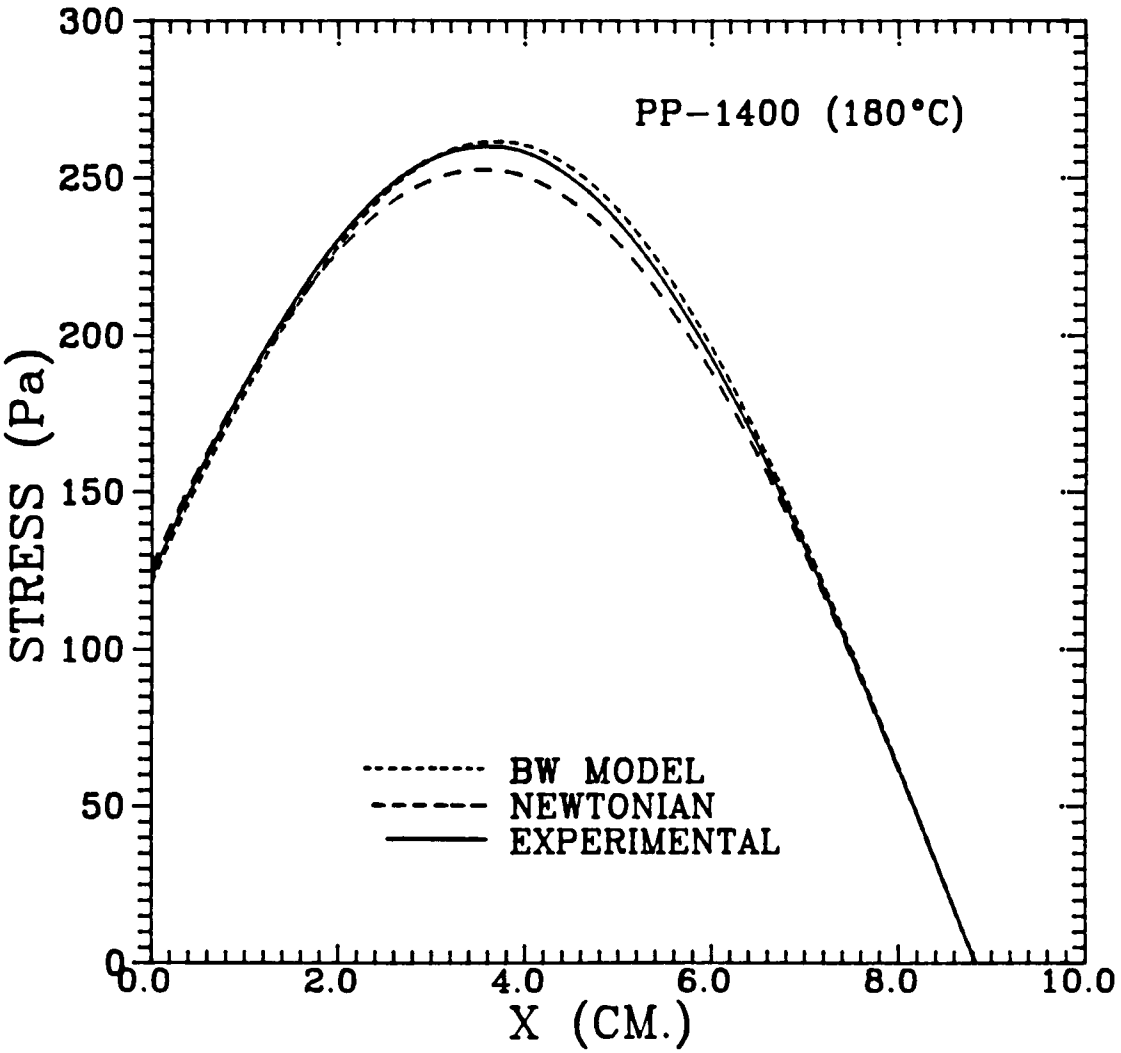


Figure 6.16. Comparison of the experimental data for PP-1400 MFR at 180 ^{o}C with the predictions of the BW model using τ=0.08 sec. and a=0.55 and the predictions assuming Newtonian behavior.

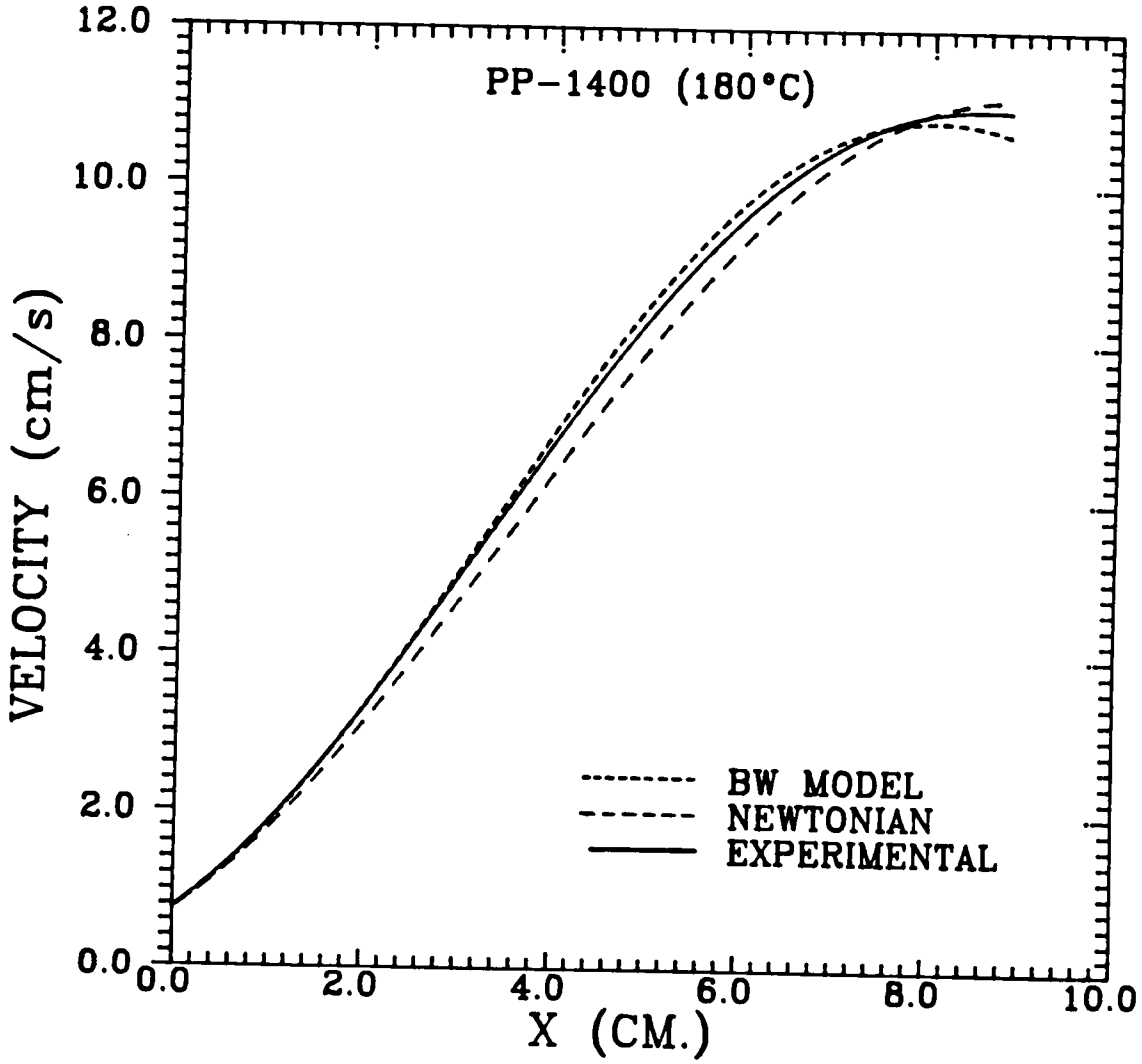


Figure 6.17. Comparison of the experimental data for PP-1400 MFR at 180 °C with the predictions of the BW model using τ=0.08 sec. and a=0.55 and the predictions assuming Newtonian behavior.

observed in the case of PP-300 MFR at 180 ^{o}C (see Figure 5.13). This unknown take-up forces can be estimated with the help of any suitable rheological models. A rheological constitutive equation does predict this reverse loop, if a non-zero stress boundary condition is used and the corresponding take-up force is subtracted from the force predicted by the model at each point along the spinline (as the take-up force was not accounted for when calculating the force from the measured diameter profile). The model predictions (using τ=0.45 sec. and a=1.1) based on an estimated take-up force of 4.0 dyne when applied to the spinline (giving corresponding nonzero stress boundary condition) and not accounted for (by subtracting it from the model predictions) quantitatively fits the experimental data as seen in Figures 6.18 and 6.19. Note that the observed "reverse" loop for PP-300 MFR at 180 ^{o}C at the take-up velocity of 12.5 cm./s is predicted by the BW model as shown in Figure 6.18. Note that a higher value of thinning parameter "a" is used (compared to the value of about 0.75 obtained by fitting the shear data) as is necessary for quantitative fits.

A run with a lower take-up velocity (= 10.3 cm/sec) was also carried out for PP-300 MFR at 180 ^{o}C. It was possible to reduce the take-up velocity little further (leading closer to a zero stress condition at the end of the spinline) but the run resulted in significant spinline vibrations and subsequent breaking of the spinline as it touched the chamber. Also due to the limitations of the take-up device it was not possible to keep precise constant take-up velocity. Hence, take-up velocity was kept a little higher to

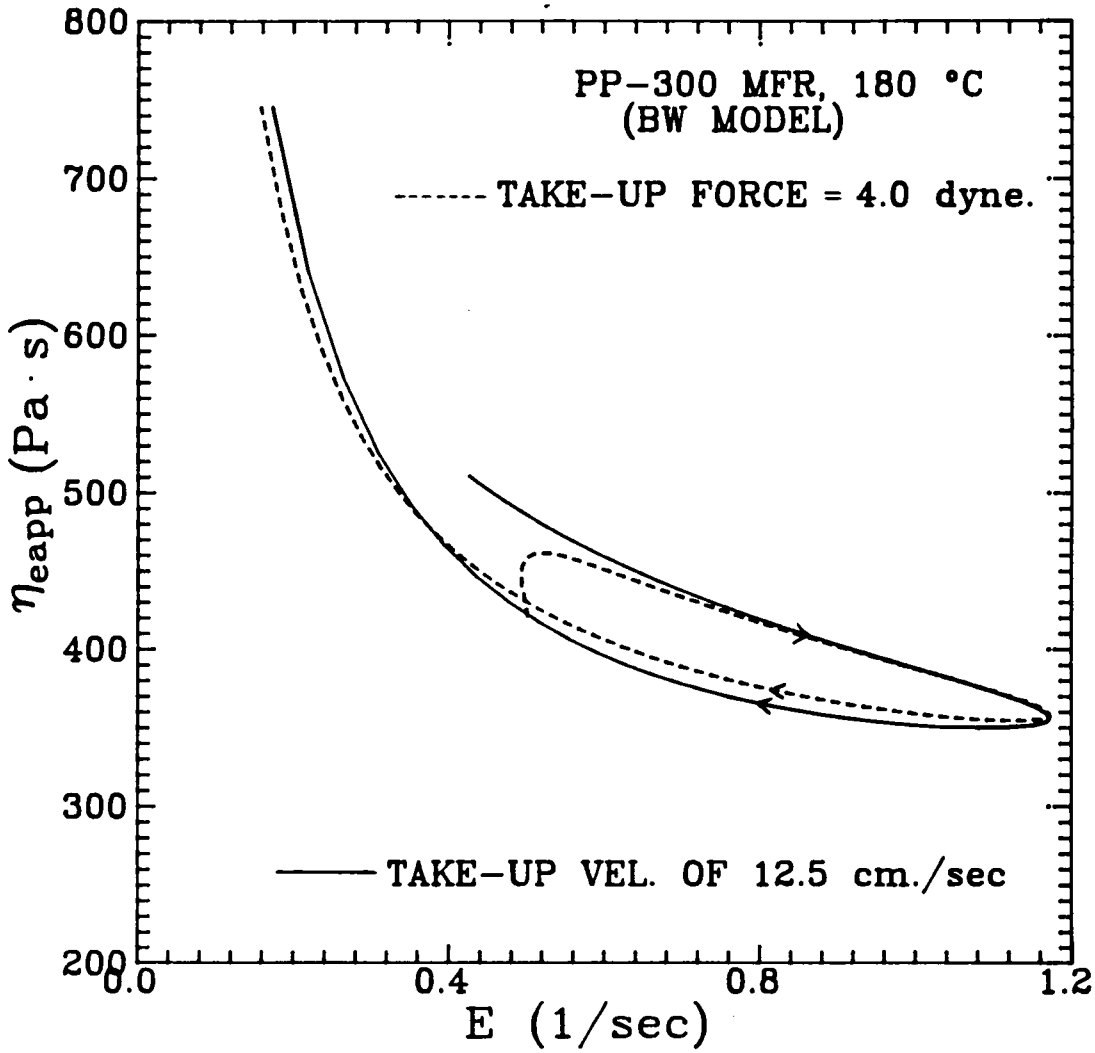


Figure 6.18. Comparison of the experimental data (solid line) for PP-300 MFR at 180 °C at the take-up velocity of 12.5 cm./sec with the predictions of the BW model (dashed line) using τ=0.45 sec. and a=1.1 and subtracting an estimated take-up force of 4.0 dyne from the model predictions.

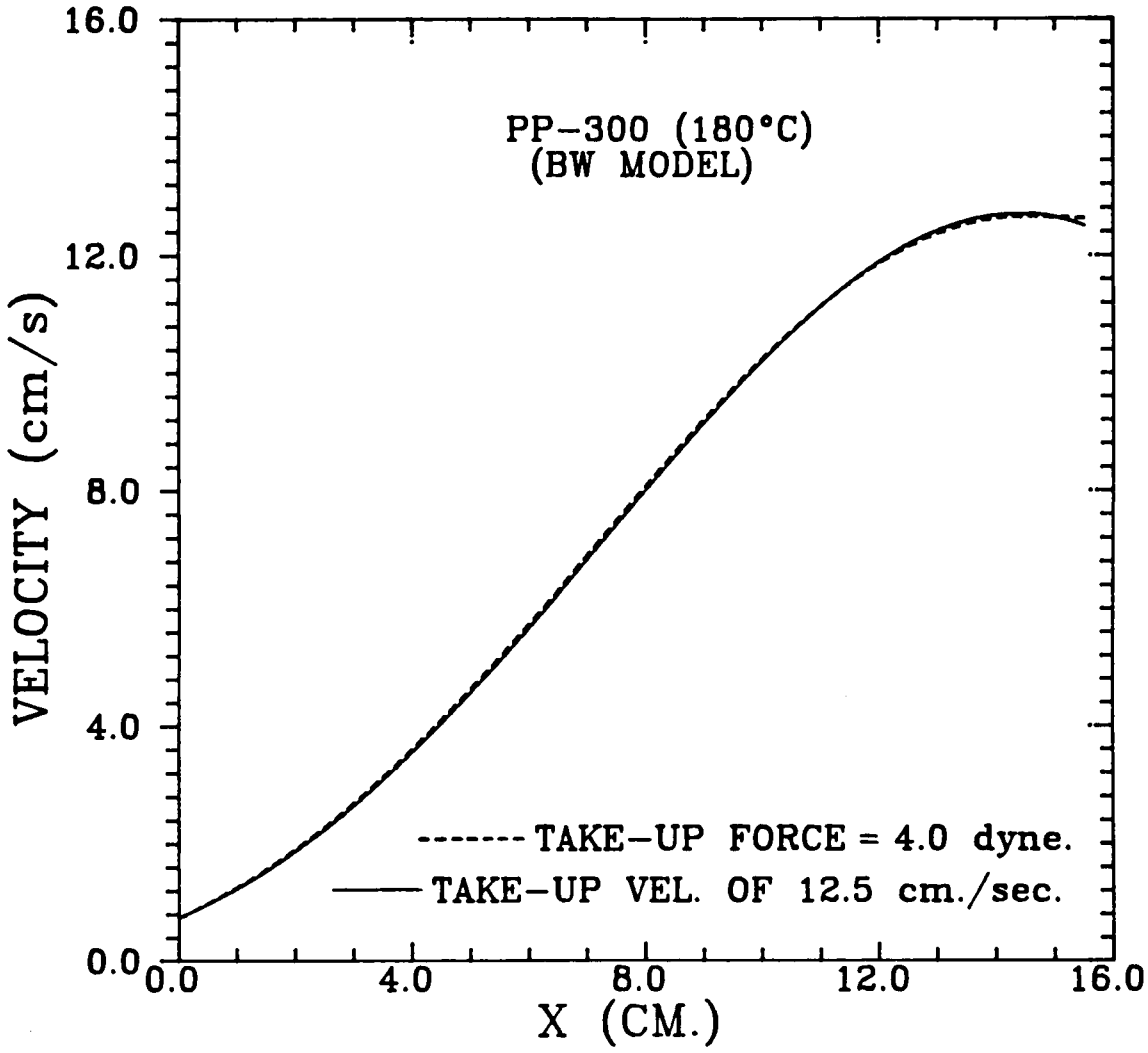


Figure 6.19. Comparison of the experimental data (solid line) for PP-300 MFR at 180 °C at the take-up velocity of 12.5 cm./sec with the predictions of the BW model (dashed line) using τ=0.45 sec. and a=1.1 and subtracting an estimated take-up force of 4.0 dyne from the model predictions.

minimize vibrations in the spinline. The data when plotted with the apparent elongational viscosity versus the elongation rate gave the usual but a narrow hysteresis loop as expected (as the take-up forces were not accouned for) (see Figure 5.11). While predicting the reverse hysteresis loop, the unknown take-up force was estimated and subtracted from force prediction at each point to match the model prediction with the data which did not take into account the applied take-up force. In this case the predictions of the BW model with a non-zero stress boundary condition (corresponding to an estimated take-up force) are compared with the experimental data, but now taking into account the same estimated take-up force ("retreated" data). The BW model predictions with a non-zero stress boundary condition are compared the experimental data with (retreated data) and without taking into account the applied take-up force in Figures 6.20 and 6.21. Note that the measured kinematics (velocity and elongation rate profile) already reflects to the given force condition (with the applied take-up force) in the spinline. So while treating the experimental data, the applied take-up force should have been accounted for. Observe that the width of the hysteresis loop is larger when the applied take-up force is accounted for. The model predictions match the retreated experimental data reasonably well. In the same plots, the model predictions with the zero stress boundary condition (corresponding to a "pure" gravity spinning experiment) are shown. The difference in the take-up velocity predictions with and without applied take-up force was in resonably good agreement with the experimental observation. Observe that the

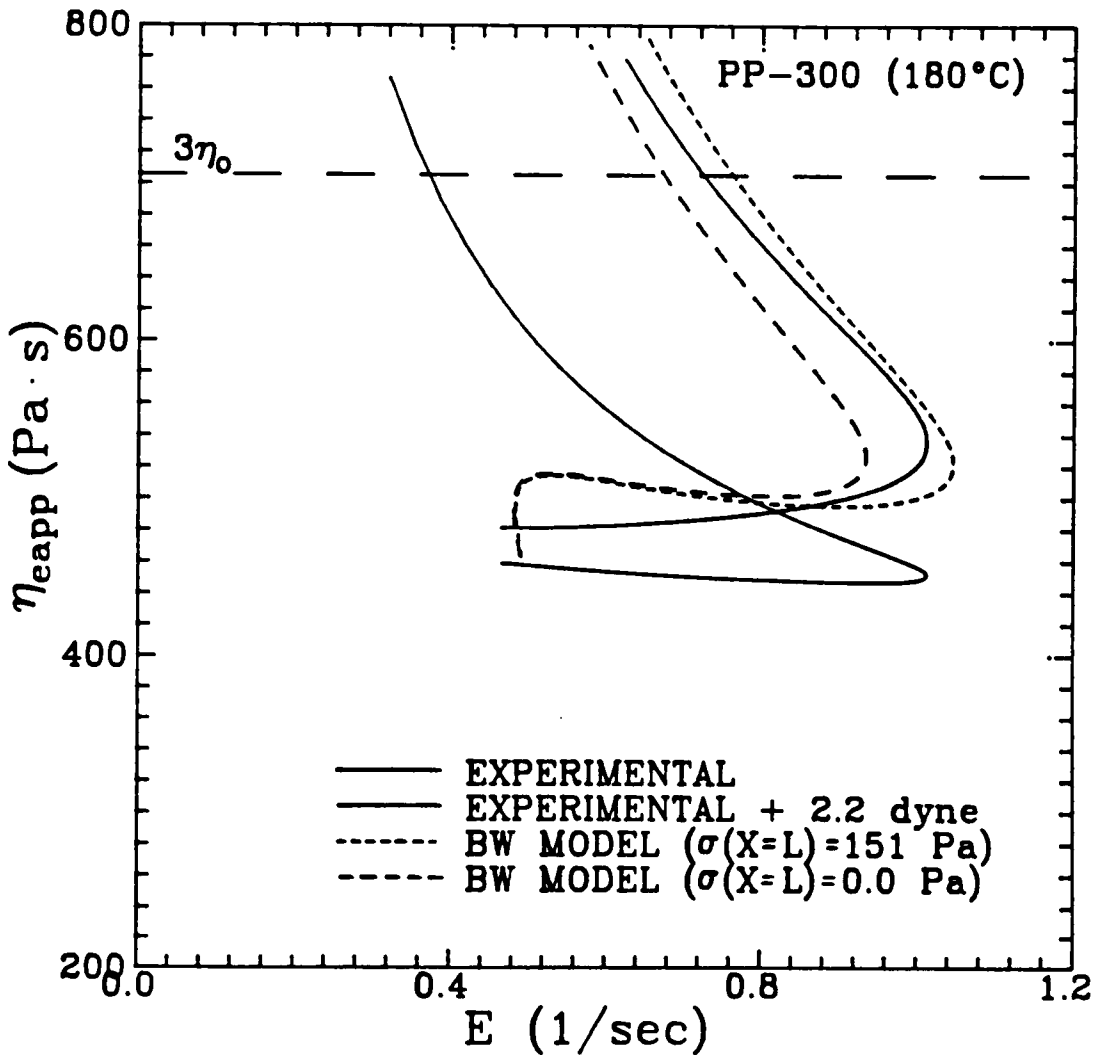


Figure 6.20. Comparison of the experimental data for PP-300 MFR at 180 °C at the take-up velocity of 10.3 cm./sec with the predictions of BW model using τ=0.45 sec. and a=1.1.

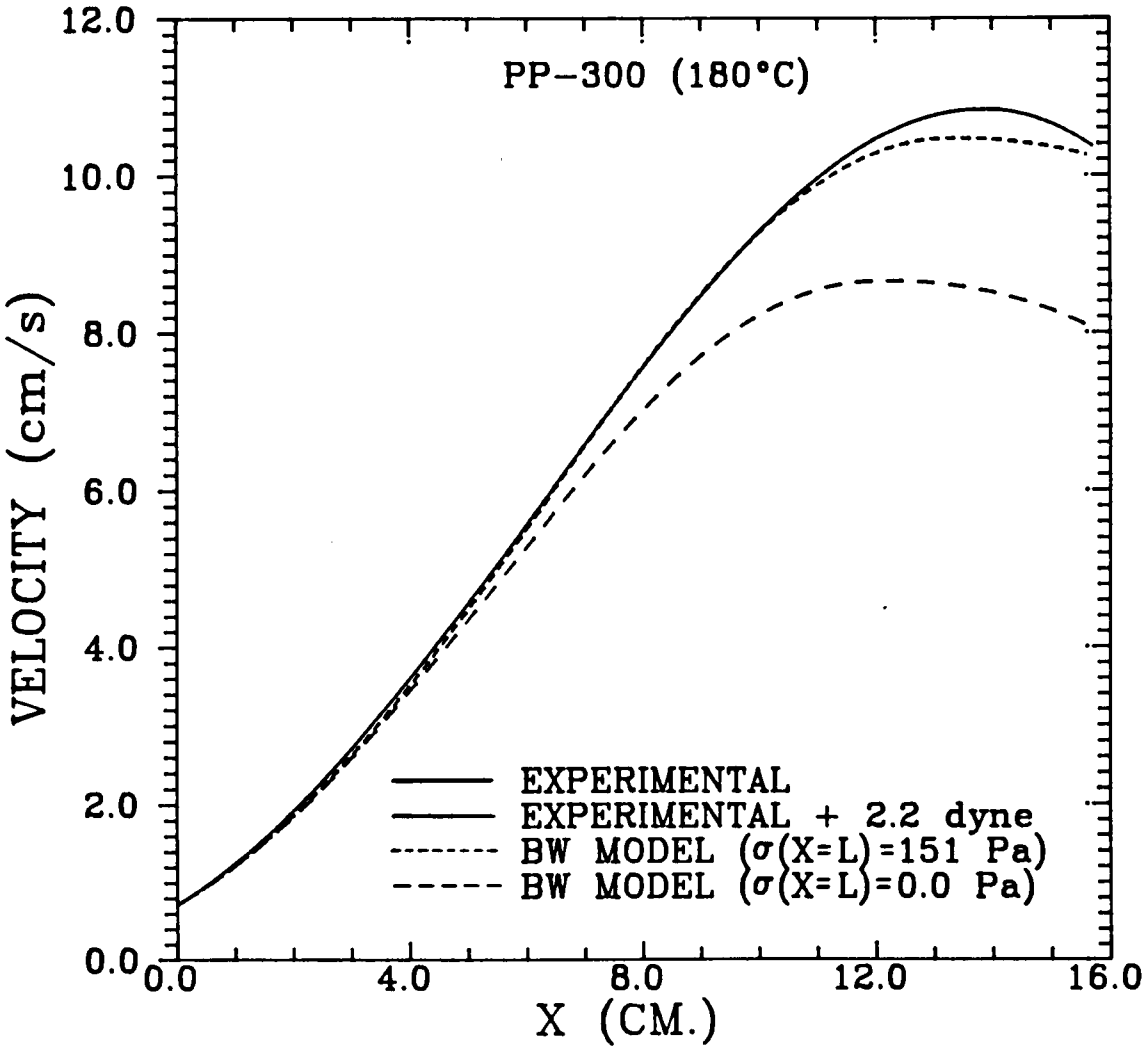


Figure 6.21. Comparison of the experimental data for PP-300 MFR at 180 °C at the take-up velocity of 10.3 cm./sec with the predictions of BW model using τ=0.45 sec. and a=1.1.

apparent elongational viscosity in the upper part of the spinline is lower than three times the zero-shear viscosity. Note that the corresponding results for PP-700 MFR and PP-1400 MFR were close to three times their zero-shear viscosities.

For modelling the elongational flow data of PP-1400 MFR and PP-700 MFR at 180 ^{o}C, T_{11}/T_{22} ratio was assumed to be zero while for PP-300 MFR, the ratio was assumed to be -0.5. Note that this ratio lies between 0 to -0.5 (71) as mentioned before. The model predictions for PP-300 MFR at 180 ^{o}C with the same non-zero stress boundary condition, but now using $T_{11}/T_{22} = 0$, are shown in Figure 6.22. The predictions are compared with those using the ratio of -0.5 and the retreated experimental data. It can be observed that even for the extreme values of the ratio of T_{11}/T_{22} for this most elastic material studied, model predictions are almost same except in the initial part of the spinline. The value of -0.5 for the ratio give somewhat better agreement with the experimental data in the initial part of the spinline. This ratio of the radial to the axial extra stresses probably reflects the die-flow effects on the subsequent spinning dynamics. For less elastic materials (having very low τ values) as in the case of PP-1400 MFR, the model predictions with the extreme values of the ratio are identical as shown in Figure 6.23. Hence, the model predictions are insentitive to any particular value of the ratio assumed.

The Bogue-White model predictions (τ=0.22 sec. and a=1.1) for PP-300 MFR at 200 ^{o}C are shown in Figures 6.24 and 6.25. Note that the same value of "a" is used as used for fitting the data of PP-300

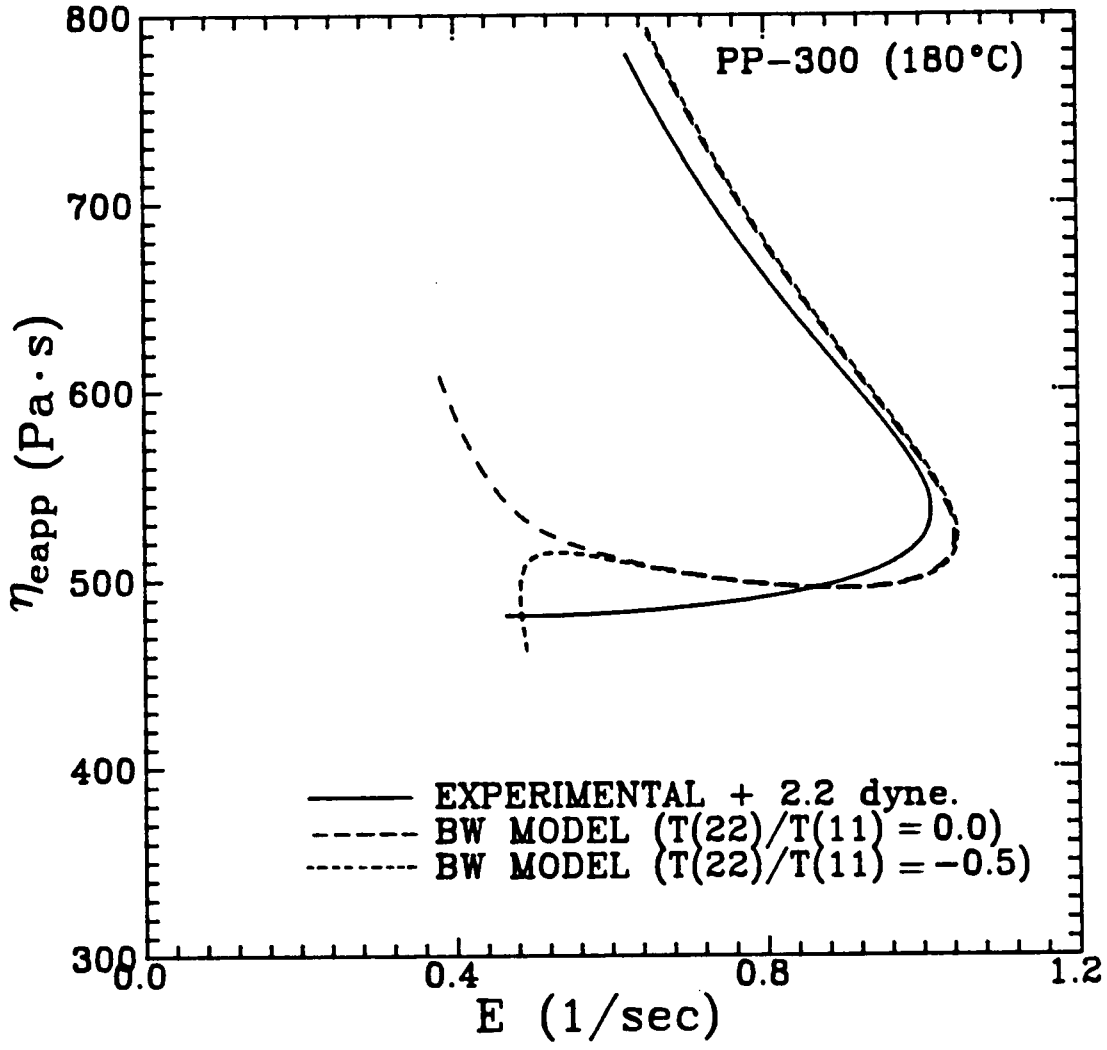


Figure 6.22. Comparison of the experimental data for PP-300 MFR at 180 °C at the take-up velocity of 10.3 with taking into account small estimated take-up forces with the BW model predictions using extreme values of (T_{11}/T_{22}) ratio (τ=0.45 sec. and a=1.1).

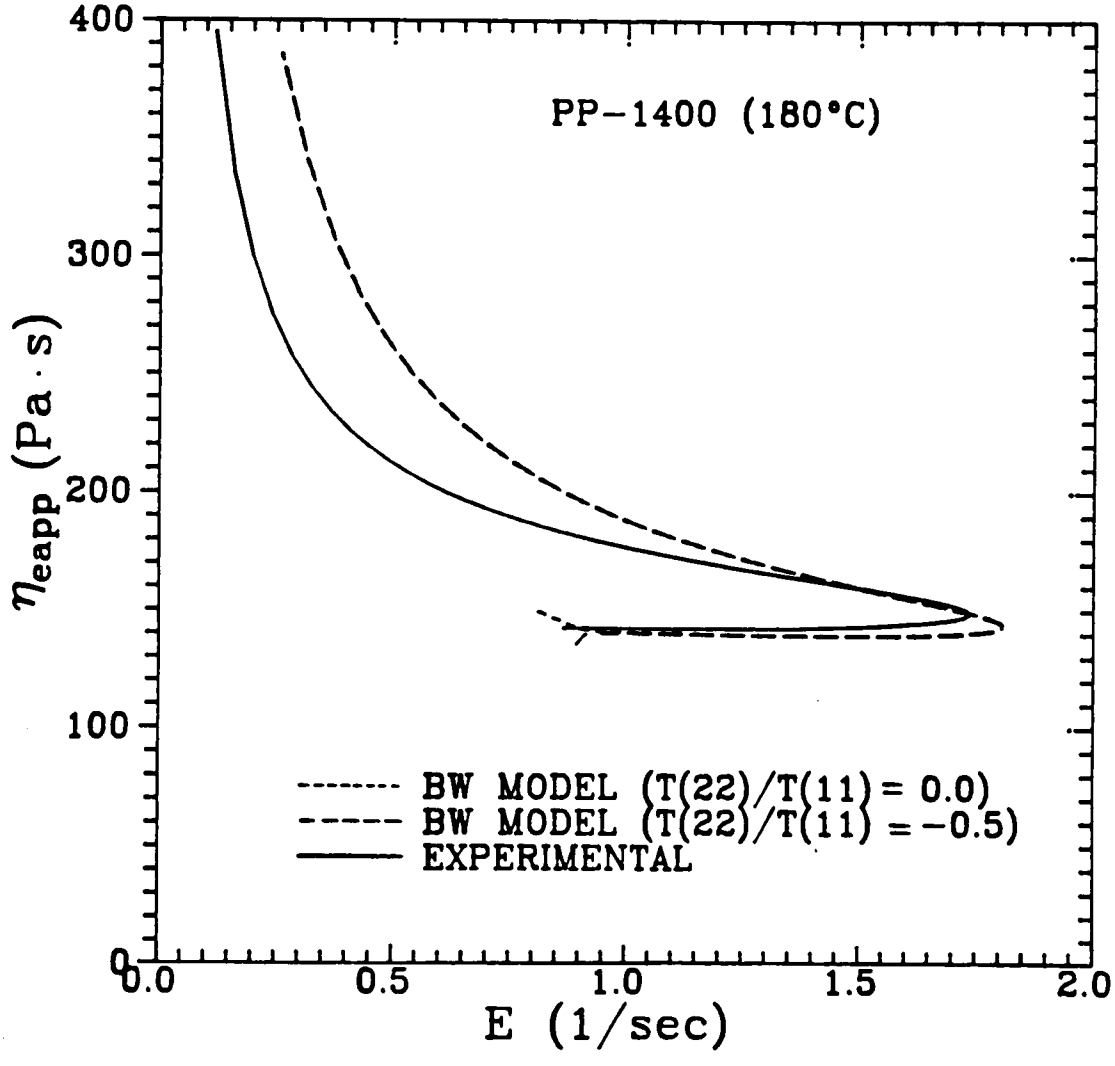


Figure 6.23. Comparison of the experimental data for PP-1400 MFR at 180 °C with the predictions of the BW model using extreme values of (T_{11}/T_{22}) ratio (τ=0.08 sec. and a=0.55).

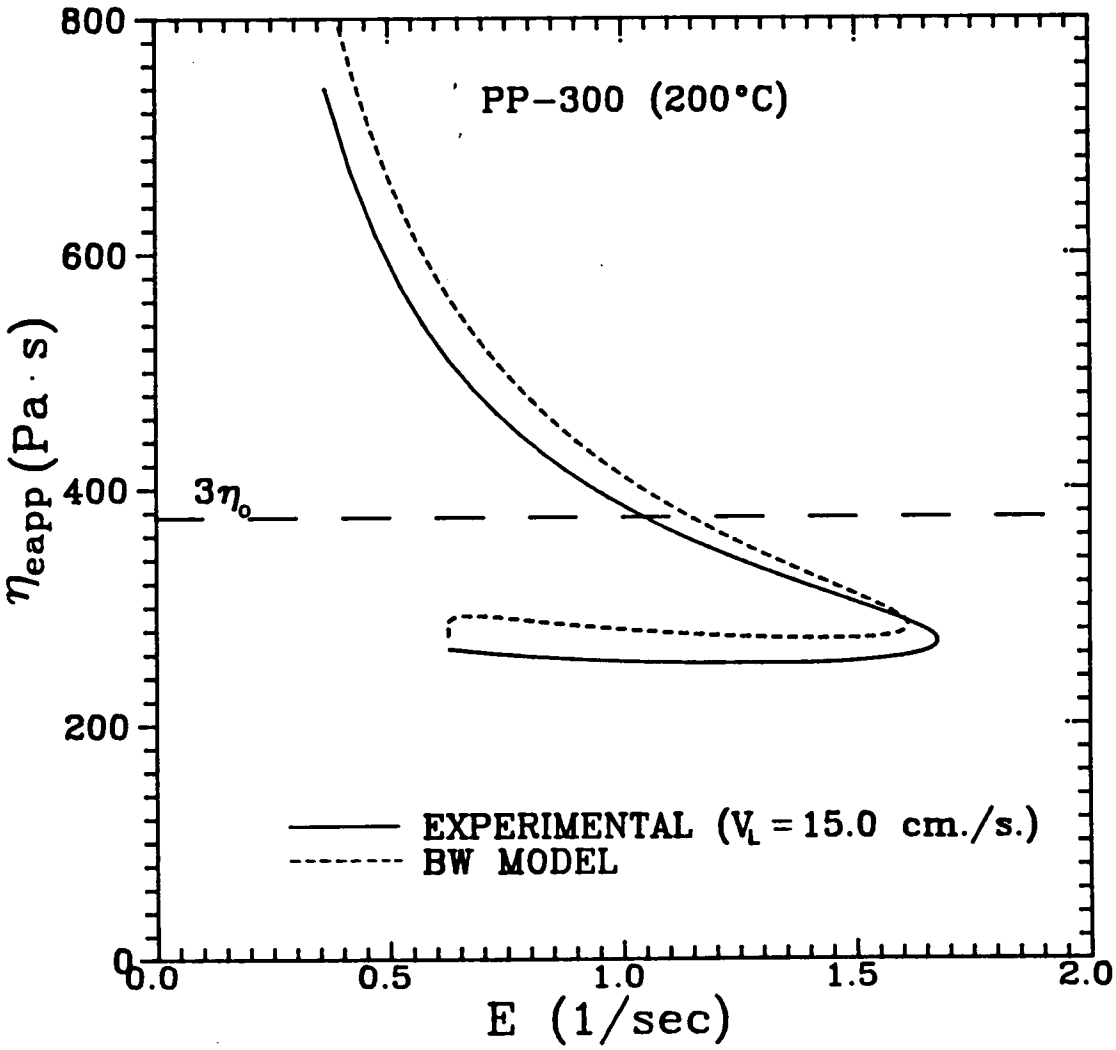


Figure 6.24. Comparison of the experimental data for PP-300 MFR at 200 °C with the predictions of the BW model using τ=0.22 sec. and a=1.1.

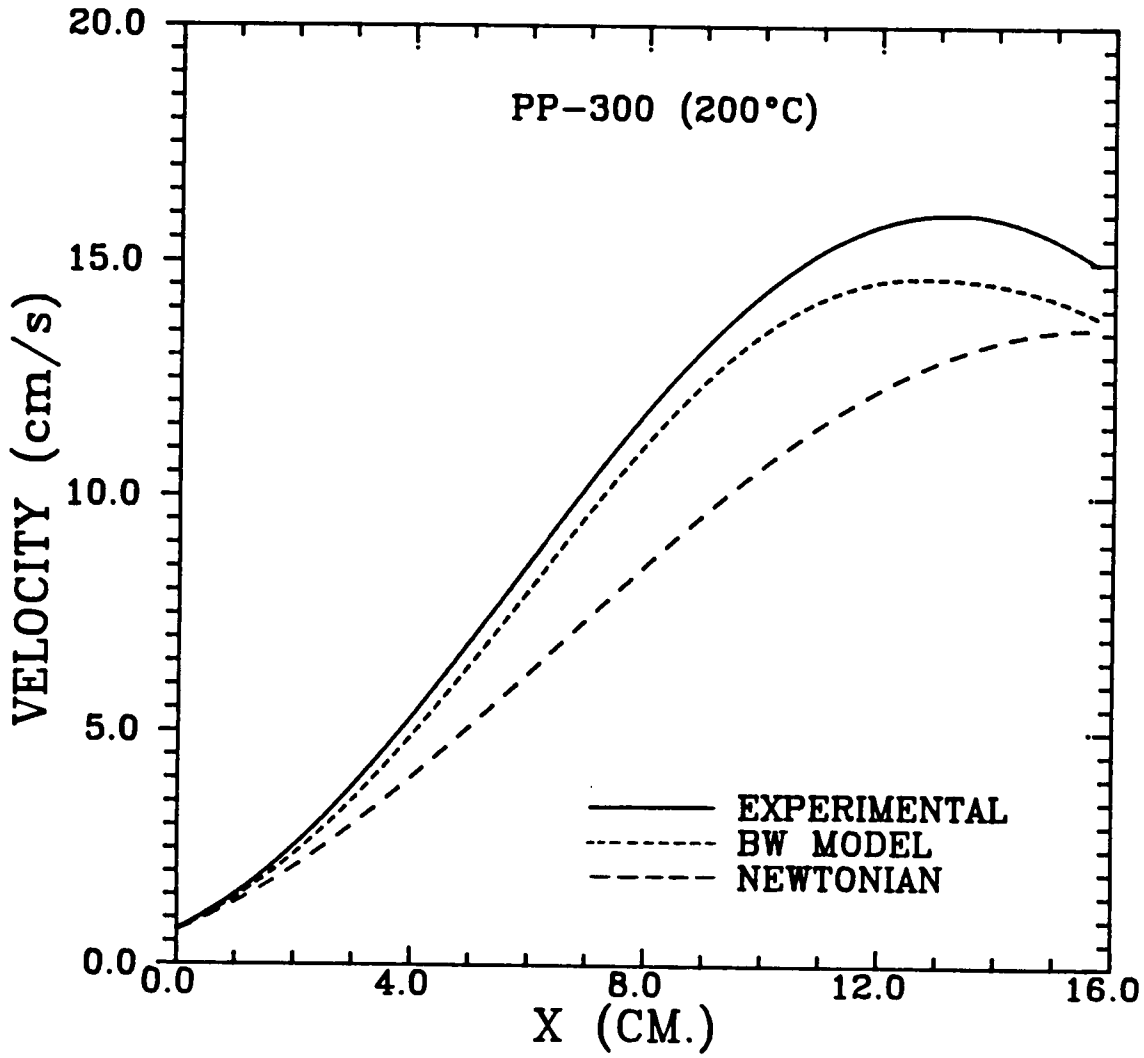


Figure 6.25. Comparison of the experimental data for PP-300 MFR at 200 ^{o}C with the predictions of the BW model using τ=0.22 sec. and a=1.1 and the predictions assuming Newtonian behavior.

MFR at 180 ^{o}C. The model predictions are compared with the experimental data and the predictions assuming Newtonian behavior. Observe that the apparent elongational viscosities in the upper part of the spinline are lower than the three times the zero-shear viscosity (or Trouton's viscosity). The comparison of the BW model predictions for the velocity profile with the experimental data suggests that even higher value of thinning parameter "a" could be used.

The plots of the average relaxation times obtained by fitting the gravity spinning data versus the zero-shear viscosity data and the Z-average molecular weight are shown as Figures 6.26 and 6.27 respectively. The values of the average relaxation times correlated very well with the zero-shear viscosity data (note that $\eta_o=G\tau$ and G's are assumed to be independent of temperature). Many of the important rheological parameters obtained by measuring the shear and the elongational properties of the polypropylene melts studied are tabulated in Table VI.I. The important conclusions drawn from the these rheological measurements and analysis will be presented in the following chapter.

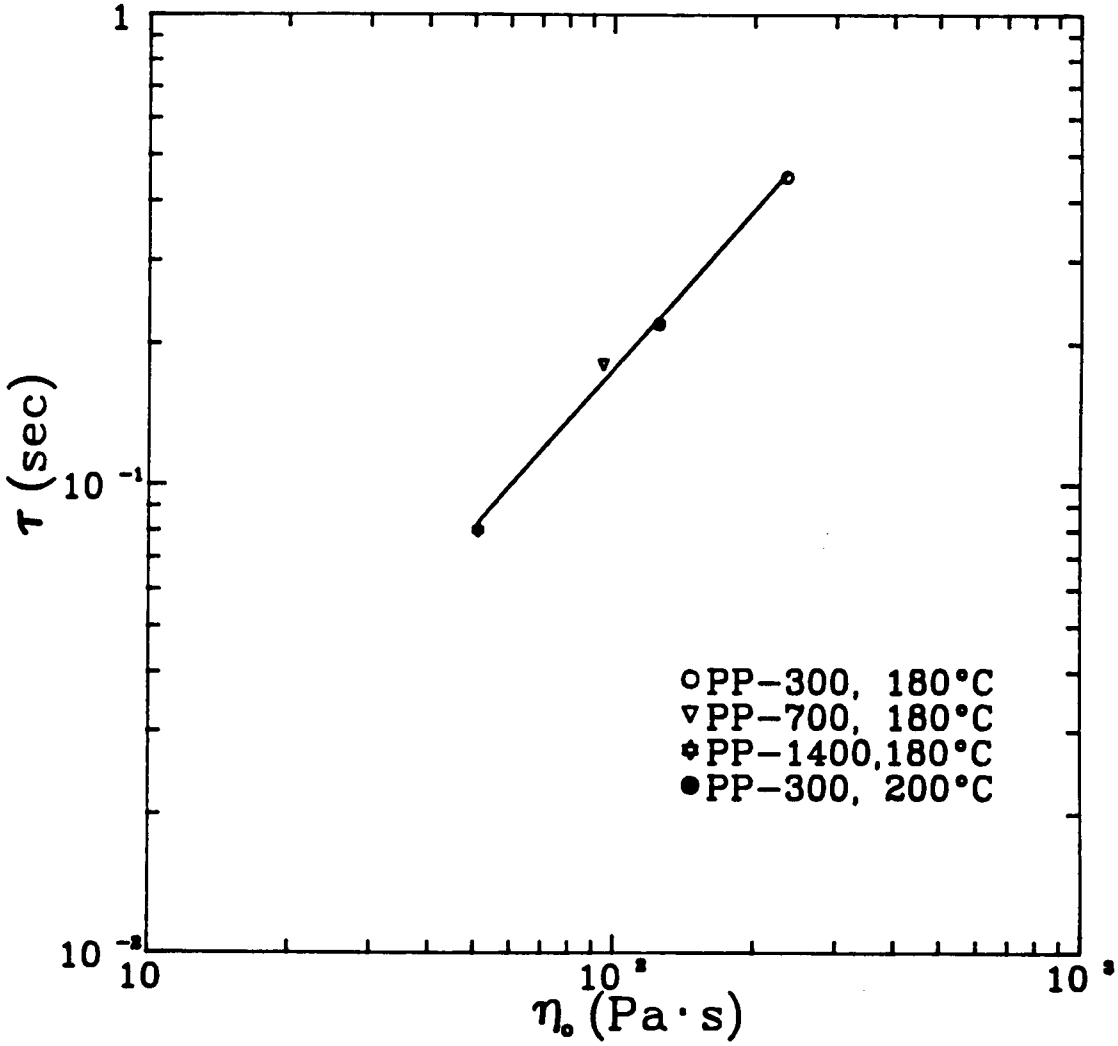


Figure 6.26. Plot of the average relaxation times versus the zero-shear viscosities.

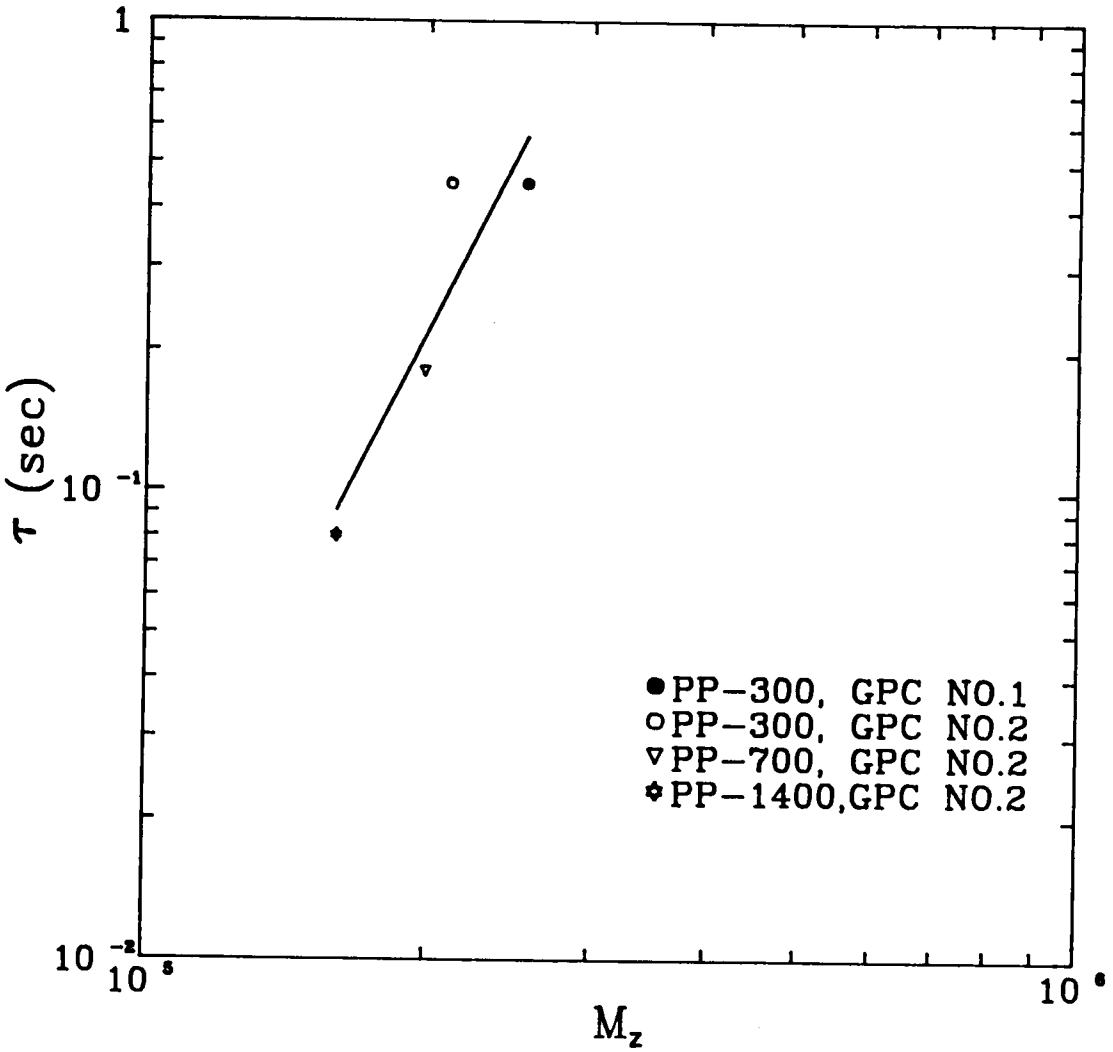


Figure 6.27. Plot of the average relaxation times versus the Z-average molecular weights.

Table VI.I. Tabulation of important parameters.

Material /MFR	Temp.	Shear	Elongation		Time Const.
		Measured $\eta_{(o)}$	Modelled $\eta_{e(o)}$	Observed $\eta_{eapp}(x=1\ cm)$	
	oC	(Pa s)	(Pa s)	(Pa s)	sec.
PP-1400	180	51	153	142	0.08
PP-700	180	95	285	273	0.18
PP-300	180	235	705	480a	0.45
PP-300	200	125	375	254	0.22

a : Taking into account estimated small applied take-up force.

Note :

$$\tau = 1.02E\text{-}03\ \eta_o^{1.1}$$

$$= 2.26E\text{-}22\ M_z^{3.96}$$

$$a_T = 5.85E\text{-}07\ e^{E/RT}$$

Where,

E = Activation energy for flow

= 12.9 Kcal/gmole.

R = Universal gas constant.

CHAPTER 7

CONCLUSIONS

1. For the deformation rates observed in the gravity spinning experiments, PP-700 MFR and PP-1400 MFR showed that the apparent elongational viscosities in the upper part of the spinline were close to three times the zero-shear viscosity, in agreement with Trouton's viscosity result for Newtonian fluids. The same result can be deduced (in the limit of zero elongation rate) indirectly for PP-300 MFR as well from the viscoelastic modelling; however, the measured apparent elongational viscosities in the upper part of the spinline were lower than three times the zero-shear viscosity.

2. Comparison of the shear viscosity data of PP-300 MFR with the remelted web sample obtained from it suggests that significant thermal degradation occurred in the screw extruder. In fact, the shear viscosities of the remelted web are not very much different from those of PP-700 MFR. Hence, the elongational viscosity of this degraded material can reasonably be taken as three times the zero-shear viscosity.

3. Under certain conditions (those giving higher elongation rates than observed for stable spinning), draw resonance was observed in all the materials studied. This suggests that probably all of these materials will be susceptible to instabilities at high elongation rates (above about 2 sec^{-1}).

4. A rheological model is necessary to analyze and obtain meaningful results from any unsteady state experiments, such as the gravity spinning experiments of the present work. The convected Maxwell model with an Oldroyd contravariant time derivative provides a convenient frame work for analyzing viscoelastic fluids. But the use of a rate dependent relaxation time (as used in the Bogue-White model and the Phan-Thien and Tanner model) is necessary to account for the shear thinning behavior and to quantitatively predict the elongational data.

5. The viscoelastic modelling showed that the time constants obtained from fitting the shear data could not be used to predict the gravity spinning data quantitatively. A higher value of the average relaxation time was therefore necessary.

6. These higher values of the average relaxation times gave quantitative fits of the elongational flow data. In fitting the elongational data for PP-300 MFR, it was necessary to take into account a small applied take-up force consistent with the experimental observations. The data for PP-700 MFR and PP-1400 MFR could be fit directly without introducing any take-up force.

7. The zero-shear viscosities (and hence the zero-elongation viscosity) of the polypropylene melts studied varied with about 3.75 power of the weight average molecular weight. The shear viscosity data and the relaxation time constants obtained from the elongational data could be shifted with temperature using an Arrhenius equation (which is a simplified form of WLF equation). The relaxation time constants obtained from the elongation data varied with about 1.1

power of the zero-shear viscosity and about 3.95 power of the Z-average molecular weight.

8. Gravity spinning is a useful method for measuring the elongation behavior of low viscosity polymer melts and solutions because it is not necessary to measure the small forces involved. The method could also be extended to higher viscosity polymer melts by increasing the spinline length to achieve higher (and accurately measurable) elongation rates.

LIST OF REFERENCES

LIST OF REFERENCES

1. A. M. Jones and L. C. Wadsworth, Presented at TAPPI Nonwovens Conference, April (1986).

2. Fu-Min Lu and J. E. Spruiell, J. Appl. Polym. Sci., 34, 1521 (1987); J. Appl. Polym. Sci., 34, 1541 (1987).

3. L. C. Wadsworth and A. M. Jones, Presented at INDA/TEC, The International Nonwovens Technological Conference, June (1986).

4. C. D. Han, "Rheology in Polymer Processing", Academic Press, New York (1976).

5. W. F. Bueche, J. Polym. Sci., A-2, 5, 1261 (1961).

6. W. W. Graessley, "Advances in Polym. Sci.", Vol. 16, Springer Verlay (1974).

7. D. C. Bogue, Ind. Eng. Chem. Fund., 5, 253 (1966).

8. D. C. Bogue and J. L. White, "Engineering Analysis of Non-Newtonian Fluid", NATO Agardograph, #144 (1970).

9. D. C. Bogue and J. O. Doughty, Ind. Eng. Chem. Fund., 5, 243 (1966).

10. J. O. Doughty and D. C. Bogue, Ind. Chem. Eng. Fund., 6, 393 (1967).

11. C. J. S. Petrie, "Elongational Flows", Pitman, London (1979).

12. R. I. Tanner, "Engineering Rheology", Clarendon Press, Oxford (1985).

13. M. Yamamoto, Trans. Soc. Rheol., 15, 783 (1971).

14. M. H. Wagner, J. Non-Newtonian Fluid Mech., 4, 39 (1978).

15. A. C. Papanastasiou, L. E. Scriven, and C. W. Macosko, J. Rheol., 27, 387 (1983).

16. J. G. Oldroyd, Proc. Roy. Soc., A77, 426 (1950).

17. J. G. Oldroyd, Proc. Roy. Soc., A200, 523 (1958).

18. W. Prager, "Introduction to Mechanics of Continua", Chicago, Ginn, p. 155 (1961).

19. S. Middleman, Trans. Soc. Rheol., 13, 123 (1969).

20. I-Jen Chen and D. C. Bogue, Trans. Soc. RHeol., 16, 59 (1972).

21. I-J. Chen, G. E. Hagler, L. E. Abbott, D. C. Bogue, and J. L. White, Trans. Soc. Rheol., 16, 473 (1972).

22. I. Furuta, V. M. Lobe, and J. L. White, J. Non-Newtonian Fluid Mech., 1, 207 (1976).

23. Y. Ide and J. L. White, J. Appl. Polym. Sci., 22, 1061 (1978).

24. T. Takaki and D. C. Bogue, J. Appl. Polym. Sci., 19, 419 (1975).

25. N. Phan-Thien and R. I. Tanner, J. Non-Newtonian Fluid Mech., 2, 353 (1977).

26. N. Phan-Thien, J. Rheology, 22, 259 (1978).

27. R. I. Tanner, J. Non-Newtonian Fluid Mech., 5, 103 (1979).

28. K. Missaghi and C. J. S. Petrie, J. Non-Newtonian Fluid Mech., 11, 283 (1982).

29. R. B. Bird, O. Hassager and R. C. Armstrong, "Dynamics of Polymer Liquid : Vol. 1 and Vol. 2", Wiley, N. Y. (1978).

30. T. W. Spriggs, J. D. Huppler and R. B. Bird, Tran. Soc. Rheol., 10, 191 (1966).

31. S. Ramachandran, H. W. Gao, and E. B. Christiansen, Macromolecules, 18, 695, (1985).

32. B. L. Lee and J. L. White, Trans. Soc. Rheol., 18, 467 (1974).

33. K. Oda, J. L. White, and E. S. Clark, Polym. Eng. Sci., 18, 25 (1978).

34. L. E. Nielsen, "Polymer Rheology", Marcel Dekker Inc., New York (1977).

35. J. D. Ferry, "Viscoelastic Properties of Polymers", 3rd ed., Wiley, N. Y. (1980).

36. C. D. Denson, Poly. Engg. Sci., 13, 125 (1973).

37. M. Van Den Tempel, The Chemical Engineer, P.95, Feb. (1977).

38. F. C. Frank, Proc. Roy. Soc., A.319, 127 (1970).

39. F. Trouton, Proc. Roy. Soc. (London), A, 77, 426 (1906).

40. D. C. Bogue, Polym. Sci. and Eng., Report No. 123, Univ. of Tenn. (1978).

41. J. M. Dealy, Polym. Eng. Sci., 11, 433 (1971).

42. J. W. Hill and J. A. Cuculo, J. Macromol. Sci. (Rev.), C14, 107 (1976).

43. C. D. Denson, Polym. Eng. Sci., 13, 125 (1973).

44. J. Meissner, Polym. Eng. Sci., 27, 537 (1987).

45. R. S. Porter and J. F. Johnson, Chem. Rev., 66, 1 (1966).

46. W. Minoshima, J. L. White, and J. E. Spruiell, J. of Appl. Polym. Sci., 25, 287 (1980).

47. W. Minoshima, J. L. White, and J. E. Spruiell, Polym. Eng. Sci., 20, 1166 (1980).

48. C. D. Han and R. R. Lamonte, Trans. Soc. Rheol., 16, 447 (1972).

49. O. Ishizuka, K. Koyama, and H. Nokubo, Polymer, 21, 691 (1980).

50. C. D. Han and Y. M. Kim, J. Appl. Polym. Sci., 20, 1555 (1976).

51. T. Trzebiatowski, and H. Wilski, Rheol. Acta., 24, 582 (1985).

52. S. Onogi, T. Masuda, and K. Kitagawa, Macromolecules, 3. 109 (1970); T. Masuda, K. Kitagawa, T. Inoue, and S. Onogi, Macromolecules, 3, 116, (1970).

53. D. C. Bogue, T. Masuda, Y. Einaga, and S. Onogi, Polym. J., 1, 563 (1970).

54. W. W. Graessley and L. Segal, Macromolecules, 2, 49 (1969); AIChE J., 16, 261 (1970).

55. W. W. Graessley, J. Chem. Phys., 54, 5143 (1971).

56. W. M. Prest, R. S. Porter, and J. M. O'Reilly, J. Appl. Polym. Sci., 14, 2697 (1970).

57. W. M. Prest and R. S. Porter, Polym. J., 4, 154 (1973).

58. W. M. Prest, Polym. J., 4, 154 (1973).

59. R. Racin and D. C. Bogue, J. of Rheo., 23(3), 263, (1979).

60. G. G. Fuller, C. A. Cathey, B. Hubbard, and B. E. Zebrowski, J. Rheol., 31(3), 235 (1987).

61. J. Meissner, Rheol. Acta., 8, 78 (1969); 10, 230 (1971); Trans. Soc. Rheol., 13, 123 (1969); 16, 405 (1972).

62. J. C. Chang, M. M. Denn and F. T. Geyling, Ind. Eng. Chem. Fundam., 20, 147 (1981).

63. Y. T. Shah and J. R. A. Pearson, Ind. Eng. Chem. Fundam., 11, 150 (1972).

64. C. B. Weinberger and J. D. Goddard, Int. J. Multiphase Flow, 1, 465 (1974).

65. J. R. Green, "Statistical Treatment of Experimental Data", Elsevier Scientific Pub. Co. (1977).

66. J. R. A. Pearson and Y. T. Shah, Trans. Soc. Rheol., 16, 519 (1972).

67. R. J. Fisher and M. M. Denn, AIChE J., 22, 236 (1976).

68. R. J. Donnelly and C. B. Weinberger, Ind. Eng. Chem. Fundam., 14, 334 (1975).

69. M. Matsui and D. C. Bogue, Polym. Eng. Sci., 16(11), 735 (1976).

70. J. D. Tsou and D. C. Bogue, J. Non-Newtonian Fluid Mech., 17, 331 (1985).

71. R. Keuings and M. J. Crochet, Ind. Eng. Chem. Fundam., 22, 347 (1983).

72. R. J. Fisher, M. M. Denn, and R. I. Tanner, Ind. Eng. Chem. Fundam., 19, 195 (1980).

73. J. C. Chang and M. M. Denn, J. Non-Newtonian Fluid Mech., 5, 369 (1979).

74. R. J. Fisher and M. M. Denn, AIChE J., 22, 236 (1976).

75. K. M. Baid and A. B. Metzner, Trans. Soc. Rheol., 21, 237 (1977).

76. M. M. Denn and G. Marrucci, J. Non-Newtonian Fluid Mech., 2, 159 (1977).

77. S. Nam and D. C. Bogue, Ind. Eng. Chem. Fundam., 23, 1 (1984).

APPENDICES

APPENDIX A

Table A-1. Shear Flow Data of PP-35 MFR.

at 180 °C			at 200 °C		
$\dot{\gamma}$ (1/sec)	η (Pa s)	N (Pa)	$\dot{\gamma}$ (1/sec)	η (Pa s)	N (Pa)
0.16	1215	-	0.16	736	-
0.25	1208	36	0.26	728	-
0.4	1190	85.4	0.4	692	34.8
0.6	1171	169	0.64	679	68
1.0	1145	328	1.0	666	152
1.6	1084	680	1.7	644	300
2.6	1030	1261	2.7	628	616
3.0	1012	-	4.2	601	1182
6.2	909	-	2.96	634	-
15.9	736	-	6.0	571	-
32.9	603	-	15.6	474	-
68	444	-	32.0	403	-
181.5	275.5	-	66.3	317	-
385	175.9	-	175	211	-
831	103	-	369	143	-
2393	46.1	-	790	90.3	-
-	-	-	2230	44.7	-
-	-	-	5102	24.2	-

Table A-2. Shear Flow Data of PP-300 MFR.

at 180 °C			at 200 °C		
$\dot{\gamma}$ (1/sec)	η (Pa s)	N (Pa)	$\dot{\gamma}$ (1/sec)	η (Pa s)	N (Pa)
0.64	231	-	1.0	123	-
1.0	226	-	1.7	117	-
1.6	219	46.0	2.8	111	27.4
2.5	215	94.4	4.4	105	66
4	209	202	7	99	145
6.4	200	385	11.6	97	323
10.3	190	785	18.6	-	785
61.6	102	-	59.2	62.9	1182
159	82.5	-	153	53.7	-
329	62.9	-	316	45.1	-
682	46.0	-	658	35.3	-
1808	30.5	-	1756	23.4	-
181.5	275.5	-	3756	15.9	-
-	-	-	8230	9.5	-

Table A-3. Shear Flow Data of PP-WEB.

at 180 °C			at 200 °C		
$\dot{\gamma}$ (1/sec)	η (Pa s)	N (Pa)	$\dot{\gamma}$ (1/sec)	η (Pa s)	N (Pa)
1.0	120	-	-	-	-
2.6	117	29.7	1.9	69.5	-
4.1	115	64	4.9	64.7	31.2
6.5	111	135	7.8	62.5	67
10	109	250	12.5	57.7	141
16	106	512	20.5	56.1	294
25	-	875	31.4	52.1	591

Table A-4. Shear Flow Data of PP-700 MFR.

at 180 °C			at 200 °C		
$\dot{\gamma}$ (1/sec)	η (Pa s)	N (Pa)	$\dot{\gamma}$ (1/sec)	η (Pa s)	N (Pa)
1.7	92.5	-	-	-	-
2.6	90.8	-	2.6	47.2	-
4.2	87.7	54.4	4.2	45.5	19.6
6.6	84.9	108	6.6	43.6	46.4
10.4	79.4	212	10.2	41.2	88
16.6	720	393	16.8	36.7	163
25.8	67.1	718	155	35.2	-
60.0	67.0	-	318	29.3	-
155	56.9	-	652	23.7	-
320	46.4	-	1697	16.7	-
666	36.5	-	3518	11.9	-
1773	23.8	-	7341	8.2	-
3777	15.5	-	-	-	-
8204	9.7	-	-	-	-

Table A-5. Shear Flow Data of PP-1400 MFR.

at 180 °C			at 200 °C		
$\dot{\gamma}$ (1/sec)	η (Pa s)	N (Pa)	$\dot{\gamma}$ (1/sec)	η (Pa s)	N (Pa)
2.7	49.9	-	-	-	-
4.1	48.4	-	4.1	24.5	-
6.5	47.3	-	10.0	23.6	-
10.2	46.8	62	16.0	22.7	33.2
16.5	45.4	122	25.1	21.7	70.8
25.9	42.2	232	40.0	-	144
41.3	41.4	496	63.0	20.3	268
58.8	39.9	-	149	20.8	540
65	39.7	968	303	19.3	-
151	34.4	-	621	16.5	-
309	30.1	-	1610	13.1	-
635	27.0	-	3330	10.2	-
1655	20.0	-	6930	7.4	-
3445	14.7	-	-	-	-
7227	9.6	-			

APPENDIX B

B.1. Computer Program for Newtonian Gravity Spinning

This program is prepared by MR. RAJEN M. PATEL.
It solves second order differential equation obtained for Newtonian jet gravity spinning. It is written in FORTRAN using 4^{th} order Runge-Kutta method. It calls subroutine for Runge-Kutta method from Wiley subroutine library.

It requires two boundary conditions, one of which is the initial velocity (y(1)), fixed by die diameter and the cross head speed (C.H.S.) of Instron Capillary Rheometer. Elongation rate (dy(1)) is found by trial and error so as to obtain elongation rate at X=L to be zero, a kinematic boundary condition for Newtonian jet gravity spinning.

L = Spinline length (cm.),
vis = Newtonian viscosity (poise),
V = Instron cross head speed (inch/min),
Q = Vol. flow rate (cc/sec),
h = Differential increment,
iter = No. of iterations.

```
      program scitest

      dimension x(101), y(101), dy(101)
        L=8.83
        X(1)=0.0
       DO 6 I=2,101
        X(I)=X(I-1)+L/100
 6     CONTINUE

        vis=510

        PI=3.1415917
        V=.5
        Q=.030165*V
c
      open(3,file='t2.dat')
      write (3,*) 'test results from desork.tst'
      iter=101
      h=0.086
      iflag=1

c     y(1) is initial velocity and dy(1) is elongation rate
c     at X =0.
```

```
      y(1)=1.76965666*V
      dy(1)=.893

c     Desork is the name of Wiley subroutine for Runge-Kutta
c     method stored in science library on IBM PC.

            Call desork(iter,h,x,y,dy,iflag)

      do 10 i=1,ITER
        WRITE(*,5) X(I),DY(I),3*VIS*DY(I),Y(I),
                   SQRT(Q*4/(PI*Y(I)))
       WRITE(3,5) X(I),DY(I),3*VIS*DY(I),Y(I),
                  SQRT(4*Q/(PI*Y(I)))
  5   FORMAT(1X,5E12.5)
 10   CONTINUE
      WRITE (3,*) ' '
      END

c     YDOPRI is the function representing second order
c     differential equation.

      FUNCTION YDOPRI(XN,YN,DYN,IFLAG)
      YDOPRI=1/YN*DYN*DYN-0.49

      RETURN
      END
```

B.2. Computer program for analyzing gravity spinning experimental data.

This program is prepared by MR. RAJEN M. PATEL.
It analyses gravity spinning experimental data which is in the form of polynomial curve fitting equation of fourth degree, fitting diameter profile in the form of (1/D) (1/cm.) versus X (cm.)

```
10 DIM X(120),DX(120),DV(120),DD(120),VIS(120),F(120)
```

The input data are the coefficients of the polynomial curve fitting equation and the spinline length.

```
20 A=6.100988
30 B=2.274731
40 C=-0.1034869
50 D=5.036054E-03
60 E=-2.063538E-04

70 Q=.0150825       'Q = Vol. flow rate (cc/sec).
80 PI=3.14159
90 G=980
100 R=.7650001      'R = Density in (gm/cc).
```

Specify the spinline length and the file names.

```
110 INPUT "total spinline length =";L
120 CON = PI*R*G/4
130 INPUT "FILE NAME FOR OUTPUT = ";NAM$
140 NAM$="B:"+NAM$+".DAT"
150 INPUT "FILE NAME FOR DIGITISED PROFILE =";DIGI$
160 DIGI$="B:"+DIGI$+".DAT"
170 OPEN NAM$ FOR OUTPUT AS #1

180 LPRINT " FOURTH DEGREE FIT "
185 LPRINT
190 LPRINT " FILE OF VISCOSITY DATA =";NAM$
200 LPRINT
210 LPRINT "FILE OF DIAMETER PROFILE =";DIGI$
220 LPRINT
230 LPRINT "SPINLINE LENGTH (CM.) =";
```

```
235 LPRINT USING "##.###";L
240 OPEN DIGI$ FOR OUTPUT AS #2
```

This block of lines perform integration by simpson rule to obtain the weight of spinline below given axial position X.

```
250 DEF FNDIA(X)=1/(A+B*X+C*X*X+D*X*X*X+E*X*X*X*X)^2
260 N=210
270 FOR I= 0 TO 100
280 X=0
290 X=I*L/100
300 X(I)=X: N=N-2
310 H=(L-X)/N
320 S1=FNDIA(X) : S2=FNDIA(L)
330 S=S1+S2
340 FOR J= 1 TO N-1
350 IF 2*INT((J+1)/2) = J THEN CO=2 ELSE CO=4
360 X=X+H
370 S=S+CO*FNDIA(X)
380 NEXT J
390 X=I*L/100
400 F(I)=CON*H/3*S     'F(I) = Weight below X.
```

This block of lines calculates the residence time of an element of fluid in spinline.

```
410 IF I <> 0 THEN 440
420 RES= PI/4/Q*S*H/3
430 LPRINT "RESIDENCE TIME (SEC.) =";
435 LPRINT USING "#.####";RES :LPRINT : LPRINT

437 LPRINT  "    X(I)      DIA.      VEL.    FORCE
    STRESS     dV/dX     VISCOSITY "
439 LPRINT
```

Elongation rate (DV(I)), velocity (UU) and elongational viscosity (VIS(I)) are computed. Relevant data are printed as well as stored as files on disk.

```
440 DX(I)=A+B*X+C*X*X+D*X*X*X+E*X*X*X*X
450 DD(I)= -(B+2*C*X+3*D*X*X+4*E*X*X*X)/DX(I)/DX(I)
460 DV(I)=-8*Q/PI*DX(I)^3*DD(I)
470 UU=4*Q/PI*DX(I)*DX(I)
```

B.3. Computer program for simulation of gravity spinning using Bogue-White model (one G and one τ case).

```
      This program is prepared by MR. RAJEN M. PATEL for the
      simulation of spinline, for gravity spinning using
      the Bogue-White model. T(11), T(22) and the velocity
      all at x=0, are the initial conditions to be specified.

      Y0P = T(11), Y2P = T(22), Y4P = σ11 (dyne/sq.cm.)
      R = Density (gm/cc),        Q = Vol. Flow Rate (cc/s)
      H = Differential Increment, Vel.(at x=0) = UU (cm/sec)
      T0 = Relaxation Time (sec), G = Modulus (dyne/sq.cm)
      AA = Thinning parameter in B-W model.

10 Y0P=1470.0
20 Y2P=-735.0
30 Y4P=Y0P-Y2P
40 T0=.40
50 PI=3.14159
60 R=.7650001
70 GR=980
80 Q=.0150825
90 H=.005
100 AA=1.43
110 G=5875.0
120 UU=.72278


      To store model predictions in two files on disk.

140 VEL$="C:U"+RAJ$+".DAT"
150 RAJ$="C:"+RAJ$+".DAT"
160 OPEN RAJ$ FOR OUTPUT AS #1
170 OPEN VEL$ FOR OUTPUT AS #2


      To print model parameter and conditions.

180 LPRINT "G =";
190 LPRINT USING "#####.##";G;
200 LPRINT TAB(20) "TAU =";
210 LPRINT USING "#.##";T0;
220 LPRINT TAB(40) "AA =";
230 LPRINT USING "#.###";AA;
```

```
480 AA=PI/4/DX(I)^2          'AA = cross-sectional area.
490 VIS(I)=F(I)/AA/DV(I)
500 PRINT USING "##.###   #.####    ##.###    ##.###
    #####.###.###########.##";X(I),1/DX(I),UU,F(I),
    F(I)/AA,DV(I),VIS(I)
510 LPRINT USING "   ##.###   #.####    ##.###    ##.###
    #####.####.###########.##";X(I),1/DX(I),UU,F(I),
    F(I)/AA,DV(I),VIS(I)
520 WRITE #1, X(I),DV(I),VIS(I),DX(I)
530 WRITE #2, X(I),DX(I),1/DX(I),UU,F(I)/AA
540 NEXT I
550 CLOSE #1
560 CLOSE #2
570 END
```

```
240 LPRINT TAB(60) "Y4(0) =";
250 LPRINT USING "#####.##";Y4P
260 LPRINT : LPRINT "   U(0) =";
270 LPRINT USING "#.#####";UU;
280 LPRINT TAB(25) "  H =";
290 LPRINT USING "#.###";H;
292 LPRINT TAB(41) "TAU(11) =";
293 LPRINT USING "#####.##";Y0P;
294 LPRINT TAB(61) "TAU(22) =";
295 LPRINT USING "#####.##";Y2P
300 LPRINT :LPRINT
310 LPRINT "OUTPUT FILE NAME =";RAJ$ :LPRINT:LPRINT
320 LPRINT "X(I)";TAB(11) "Ne(I)";TAB(22) "Du/Dx";TAB(33)
    "VEL"; LPRINT TAB(42) "SIGMA(11)";TAB(55)
    "T(11)";TAB(64) "T(22)"



330 DU=1!       ' Initial guess for elongation rate at x=0.
340 FOR I=1 TO 40000
350 X=(I-1)*H
```

Boundary condition for gravity spinning is $\sigma_{11} = 0$. using this boundary condition model predicts spinline length with given initial conditions and model paramters.

```
370 IF Y4G < 0.0 THEN 940
```

This block solves the differential eqs. using 4^{th} order Runge-Kutta method with the specified guess value of DU (elongation rate).

```
372 YN=Y0P
380 YN2=Y2P
390 YN4=Y4P
400 U=UU
410 GOSUB 990
420 TK1=H*YP
430 T1=H*YP2
440 S1=H*YP4
450 U=U+DU*H*.5
460 YN=Y0P+TK1*.5
470 YN2=Y2P+T1*.5
480 YN4=Y4P+S1*.5
490 GOSUB 990
500 TK2=H*YP
510 T2=H*YP2
```

```
520 S2=H*YP4
530 YN=Y0P+TK2*.5
540 YN2=Y2P+T2*.5
550 YN4=Y4P+S2*.5
560 GOSUB 990
570 TK3=H*YP
580 T3=H*YP2
590 S3=H*YP4
600 U=U+DU*H*.5
610 YN=Y0P+TK3
620 YN2=Y2P+T3
630 YN4=Y4P+S3
640 GOSUB 990
650 TK4=H*YP
660 T4=H*YP2
670 S4=H*YP4
680 Y0G=Y0P+(TK1+2*TK2+2*TK3+TK4)/6
690 Y2G=Y2P+(T1+2*T2+2*T3+T4)/6
700 Y4G=Y4P+(S1+2*S2+2*S3+S4)/6
```

The values of σ_{11} predicted by the force balance eq. and the Bogue-White model ($\sigma_{11} = T_{11} - T_{22}$) are compared.

```
710 DIFF=Y4G-(Y0G-Y2G)
730 IF ABS(DIFF) < .005 THEN 805
740 IF IFLAG=1 THEN 770
```

If the difference is more than the tolerence, new value of DU is guessed by this block (by method of interval halving) such that convergence to the correct value is rapidly attained and the differential equations are agained solved till the required tolerence is achieved between the force balance eq. and the BW model.

If the difference is greater than zero then DU is incremented till it becomes within tolerable value or less than zero at which the value of DU forms the upper limit (DUG) on DU. Once difference is less than zero, IFLAG is set at one. The lower limit of DU (DUB) is set in line 910.

```
750 IF DIFF > 0 THEN DU=DU+.2 :GOTO 370
760 IFLAG=1 :DUB=DU
770 IF DIFF > 0 THEN DUG=DU : DU=(DU+DUB)/2 : GOTO 370
780 DUB=DU : DU=(DU+DUG)/2  : GOTO 370
```

To obtain desired printout and the files.

```
805 IF Y4G < 20.0 THEN 820
807 IF FLG = 0 THEN 820      ' FLG is a counter.
810 IF FLG < 20 THEN 890
820 NE=Y4P/DU
830 IF NE > 8000 OR NE < 0.1 THEN 850
```

Model predictions are converted in to SI units before storing in the soft diskett.

```
840 WRITE #1, X;DU;NE/10 'conversion factor = 10 to convert Pa-s.
850 WRITE #2, X,DU,SQR(4*Q/PI/UU),UU,Y4P/10  ' to convert to Pascal.
870 LPRINT USING "##.### ########.##  ##.######   ##.###
    ######.##  ######.## #######.##";X,NE,DU,UU,Y4P,Y0P,Y2P
880 FLG=0
```

Predicted velocity now naturally becomes starting value.

```
890 UU=U : FLG=FLG+1
```

Predicted stresses now become starting values for next X.

```
900 Y0P=Y0G : Y2P=Y2G : Y4P=Y4G
```

The lower limit for elongation rates (DUB) is fixed.

```
910 IF DU < 0.01 THEN DUG=-.9 ELSE DUG=-0.01: IFLAG=0
```

DU is arbitrarily increased. (may be omitted)

```
920 DU=DU+.004
930 NEXT I
940 CLOSE #2
950 CLOSE #1
960 LPRINT : LPRINT : LPRINT "        SPINLINE LENGTH =";
970 LPRINT USING "##.###";X
980 END
```

cont.

The Bogue-White model and the Force balance eqs.

```
990 T=T0/(1+(1.7320508#*AA*T0*ABS(DU))^0.75)
1000 YP = -(1/(U*T)-2*DU/U)*YN+2*G/U*DU
1010 YP2= -(1/(U*T)+DU/U)*YN2 - G/U*DU
1020 YP4=-R*GR+YN4/U*DU
1030 RETURN
1040 END
```

B.4. Computer program for simulation of gravity spinning using Bogue-White model (two G and two τ case)

This program is prepared by MR. RAJEN M. PATEL for the simulation of spinline for gravity spinning using
the Bogue-White model with two G's and two τ's. For complete documentation, refer to the case for one G and one τ.

```
10 Y0P=1217.2326      'T(11) corresponding to G1 and TAU10.
20 Y1P=458.6674       'T(11) corresponding to G2 and TAU20.
30 Y2P=0!             'T(22) corresponding to G1 and TAU10.
40 Y3P=0!             'T(22) corresponding to G2 and TAU20.
50 Y4P=Y0P+Y1P-Y2P-Y3P
60 TAU10=.0023
70 G1=300000!
80 TAU20=0.11
90 G2=2363.6
100 R=.7650001
110 GR=980
120 Q=.0150825
130 H=.0005
140 AA=0.70
150 PI=3.14159
160 UU=.70992


170 INPUT " OUTPUT FILE NAME =";RAJ$
180 VEL$= "C:"+"U"+RAJ$+".DAT"
190 RAJ$="C:"+RAJ$+".DAT"
200 OPEN RAJ$ FOR OUTPUT AS #1


210 LPRINT "  G1 =";G1;TAB(30) "T1 =";  : LPRINT USING "#.####"
;TAU10
220 LPRINT "  G2 =";
230 LPRINT USING "####.##" ;G2;
240 LPRINT TAB(30) "T2 =";
250 LPRINT USING "##.####" ;TAU20;
260 LPRINT TAB(50) "NEWTONIAN VISCOSITY =";
270 LPRINT USING "####.##";G1*TAU10+G2*TAU20
280 LPRINT
290 LPRINT "Y0P =";
300 LPRINT USING "####.###" ;Y0P;
310 LPRINT TAB(30) "Y2P =";
320 LPRINT USING "####.##" ;Y2P
330 LPRINT "Y1P =";
```

```
340 LPRINT USING "####.###" ;Y1P;
350 LPRINT TAB(30) "Y3P =";
352 LPRINT USING "####.##";Y3P;
360 LPRINT TAB(50) " INITIAL VELOCITY =";
370 LPRINT USING "#.#####"; UU
390 LPRINT
400 LPRINT "Y4P =";
410 LPRINT USING "####.##" ;Y4P;
420 LPRINT TAB(30) "AA =";
430 LPRINT USING "#.###" ;AA;
440 LPRINT TAB(60) "H =";
450 LPRINT USING "#.####";H
460 LPRINT
470 LPRINT "FILE NAME =";RAJ$
480 LPRINT  : LPRINT
490 OPEN VEL$ FOR OUTPUT AS #2
500 LPRINT TAB(1);"X(I)";TAB(12) "Ne(I)";
    TAB(23) "Du/Dx";TAB(36) "VEL";TAB(46)
    "SIGMA(11)";TAB(59) "T(11)";TAB(71) "T(22)"


510 DU=1!

520 FOR I=1 TO 400000!
530 X=(I-1)*H

540 IF Y4G < 0 THEN 1290



550 YN=Y0P
560 YN1=Y1P
570 YN2=Y2P
580 YN3=Y3P
590 YN4=Y4P
600 U=UU
610 GOSUB 1340
620 TK1=H*YP
630 CK1=H*YP1
640 T1=H*YP2
650 C1=H*YP3
660 S1=H*YP4
670 U=U+DU*H*.5
680 YN=Y0P+TK1*.5
690 YN1=Y1P+CK1*.5
700 YN2=Y2P+T1*.5
710 YN3=Y3P+C1*.5
720 YN4=Y4P+S1*.5
730 GOSUB 1340
740 TK2=H*YP
750 CK2=H*YP1
```

```
760 T2=H*YP2
770 C2=H*YP3
780 S2=H*YP4
790 YN=Y0P+TK2*.5
800 YN1=Y1P+CK2*.5
810 YN2=Y2P+T2*.5
820 YN3=Y3P+C2*.5
830 YN4=Y4P+S2*.5
840 GOSUB 1340
850 TK3=H*YP
860 CK3=H*YP1
870 T3=H*YP2
880 C3=H*YP3
890 S3=H*YP4
900 U=U+DU*H*.5
910 YN=Y0P+TK3
920 YN1=Y1P+CK3
930 YN2=Y2P+T3
940 YN3=Y3P+C3
950 YN4=Y4P+S3
960 GOSUB 1340
970 TK4=H*YP
980 CK4=H*YP1
990 T4=H*YP2
1000 C4 =H*YP3
1010 S4=H*YP4
1020 Y0G=Y0P+(TK1+2*TK2+2*TK3+TK4)/6
1030 Y1G=Y1P+(CK1+2*CK2+2*CK3+CK4)/6
1040 Y2G=Y2P+(T1+2*T2+2*T3+T4)/6
1050 Y3G=Y3P+(C1+2*C2+2*C3+C4)/6
1060 Y4G=Y4P+(S1+2*S2+2*S3+S4)/6


1070 DIFF=Y4G-(Y0G+Y1G-Y2G-Y3G)
1080 IF ABS(DIFF) < .001 THEN 1140


1090 IF IFLAG=1 THEN 1120
1100 IF DIFF > 0 THEN DU=DU+.2 : GOTO 540
1110 IFLAG=1 :DUB=DU
1120  IF DIFF > 0 THEN DUG=DU : DU=(DU+DUB)/2 : GOTO 540
1130 DUB=DU : DU=(DU+DUG)/2 : GOTO 540



1140 IF FLG = 0! THEN 1170
1150 IF Y4G < 5 THEN 1170
1160 IF FLG < 200 THEN 1230
1170 NE=Y4P/DU
1180 IF NE > 4000 THEN 1200
1190 WRITE #1, X;DU;NE/10    ' to convert to Pa-s.
```

```
1200 WRITE #2, X;DU;SQR(4*Q/PI/UU);UU;Y4P/10 ' to convert to pascal.
1210 LPRINT USING "##.### ########.##    ##.######      ##.###
     ######.##    ######.##   #######.##";X,NE,DU,UU,Y4P,Y1P,Y3P
1220 FLG=0
1230 FLG=FLG + 1


1240 UU=U
1250 Y0P=Y0G : Y1P=Y1G : Y2P=Y2G : Y3P=Y3G : Y4P=Y4G


1260 IF DU < 0.0 THEN DUG=-0.9 ELSE DUG=-.01 : IFLAG = 0

1270 DU=DU+.02
1280 NEXT I
1290 CLOSE #1
1300 CLOSE #2

1310 LPRINT : LPRINT : LPRINT "         SPINLINE LENGTH =";
1320 LPRINT USING "##.###";X
1330 END



1340 TAU1=TAU10/(1+(1.7320508#*AA*TAU10*ABS(DU))^.75)
1350 TAU2=TAU20/(1+(1.7320508#*AA*TAU20*ABS(DU))^.75)
1360 YP = -(1/(U*TAU1)-2*DU/U)*YN+2*G1/U*DU
1370 YP1= -(1/(U*TAU2)-2*DU/U)*YN1+2*G2/U*DU
1380 YP2= -(1/(U*TAU1)+DU/U)*YN2 - G1/U*DU
1390 YP3= -(1/(U*TAU2)+DU/U)*YN3 - G2/U*DU
1400 YP4=-R*GR+YN4/U*DU
1410 RETURN
1420 END
```

APPENDIX C

Force Balance Equation :

$$\sigma_{11}\, A(x) = F_L + F_G - F_D - F_S - F_I$$

$F_L = 0$ for gravity spinning. Neglecting F_D, F_S, and F_I,

$$\sigma_{11}\, A(x) = \int_x^L \rho g\, A(x)\, dx$$

Differentiating this equation and using $A(x) = Q/U_1(x)$, we get,

$$d\sigma_{11}/dx = -\rho g + \sigma_{11}/U_1(x)\; dU_1/dx$$

The Bogue-White Model :

The Bogue-White model is a convected Maxwell model with contravariant time derivative with deformation rate dependent relaxation time.

$$T_{ij} + \tau_{neff}(\delta T_{ij}/\delta t) = G\tau_{neff} d_{ij}$$

Where,

$$\tau_{neff} = \frac{\tau_n}{1 + (a\tau_n \langle \pi_d^{1/2} \rangle)^b}$$

$\delta T_{ij}/\delta t$ = Oldroyd contravariant time derivative

$$= DT_{ij}/Dt - \partial U_i/\partial x_k\, T_{kj} - \partial U_j/\partial x_k\, T_{ik}$$

$$d_{ij} = \text{Deformation rate tensor}$$

$$= (dU_i/dx_j + dU_j/dx_i)$$

For isothermal melt spinning,

$$\delta T_{11}/\delta t = U_1 \; dT_{11}/dx_1 - 2 \; dU_1/dx_1 \; T_{11}$$

$$\delta T_{22}/\delta t = U_1 \; dT_{22}/dx_1 + dU_1/dx_1 \; T_{22}$$

(From eqn. of continuity : $dU_1/dx_1 = -2dU_2/dx_2 = -2dU_3/dx_3$)

and hence, the governing differential equations for T_{11} and T_{22} can be written as follows :

$$T_{11} + \tau_{neff}(U_1 dT_{11}/dx_1 - 2 \; dU_1/dx_1 \; T_{11}) = 2G\tau_{neff} dU_1/dx_1$$

$$T_{22} + \tau_{neff}(U_1 dT_{22}/dx_1 + dU_1/dx_1 \; T_{22}) = - G\tau_{neff} dU_1/dx_1$$

In case of discrete spectrum of relaxation times, for each pair of values of τ's and G's, there will be differential equations for T_{11} and T_{22}.

The Phan-Thien and Tanner Model :

The governing differential equations for T_{11} and T_{22} are as follows :

$$dT_{11}/dx_1 = 2(1-\xi)/U_1 \; dU_1/dx_1 \; T_{11} - T_{11}/(\tau U_1) \exp(\varepsilon/G(T_{11}+2T_{22}) + 2G/U_1 \; dU_1/dx_1$$

$$dT_{22}/dx_1 = -(1-\zeta)/U_1 \; dU_1/dx_1 \; T_{22}-T_{22}/(\tau U_1) \exp(\varepsilon/G(T_{11}+2T_{22}) - G/U_1 \; dU_1/dx_1$$

Note that these are two simultaneous differential equations.

VITA

Rajen Patel was born in Ahmedabad, India, on June 4, 1963. After graduating from Jai Hind College, Bombay, he entered Department of Chemical Technology, University of Bombay (U.D.C.T.), in July 1980. He received the Bachelor of Engineering degree in Chemical Engineering in July 1984. He worked for a year as a research assistant at Central Research Station, ACC Ltd. He entered the University of Tennessee, Knoxville in September 1985 and received the Master of Science degree in Polymer Engineering in January 1988.

He is a member of Phi Kappa Phi, the Society of Rheology and the Society of Plastics Engineers.